

The D -dimensional charged AdS black holes solutions in polytropic dark energy from Barrow entropy

Y. Sekhmani*

*Center for Theoretical Physics, Khazar University,
41 Mehseti Street, Baku, AZ1096, Azerbaijan.*

*Centre for Research Impact & Outcome, Chitkara University Institute of Engineering and Technology,
Chitkara University, Rajpura, 140401, Punjab, India. and
Chitkara Centre for Research and Development,
Chitkara University, Baddi, Himachal Pradesh, 174103, India*

B. Hazarika†

Department of Physics, Dibrugarh University, Dibrugarh, Assam,786004

P. Phukon‡

*Department of Physics, Dibrugarh University, Dibrugarh, Assam,786004 and
Theoretical Physics Division, Centre for Atmospheric Studies,
Dibrugarh University, Dibrugarh, Assam,786004*

A. Landry§

*Department of Mathematics and Statistics,
Dalhousie University, Halifax, Nova Scotia, Canada, B3H 3J5*

S. K. Maurya¶

*Department of Mathematical and Physical Sciences, College of Arts and Sciences,
University of Nizwa, Nizwa 616, Sultanate of Oman and
Research Center of Astrophysics and Cosmology,
Khazar University, Baku, AZ1096, 41 Mehseti Street, Azerbaijan*

J. Rayimbaev**

*Institute of Fundamental and Applied Research,
National Research University TIIAME, Kori Niyoziy 39, Tashkent 100000, Uzbekistan
University of Tashkent for Applied Sciences,
Gavhar Str. 1, Tashkent 100149, Uzbekistan*

*Urgench State University, Kh. Alimdjan str. 14, Urgench 220100, Uzbekistan
Shahrisabz State Pedagogical Institute, Shahrisabz Str. 10, Shahrisabz 181301, Uzbekistan and
Tashkent State Technical University, Tashkent 100095, Uzbekistan*

Abstract

This paper mainly aims to solve the Anti deSitter Black Holes (AdS BH) under the Barrow entropy under polytropic gas fluid, especially the Chaplygin Gas. First, we develop this last polytropic model in detail to then obtain the possible solutions and thermodynamic conditions on the Energy-Momentum and the Barrow Entropy for spacetimes of spatial dimension $D > 3$. Then, we focus on thermodynamic solutions and the different impacts on the Barrow entropy of the black hole, the temperature profile, the mass and the various physical quantities involved. Afterwards, we focus on the specific cases of the solutions of dimensions $D = 4$ and 5 in order to concretely test the models, especially from the point of view of the thermodynamic topology. Finally, we generalize everything by elaborating and testing the stability of the models to arrive at the thermal geometry of the AdS BH.

I. INTRODUCTION

The spherically symmetric spacetime physical problem is a well-interesting challenge, especially concerning a black hole (BH) as a gravitational source in General Relativity (GR) and some more generalized and complex gravity theories. Not only the BH horizon solutions are in the most interest for physicists in gravity, but there are also neutron stars (NS) and white dwarf (WD) solutions as interesting physical process using the same formalism. However, there has been an increasing interest since a while toward the thermodynamic aspects of physical process implying BH and any remnants. This interest was leading to the thermal radiation emission from spherically symmetric masses process as the Hawking Radiation [1–11]. This type of thermal radiation leads to the Hawking Temperature, which is essentially the BH evaporating temperature can be measured from the BH horizon surface as in infinity. A BH will evaporate its thermal energy in some conditions as a black body radiation. There are several works in the literature on the various physical processes leading to Hawking BH radiation and may also imply BH and accretion systems [7–11]. We should note that there is an equivalent for linear accelerated mass thermal radiation called the Unruh radiation working a bit on the same principles [12–14].

From this point, because the thermal radiation from spherically symmetric astrophysical objects leads to thermodynamic process, we need to get interested on the entropy related to this thermal radiation. Because a BH has an intrinsic temperature, the Hawking temperature $T_H = T_H(r \rightarrow \infty) = \frac{1}{8\pi M}$, this consideration implies that the first thermodynamic law needs to be satisfied as $dE = T dS - P dV$ where T can be expressed in terms of the Hawking temperature T_H and dS will be the related instant entropy of this same BH. We can also express this in a macroscopic manner as $(S - S_0) \approx 8\pi M dE$ and the BH entropy is proportional to its surface area [3–10]. The Hawking BH evaporation temperature leads to the Hawking-Bekenstein entropy described by $S \sim A_H$ where A_H is the horizon surface area. Depending on the type of BH, there are several type of more developed entropy processes and specific relations.

One of the most important class of entropy processes arises to a particular interest for the anthropic principle and some related physical models. This principle states that all universe obser-

* sekhmaniyassine@gmail.com

† rsbidyuthazarika@dibru.ac.in

‡ prabwal@dibru.ac.in

§ a.landry@dal.ca

¶ sunil@unizwa.edu.om

** javlon@astrin.uz

vation should be done by a biological observer (a human) [15]. There are two Anthropic principle: i. the Weak Anthropic Principle (WAP) where the location in Universe is privileged as observer and ii. Strong Anthropic Principle (SAP) stating that the universe must have fundamental laws, constant and parameter making possible the observer existence [15]. Then J.D. Barrow in 1986 made the anthropic universe formulation slightly different from Carter's anthropic philosophical principles. The Barrow-Tipler anthropic principles version are stated as: The WAP states that the observables of all physical and cosmological quantities are not equally probable and their values are restricted by sites where carbon-based life exists. The SAP will state that Universe must have properties allowing life and a development within some stages in its history. This last principle arises to some consequences such as the observer existence in universe, the information transmission from the rest of universe to an observer and multiple universes possibility [16–19]. This anthropic model is going to the all observer-based universe principle as we could really summarize this philosophical thought. There are several implications of this principle, including on the cosmic expansion in string theory [20]. However, the cosmic inflation models does not really explain the time asymmetry and the arrow of time existence [21].

Before going into the Barrow entropy more in-depth discussion and precision, we need to discuss more about the possible cosmological fluids might satisfy the anthropic principle. As a well suitable cosmological fluid equation of state (EoS), there is a special class called the polytropic cosmological gases satisfying the anthropic principle. The polytropic fluids are usually described by [22–29]:

$$P(\rho) = -\gamma\rho^{1+\frac{1}{n}}, \quad (1)$$

where n is the polytropic index and the possible values are $1 < n < \infty$. Eqn (1) is made for negative pressure as required for dark energy fluids. By setting $\frac{1}{3} < \gamma < 1$ and $n \rightarrow \infty$ inside eqn (1), we obtain the quintessence dark energy fluid solutions. This state constitutes a fifth matter form in the universe and this quintessence process is related to an associated scalar field. The cosmological constant Λ_0 is obtained by setting $\gamma = 1$ and $n \rightarrow \infty$, but this also constitutes the primarily dark energy form (cite cosmology paper). However, the quintessence is a second dark energy form as stated by P. Steinhardt works predicting the accelerating universe expansion [30–32]. The quintessence dark energy form is in meantime a specific subcase of polytropic gas according to eqn (1). This EoS as stated by eqn (1) can be generalized by using scalar field EoS with P_ϕ and ρ_ϕ as pressure and fluid density function [33, 34] as:

$$\rho_\phi = \frac{\dot{\phi}^2}{2} + V(\phi), \quad (2)$$

$$P_\phi = \frac{\dot{\phi}^2}{2} - V(\phi), \quad (3)$$

where $\dot{\phi}$ is the time-derivative of the scalar field ϕ and $V(\phi)$ is the scalar potential. The quintessence ratio is defined as $w_Q = -\gamma = \frac{P_\phi}{\rho_\phi}$.

In addition, there are some possible generalization of this eqn (1) EoS such as logatropic and the double polytropic fluids with an EoS as [35, 36]:

$$P(\rho) = -\gamma_1\rho^{1+\frac{1}{n_1}} - \gamma_2\rho^{1+\frac{1}{n_2}}, \quad (4)$$

where n_1 and n_2 are polytropic indexes. One special case of double polytropic fluid is the Murnaghan fluids where eqn (4) will simplify as [35, 36]:

$$P(\rho) = -\gamma\rho^{1+\frac{1}{n}} + P_2, \quad (5)$$

where the second part of fluid is a isobar fluid (constant pressure). From all of these previous EoS, we can easily find several types of BH and cosmological solutions.

There are some literature on the polytropic cosmological structure models explaining BH and cosmological solutions with dark energy models [22–29]. From this consideration, there is the polytropic EoS leading to the polytropic cosmological γ -models. One of the important study on polytropic gas system was on Dark Energy system with cold matter scenario [28]. This study was done with some specific polytropic gases, especially with Chaplygin gas. This last kind of gas is originally described by $P(\rho) = -\gamma\rho^{-1}$, where $n = -\frac{1}{2}$ as polytropic index inside eqn (1). This original Chaplygin gas EoS leads to Quartessence phenomena, a generalization and more complete process in comparison to quintessence models [37–39]. This physical process can be described by two different manifestations of a one and single dark fluid leading to two thermodynamic states: Dark Matter (DM) and Dark Energy (DE). This explanation was also confirmed by cosmological background observations [38, 39]. The both states Quartessence process will have some topological consequences and especially will allow the Anti deSitter Black Hole (AdS BH) solutions by this thermodynamic and topological approach.

Another good example of polytropic gas application is the matter accretion by a charged BH inside a such gas [29]. In this case, the authors found some critical points of possible accretion and the temperature profile and limits close to the event horizon for a Maxwell-Boltzmann gas. These previous solutions are still using the Hawking thermal radiation formalism even if these papers resolve the physical problem for a EoS of some polytropic gases. But the most important consequence on the thermodynamic process is that a BH thermal process can easily be expressed by the Barrow entropy.

The Barrow entropy is the cosmological anthropic entropy of apparent Black Hole (BH) horizons in the universe satisfying first the Friedmann-Lemaître-Robertson-Walker (FLRW) equations. This special entropy from Black hole horizons is described by [40–44]:

$$S_B = \left(\frac{A_H}{A_{Pl}} \right)^{1+\frac{\Delta}{2}}, \quad (6)$$

where $0 < \Delta < 1$ with Δ is the quantum deformation, A_H and A_{Pl} are respectively the horizon and Planck surface areas. The maximal quantum deformation is occurring when $\Delta = 1$ and the Hawking-Bekenstein entropy is recovered for $\Delta = 0$ [43]. But the Barrow entropy leads to several possible solutions and one of them are the BH under AdS/CFT correspondence [45]. This case leads to the restricted phase space (RPS) thermodynamics and then there are charged Anti-deSitter BH solutions with double horizon radius. In this case, the Barrow entropy will be described as

$S_B = \left(\frac{\pi r_+^2}{G} \right)^{1+\frac{\Delta}{2}}$ with r_+ is the outside charged BH horizon. Another possible case of BH solution concerns the BH fragmentation leading to an upper bound on Δ parameter [46]. This result shows that some BHs are unstable and lead to non-negligible corrections on the Barrow entropy in some situations.

All these possible BH solutions are also linked to the modified FLRW cosmological solutions under Barrow entropy [46–50]. The FLRW modified cosmological equations under Barrow entropy are [47]:

$$\kappa_{eff}\rho = 3 \left(H^2 + \frac{k}{a^2} \right)^{1-\Delta/2}, \quad (7)$$

$$-\kappa_{eff}P = (2 - \Delta) \frac{\ddot{a}}{a} \left(H^2 + \frac{k}{a^2} \right)^{-\Delta/2} + (1 + \Delta) \left(H^2 + \frac{k}{a^2} \right)^{1-\Delta/2}, \quad (8)$$

where κ_{eff} is the Barrow modified coupling constant. As in standard cosmology, the cosmological horizon radius and temperature used for Barrow Entropy is [47]:

$$r_H = \left(H^2 + \frac{k}{a^2} \right)^{-1/2}, \quad (9)$$

$$T_{Hor} = -\frac{1}{2\pi r_H} \left(1 - \frac{\dot{r}_H}{2Hr_H} \right), \quad (10)$$

where k is the spatial cosmological curvature, \dot{r}_H is the horizon radius time-derivative, a is the scale factor and H is the Hubble parameter. From eqns (7) and (8), the dark energy thermodynamic Barrow entropy solutions was obtained from eqns (7) and (8) by using eqns (9) and (10) as clearly showed in refs [48, 49]. For going further, there are also the FLRW modified cosmological equations under AdS/CFT correspondence solutions [50]. These changes not only concern the FLRW equations, but there are impacts also on higher dimensional AdS BH solutions, on the Barrow entropy and other more complex approaches in AdS/CFT theory. There is even discussion of AdS thermodynamics as an approach leading to an ideal gas dual in CFT as a relevant solution. So there are some common points and goals with the use of Barrow entropy for higher dimensional BH solutions in general.

Since Barrow entropy has important effects on spacetime and gravitational structures, there has even been recent work on this type of thermodynamics under modified gravity theories. First there was a first paper on BH topological solutions under Barrow entropy via the metric-affine gravity approach [51]. A bit more recently, there is a really interesting paper where Barrow entropy is directly treated and integrated into $F(T)$ -type gravity models [52]. There is even a convincing example of a quadratic $F(T)$ showing Barrow entropy under this alternative theory. This paper also shows the fractal horizon surface of BHs under Barrow entropy via $F(T)$ -type gravity. This new approach could reveal many other things. Finally, there are also some new papers concerning gravity modification under Barrow entropy as well as another more concrete work on aspects of entropic cosmology [53, 54]. So, these last examples clearly show that there are further possible developments of Barrow entropy effects and its generalizations under modified and/or alternative gravity theories.

There is a direct generalization of Barrow with a similar definition called the Tsallis entropy. The exact definition is [55–57]:

$$S_{Ts} = \gamma A^\beta, \quad (11)$$

where β is the Tsallis parameter which is in principle $0 < \beta < \infty$. Barrow entropy becomes with this generalization a specific subcase of Tsallis entropy where $\beta = 1 + \frac{\Delta}{2}$, and then $1 \leq \beta \leq \frac{3}{2}$.

Another possible entropy process case is the Kaniadakis entropy defined as [58–60]:

$$S_K = -k_B \sum_i^N n_i \frac{n_i^K - n_i^{-K}}{2K}, \quad (12)$$

where k_B is the Boltzmann constant, K is the Kaniadakis parameter with $-1 < K < 1$ and n_i is the statistical distribution function as defined in ref. [60]. For a simple BH, the eqn (12) will simplify as $S_K = \frac{\sinh(K S_{BH})}{K}$, where $S_{BH} \sim A_H$ as defined for Hawking-Bekenstein entropy. There are some other possible investigation to be done on these more complex entropy cases, but these are going further than the aims of this current paper.

We will now focus to the aims of this current paper, the thermodynamic physical problem of higher dimension AdS BH solutions under Barrow entropy defined by eqn (6) for a polytropic gas EoS defined by eqn (1). Higher dimensional spacetimes are generally defined when the total number of spatial dimensions is $D > 3$. The additional dimensions can be seen as topological and we will see additional effects related to the thermodynamic behavior of the physical system studied here. We will see in particular how the thermodynamics of the polytropic gas and the Barrow entropy of the BH will influence the parameters of higher dimensional spacetimes such as curvatures, horizons, entropy, Barrow Temperature and so on... We will finally study the thermodynamic stability conditions of these higher dimensional BHs in order to know the possible states satisfying the Barrow entropy.

The manuscript is organized as follows: in Sec. II we introduce field equations for a spherically symmetric metric in the presence of polytropic structure, featured by EoS eqn (1) and deliberate on the primary characteristics of the resulting equations [61]. In Sec. III, we first solve our main equations for the general exact BH solutions with the most important conditions to satisfy. We will then interest in Sec. IV by the general thermodynamics effects of the main solutions under Barrow entropy. We will enchain and go further in Sec. V by working on the topological effect of the BH Barrow thermodynamics. In Sections VI to IX, we will study more in details some thermodynamic concerns, with specific cases such as 4D and 5D AdS BH solutions, on stability, critical points and some other important physical aspects and solution on the higher dimensional BH Barrow solutions. We will finally conclude on all these previous part in the Sec. X.

II. POLYTROPIC GAS MODEL OF DARK ENERGY WITH EOS: $p = -\gamma\rho^{1+\frac{1}{n}}$

To set up a corresponding physical set for charged scalar gas fields with a polytropic EoS in the GR framework, an appropriate action ought to be considered. To this end, a higher-dimensional action featuring the Einstein-Hilbert term, the Maxwell term, and a polytropic background, expressed by

$$\mathcal{I} = \int d^D x \sqrt{-g} \left[\frac{1}{2\alpha^2} (\mathcal{R} + 6L^{-2}) - \frac{1}{2} F_{\mu\nu} F^{\mu\nu} \right] + \mathcal{I}_{Poly}, \quad (13)$$

where the gravity is ruled out by the scalar curvature of the Ricci scalar \mathcal{R} , the parameter L encodes information on the length of the AdS space, $g = \det(g_{\mu\nu})$ is the determinant of the metric 2-rank tensor $g_{\mu\nu}$, $F_{\mu\nu}$ is the electromagnetic 2-rank tensor associated with abelian gauge symmetry U(1) by the gauge potential φ_μ via $F_{\mu\nu} = \partial_\mu \varphi_\nu - \partial_\nu \varphi_\mu$, and \mathcal{I}_{Poly} stands for the polytropic

action ¹.

From that point on, the variation of the action (13) results in the following field equations:

$$\mathcal{I}_{\mu\nu} = \mathcal{R}_{\mu\nu} - \frac{1}{2}g_{\mu\nu}(\mathcal{R} + 6L^{-2}) - \alpha(\mathcal{T}_{\mu\nu}^{\text{Poly}} + \mathcal{T}_{\mu\nu}^{\text{em}}) = 0, \quad (14)$$

$$\partial_\mu(\sqrt{-g}F^{\mu\nu}) = 0, \quad (15)$$

where the Maxwell field equations identify by

$$\mathcal{T}_{\mu\nu}^{\text{em}} = -\frac{1}{2}g_{\mu\nu}F + 2F_{\mu\sigma}F_\nu^\sigma, \quad (16)$$

$$\varphi_a = \varphi(r)(dt)_a, \quad (17)$$

with $F = F_{\mu\nu}F^{\mu\nu}$ is the Maxwell invariant, and $\mathcal{T}_{\mu\nu}^{\text{Poly}}$ is the energy-momentum tensor for polytropic structure.

In order to model an exact BH solution, the processing has to incorporate a static, spherically symmetric D -dimensional spacetime metric ansatz with $g_{tt}g_{rr} = -1$ involving the unknown metric function $F(r)$, such that

$$ds^2 = -F(r) dt^2 + F(r)^{-1} dr^2 + r^2 d\Omega_{D-2}^2, \quad (18)$$

where $d\Omega_{D-2}^2$ identifies the line element of a $(D-2)$ -dimensional hypersurface Σ with constant curvature $(D-2)(D-3)$. It is accordingly described by

$$d\Omega_{D-2}^2 = d\theta^2 + \sin^2\theta \left[d\phi_1 + \sum_{i=2}^{D-3} \prod_{j=1}^{i-1} \sin^2\phi_j d\phi_i^2 \right], \quad (19)$$

with $\theta \in [0, \frac{\pi}{2}]$. It is then handy to specify the coordinates x_i for a spherical hypersurface as follows

$$x_1 = r \cos\theta, \quad (20)$$

$$x_i = r \sin\theta \cos\phi_{D-i-1} \quad (21)$$

$$\times \prod_{j=1}^{D-i-2} \sin\phi_j, \quad i = 2, \dots, D-2$$

$$x_{D-1} = r \sin\theta \prod_{j=1}^{D-4} \sin\phi_j, \quad (22)$$

where r is the radius of the hypersphere and the angles are of the standard ranges.

In this study, it is worth considering the perfect fluid state, which is featured in terms of the stress-energy tensor

$$\mathcal{T}_{\mu\nu} = (\rho + p) u_\mu u_\nu + p g_{\mu\nu}. \quad (23)$$

Here, ρ and p are, respectively, the energy density and the isotropic pressure, which are gauged by an observer moving with the fluid, and u_μ denotes the D -velocity vector. Numerous studies are

¹ In the following, we assume that $\alpha = 8\pi G = c = 1$, where G and c are, respectively, the Newtonian gravitational constant and the speed of light.

currently being carried out in the field of GR, implicating spherically symmetric static solutions with the surrounding part of typical perfect fluid (dust, radiation, dark energy, or ghost energy) with an EoS $p = \omega\rho$ (ω is a constant) [37, 62–68]. Multiple indicators suggest that the ideal cosmological fluid around the black hole may be considered anisotropic because of gravitational influence. By way of example, the polytropic gas with a non-linear EoS has been widely deployed in the literature to probe the features of compact objects. As polytropes are self-gravitating gaseous spheres, they can serve as a *fuzzy* approximation to more refined stellar models. Furthermore, it assists in describing the internal structure of neutron stars (NS), inclusive of their maximum mass, surface temperature, pulsar glitches, and other features, due to its efficient fit to the EoS of NS. On the other hand, certain evidence invokes a scalar tachyon field ϕ which is held to be the source of dark energy, and a potential tachyon field $V(\phi)$, with Born-Infeld type Dirac Lagrangian $\mathcal{L}_\phi = -V(\phi)\sqrt{1 - g^{\mu\nu}\partial_\mu\nu\phi}$ [69]. Further, drawing on ideas in terms of k essence scalar field concepts, the polytropic structure can be reconstructed as a scalar field gas. This reconstruction is generated in fact by considering the K -essence scalar field action, $S = \int d^4x\sqrt{-g}p(\phi, \chi)$ with $p(\phi, \chi)$ being the Lagrangian density [70, 71]. The foregoing implies that the polytropic structure is properly emulated such that its radial pressure is distinct from the tangential pressure. This is in accordance with anisotropic fluids, entailing a covariant form of the stress-energy tensor for the polytropic structure, given by

$$\mathcal{T}_{\mu\nu} = (\rho + p_t) u_\mu u_\nu - p_t g_{\mu\nu} + (p_r - p_t) \chi_\mu \chi_\nu, \quad (24)$$

in which p_r is the radial pressure along the direction of χ_μ , p_t is the tangential pressure perpendicular to χ_μ , and χ_μ is the unit spacelike vector perpendicular to the velocity u_μ . As well, u_μ and χ_μ comply with the constraint $u_\mu u^\mu = -\chi_\mu \chi^\mu = 1$.

The present examination as regards the polytropic structure is performed by considering the frame in comoving with the fluid, allowing us to have $u^a = \sqrt{F(r)}\delta_0^a$ and $\chi^a = 1/\sqrt{F(r)}\delta_1^a$. Accordingly, the stress-energy tensor of Eq. (24) can be restated as follows

$$\mathcal{T}_\mu^\nu = -(\rho + p_t)\delta_\mu^0\delta_0^\nu + p_t\delta_\mu^\nu + (p_r - p_t)\delta_\mu^1\delta_1^\nu, \quad (25)$$

where the term $p_r - p_t$ is termed the anisotropic factor, and for $p_r = p_t$, the case will be subject to the standard isotropic background.

For the purpose of exhaustiveness, we assume that the scalar field gas is in a state on either side of an event horizon identified by the stress energy (25). To be more precise, it should be pointed out that inside the horizon, where $g_{rr} < 0$ and $g_{tt} > 0$, the behaviour of the spatial coordinate r is similar to that of the temporal coordinate t . The energy density is thus $\mathcal{T}_r^r = p_r$, while the pressure along the spatial direction t is defined as $\mathcal{T}_t^t = -\rho$. On the basis of this connection, the energy density and pressure are kept continuous, provided that the criterion $p_r = -\rho$ is verified. Nevertheless, in the case of $p_r \neq -\rho$ and $\rho(r_h) \neq 0$, the pressure at the horizon is discontinuous and the relative phase of the solution evolves dynamically.

Going forward, we will address just the case where $p_r = -\rho$ [62], where the polytropic structure is static and, barring restrictions on the solution, the energy density is continuous across the horizon. Specifically, borrowing ideas from anisotropic fluids, the tangential pressure p_t is constrained by adopting isotropic averaging over the angles and asserting that $\langle \mathcal{T}_i^{(D)j} \rangle = p(r)\delta_i^j$.

Thus, it is possible to get

$$p(r) = p_t + \frac{1}{D-1} (p_r - p_t), \quad (26)$$

where the standard formula $\langle \delta_i^1 \delta_1^i \rangle \equiv \frac{1}{D-1}$ is taken into consideration. Pragmatically, in view of analogous concepts, the standard tangential pressure formulation for quintessential dark energy is given taking into account Eq. (26) as $p_t = \frac{1}{D-2} ((D-1)\omega + 1) \rho$, which is in line with the radial pressure $p_r = -\rho$.

The polytropic structure is characterised to exhibit a non-linear EoS as $p = -\gamma\rho^{1+\frac{1}{n}}$, where ξ is a positive parameter. In considering the rule $p_r = -\rho$, the tangential pressure of the polytropic structure is $p_t = \frac{1}{D-2}\rho(r) - \frac{(D-1)}{(D-2)}\gamma\rho^{1+\frac{1}{n}}$. Therefore, the elements of the stress-energy tensor of the polytropic structure can be specified in terms of the expressions

$$\mathcal{T}_t^t = \mathcal{T}_r^r = -\rho, \quad (27)$$

$$\mathcal{T}_{\theta_1}^{\theta_1} = \mathcal{T}_{\theta_i}^{\theta_i} = \frac{1}{D-2}\rho(r) - \frac{(D-1)}{(D-2)}\gamma\rho^{1+\frac{1}{n}}. \quad (28)$$

We later show that the anisotropy of the polytropic structure diminishes and that the EoS $p = -\gamma\rho^{1+\frac{1}{n}}$ is retained on the cosmological scale.

III. EXACT SOLUTIONS

Due to the static and spherically symmetric characteristics of spacetime, the requirement $\mathcal{T}_t^t = \mathcal{T}_r^r$ is fully fulfilled. Thus, the elements of the gravitational field equation (14) in D -dimensions are given by

$$\mathcal{I}_t^t = \mathcal{I}_r^r = \frac{1}{2r^2}(D-2)(D-3)(F(r)-1) + \frac{1}{2r}(D-2)F'(r) - \frac{3}{L^2}, \quad (29)$$

$$\mathcal{I}_{\theta_i}^{\theta_i} = \mathcal{I}_{\theta_1}^{\theta_1} = \frac{F''(r)}{2} + \frac{(F(r)-1)(D-3)(D-4)}{2r^2} + \frac{(D-3)F'(r)}{r} - \frac{3}{L^2}. \quad (30)$$

On the other hand, insights into the structure of Maxwell's charged source are thus explored by considering the time component of Eq. (15) in conjunction with the space-time metric (18), giving the following differential equation

$$(D-2)\varphi'(r) + r\varphi''(r) = 0, \quad (31)$$

which admits an exact electric field given by

$$\varphi(r) = \begin{cases} -\frac{q}{(D-3)r^{D-3}} + \Phi_0 & D > 3, \\ q \ln r + \Phi_0 & D = 3. \end{cases} \quad (32)$$

where q and Φ_0 are integration constants.

As a rule of thumb, the integration constant q is correlated to the physical parameter of the charge Q on a two-dimensional sphere of infinite radius by means of Gauss's law

$$\begin{aligned} Q &= \frac{1}{4\pi} \int_{S_\infty^2} \star \mathbf{F} = \frac{1}{8\pi} \int_{S_\infty^2} F^{ab} \epsilon_{abc_1c_2 \dots c_{D-2}} \\ &= \frac{1}{4\pi} \int_{S_\infty^2} \varphi'(r) \sqrt{-g} d\theta_1 d\theta_2 \dots d\theta_{D-2} \\ &= \frac{q}{4\pi} \omega_{D-2}, \end{aligned} \quad (33)$$

where ω_{D-2} is the volume of the unit $(D-2)$ -dimensional spherical topology².

Seeking an analytically exact solution for the surrounding polytropic structure in the context of GR must take into account the dual equations of the gravitational field and the matter field (14-15). Therefore, a specific analysis of the polytropic structure side using the Bianchi identity ($T_{;\nu}^{\mu\nu} = 0$) could supply a first-order differential equation in terms of $\rho(r)$ such that

$$r \rho'(r) + (D-1) \rho(r) - \gamma(D-1) \rho(r)^{1+\frac{1}{n}} = 0, \quad (34)$$

where the first prime refers to the first derivative with respect to the radial variable r . An attempt to analytically solve Eq. (34) results in an exact solution for the polytropic structure energy density in the form of

$$\rho(r) = \left(\zeta^2 r^{\frac{D-1}{n}} + \gamma \right)^{-n}, \quad (35)$$

where ζ is a normalisation parameter specifying the intensity of the polytropic scalar field gas. In closer scrutiny, Eq. (35) revolves around the result of the stress energy tensor conservation law $\partial_\mu T^{\mu\nu} = 0$.

To gain a deeper insight into the behavior of the polytropic structure, it is worth examining its criticality at certain limits. In this respect, at large radial coordinates (i.e. $\zeta^2 r^{\frac{D-1}{n}} \gg \gamma$), it gives rise to

$$\rho(r) \sim \zeta^{-2n} / r^{D-1}, \quad (36)$$

which states that the polytropic structure behaves like a matter content whose energy density varies with r^{D-1} . On the other hand, at small radial coordinates (i.e. $\zeta^2 r^{\frac{D-1}{n}} \ll \gamma$), we obtain

$$\rho(r) \sim \gamma^{-n}, \quad (37)$$

which in turn means that the polytropic structure resembles a positive cosmological constant in a small-scale scenario, and that the closer it gets to the black hole, the more it gravitationally clumps up.

Alternatively, picking $r \rightarrow \infty$ results in properties

$$p_r \rightarrow - \left(\zeta^2 r^{\frac{D-1}{n}} \right)^{-n}, \quad (38)$$

$$p_{\theta,\phi} \rightarrow \frac{1}{D-2} \left(\frac{\zeta^{-2n}}{r^{D-1}} \right) \left(1 - \gamma(D-1) \zeta^{-2} r^{-\frac{D-1}{n}} \right), \quad (39)$$

² $\omega_{D-2} = \frac{2\pi^{\frac{D-1}{2}}}{\Gamma(\frac{D-1}{2})}$

which means that the anisotropic nature is not guaranteed at large distances. In Table I, we work out the large distance bounds on the pressure components for the polytropic structure, revealing that the anisotropic factor asymptotically fails to tend to zero. This is unlike the effects observed in the quintessential fluid [62] and CDF [72], where the anisotropy decreases with distance; for the polytropic structure, the anisotropy factor reaches zero in the case of $\gamma = 2(D - 2) \left(r^{(D-1)/n} \xi^2 \right) / (D - 1)$. This lingering anisotropy raises a number of implications for the evolution of the universe, such as Hubble expansion anisotropies and the fluxes of mass phenomenon. These insights are supported by an array of observational surveys, such as those focused on galaxy clusters [73–75] and type Ia supernovae (SN Ia) within the framework of the Lematre-Tolman-Bondi (LTB) patterns [76]. Our preliminary findings pave the way for more in-depth investigations into the polytropic structure, drawing on the studies referred to herein and others.

For a slightly clearer insight into the behavior of our solution, we shall focus on the classical ECs, i.e., the null energy condition (NEC), the dominant energy condition (DEC), the weak energy condition (WEC), and the strong energy condition (SEC), defined as follows [77]:

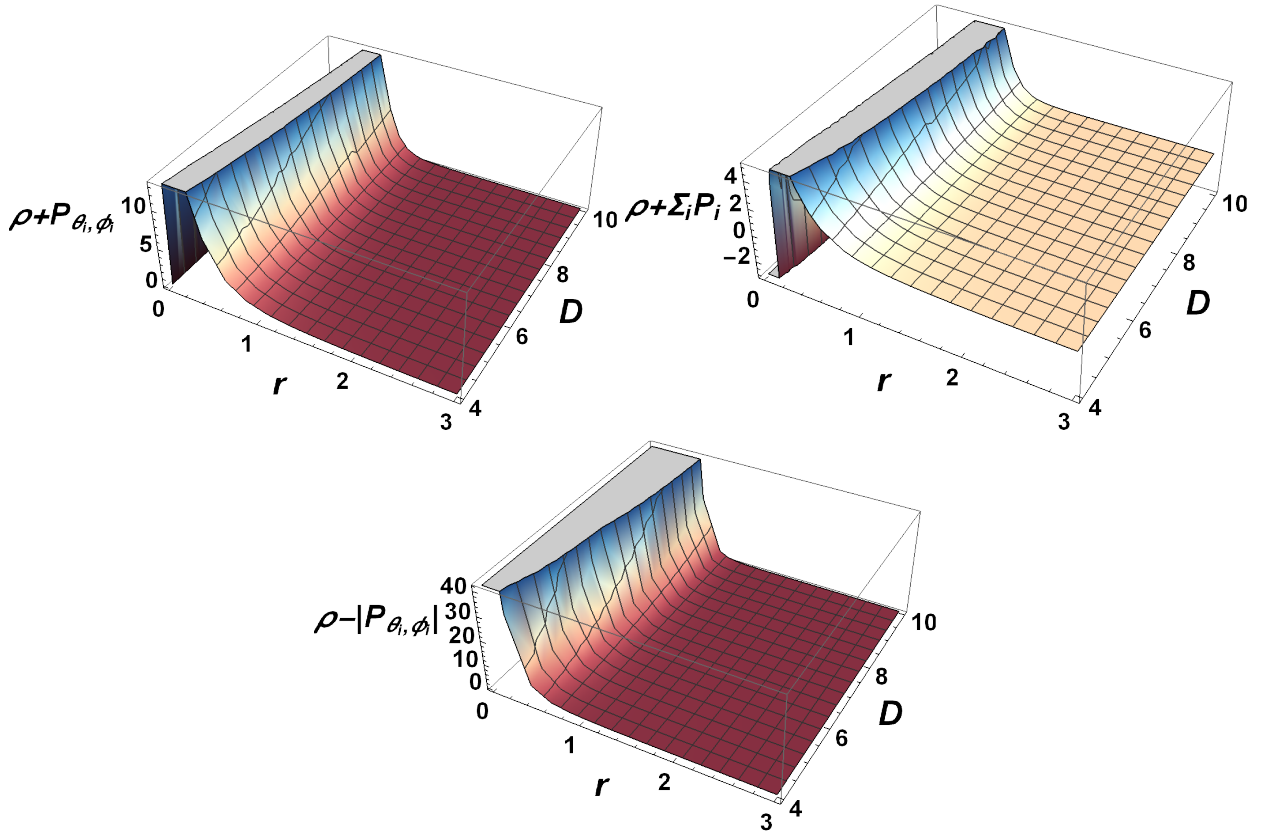


FIG. 1: The variation of $\rho + \sum_i P_i$ (strong energy condition), $\rho + P_{\theta, \phi_i}$ (null energy condition), and $\rho - |P_{\theta, \phi_i}|$ (dominant energy condition) against r for multiple values of the parameter dimension D and for the fixed set, i.e., $\gamma = 0.095$, $\xi = 1$, and $n = 2$.

$$\text{WEC} : \rho \geq 0, \rho + P_i \geq 0,$$

$$\begin{aligned}
\text{SEC} &: \rho + \sum_i P_i \geq 0, \quad \rho + P_i \geq 0, \\
\text{NEC} &: \rho + P_i \geq 0, \\
\text{DEC} &: \rho \geq 0, \quad |P_i| \geq \rho.
\end{aligned} \tag{40}$$

Accordingly, full expressions may be furnished as follows:

$$\begin{aligned}
\rho + P_r = 0, \quad \rho + P_{\theta_i, \phi_i} &= \frac{D-1}{D-2} \left(\rho - \frac{\gamma}{\rho} \right), \quad \rho + \sum_i P_i = \rho - \left(\frac{D-1}{D-2} \right) \frac{\gamma}{\rho}, \\
\rho - |P_r| = 0, \quad \rho - |P_{\theta_i, \phi_i}| &= \rho - \left| \frac{1}{D-2} \rho - \left(\frac{D-1}{D-2} \right) \frac{\gamma}{\rho} \right|.
\end{aligned} \tag{41}$$

where explicitly, in terms of the BH parameter space, one has

$$\begin{aligned}
\rho + P_{\theta_i, \phi_i} &= \frac{D-1}{D-2} \left(\left(\gamma + \xi^2 r^{\frac{D-1}{n}} \right)^{-n} - \gamma \left(\left(\gamma + \xi^2 r^{\frac{D-1}{n}} \right)^{-n} \right)^{\frac{1}{n}+1} \right), \\
\rho + \sum_i P_i &= \left(\gamma + \xi^2 r^{\frac{D-1}{n}} \right)^{-n} - \frac{\gamma(D-1) \left(\left(\gamma + \xi^2 r^{\frac{D-1}{n}} \right)^{-n} \right)^{\frac{1}{n}+1}}{D-2}, \\
\rho - |P_{\theta_i, \phi_i}| &= \frac{\left(\gamma + \xi^2 r^{\frac{D-1}{n}} \right)^{-n}}{D-2} \left(D-3 + \gamma(D-1) \left(\gamma + \xi^2 r^{\frac{D-1}{n}} \right)^{-1} \right).
\end{aligned} \tag{42}$$

To highlight the inspection of the violation/satisfaction of the constraints of ECs, Fig. 1 represents, for a multiple value of the BH parameter system, three types of ECs such as $\rho + \sum_i P_i$, $\rho + P_{\theta_i, \phi_i}$ and $\rho - |P_{\theta_i, \phi_i}|$ against the variable r . Upon detailed scrutiny, $\rho + P_{\theta_i, \phi_i}$ and $\rho - |P_{\theta_i, \phi_i}|$ are all definite positively, while $\rho + \sum_i P_i$ undergoes a sign change at $r_0 = \left(\gamma / (D-2) \xi^2 \right)^{\frac{n}{-1+D}}$, entailing a negative-to-positively switch between small r and large one (see Fig. 2). Of interest is the fact that the root r_0 is effectively the transition point in the sign of P_{θ_i, ϕ_i} , i.e. the point at which the tangential pressure switches from a repulsive to an attractive phase. In a nutshell, the concluding assessment and compliance reveals that the polytropic structure satisfies the NEC, WEC, and DEC criteria, though it is in violation of the SEC. Interestingly, this scenario is exactly the similar to the quintessential model for dark energy. Roughly speaking, any violation of the SEC in GR has been demonstrated to be a violation of the attractive nature of gravity, as manifest in the case of dark energy. However, this scenario is not necessarily viable in the context of extended severity, as shown for the extended gravity model of the model $f(R)$ [78].

It is similarly worthwhile approaching the EC set-up from a thermodynamic standpoint. Notice that the thermodynamic description of the BH system in the extended phase space is substantially given by the radius r , which is related to the thermodynamic volume by Eq. (63).

These considerations are worth contrasting with current findings in the literature. For example, logotropic fluid-type BHs can violate the SEC for high radii, as argued in [79]. In turn, the study of [80] discloses that, while the WEC is satisfied, the SEC, in fact, remains violated for regular Hayward-AdS BHs. According to [81], such new solutions are suggested for regular BHs with multihorizons, inferring that the SEC is not satisfied at all inside the event horizon for all

TABLE I: Quintessence, CDF and polytropic structures in *higher*-dimensional spacetime formulation.

anisotropic fluid	EoS	p_r	p_t	ρ	asymptotic behavior
Quintess. (DE) [62]	$p = \rho\omega$ ($-1 < \omega < -1/3$)	$-\rho$	$\frac{1}{D-2} ((D-1)\omega + 1) \rho$	$\frac{c\omega(D-1)(D-2)}{4r^{(D-1)(\omega+1)}}$	$\rho \rightarrow 0$ $p_r \rightarrow 0$ $p_t \rightarrow 0$
CDF [72]	$p = -\gamma/\rho$ ($\gamma > 0$)	$-\rho$	$\frac{1}{D-2} \left(\rho - \frac{(D-1)\gamma}{\rho} \right)$	$\sqrt{\gamma + \frac{Q^2}{r^{2(D-1)}}}$	$\rho \rightarrow \sqrt{\gamma}$ $p_r \rightarrow -\sqrt{\gamma}$ $p_t \rightarrow -\sqrt{\gamma}$
Polytropic	$p = -\gamma\rho^{1+\frac{1}{n}}$ ($\gamma > 0$)	$-\rho$	$\frac{1}{D-2} \left(\rho - \frac{(D-1)}{\gamma\rho^{1+\frac{1}{n}}} \right)$	$\left(\xi^2 r^{\frac{D-1}{n}} + \gamma \right)^{-n}$	$\rho \rightarrow \frac{\xi^{-2n}}{r^{(D-1)}}$ $p_r \rightarrow -\frac{\xi^{-2n}}{r^{(D-1)}}$ $p_t \rightarrow -p_r \left(\frac{1}{(D-2)} + \gamma(D-2)p_r^{\frac{1}{n}} \right)$

solutions, while the other ECs rely on the ratio of extreme charges of the isolated solutions. Here, in [81] further solutions for regular BHs featuring multihorizons are offered, concluding by stating that the SEC is never satisfied across the event horizon in all solutions, while the remaining ECs rely on the ratio of extreme charges of the isolated solutions. For non-rotating or spinning BHs in conformal gravity, analogous conclusions are offered in [82], where the SEC has to be satisfied for particular BH sizes that rely on the theory's ultimate scaling.

By taking into account the exact analytical solutions for the Maxwell electric field (32) with respect to Einstein's equations (14)-(15), we are able to obtain two sets of second differential equations in terms of the metric function $F(r)$, such that

$$\mathcal{I}_t^t = \mathcal{I}_r^r = \frac{1}{2r^2}(D-2)(D-3)(F(r)-1) + \frac{(D-2)}{2r}F'(r) - \frac{3}{L^2} + \frac{q^2}{4r^{2(D-2)}} - \rho(r), \quad (43)$$

$$\begin{aligned} \mathcal{I}_{\theta_i}^{\theta_i} = \mathcal{I}_{\theta_1}^{\theta_1} &= \frac{F''(r)}{2} + \frac{(F(r)-1)(D-3)(D-4)}{2r^2} + \frac{(D-3)F'(r)}{r} - \frac{3}{L^2} \\ &- \frac{q^2}{4r^{2(D-2)}} + \frac{1}{D-2}\rho(r) - \frac{D-1}{D-2}\gamma\rho^{1+\frac{1}{n}}. \end{aligned} \quad (44)$$

While considering the energy density of the polytropic structure (35), and proceeding with the $(\overset{t}{t})$ components of the field equations allows us to obtain the following differential equation

$$(D-2) \left[(3-D)(1-F(r)) + rF'(r) \right] + 2r^2 \left(\left(\xi^2 r^{\frac{D-1}{n}} + \gamma \right)^{-n} - 3L^{-2} + \frac{q^2}{4r^{2(D-2)}} \right) = 0, \quad (45)$$

where an exact analytical solution for $F(r)$ can be represented in the following form

$$F(r) = 1 - \frac{2M}{r^{D-3}} + \frac{q^2}{r^{2(D-3)}} + \frac{r^2}{L^2} - \frac{2r^2\gamma^{-n} {}_2F_1 \left(n, n; n+1; -\frac{\xi^2 r^{\frac{D-1}{n}}}{\gamma} \right)}{(D-2)(D-1)}, \quad (46)$$

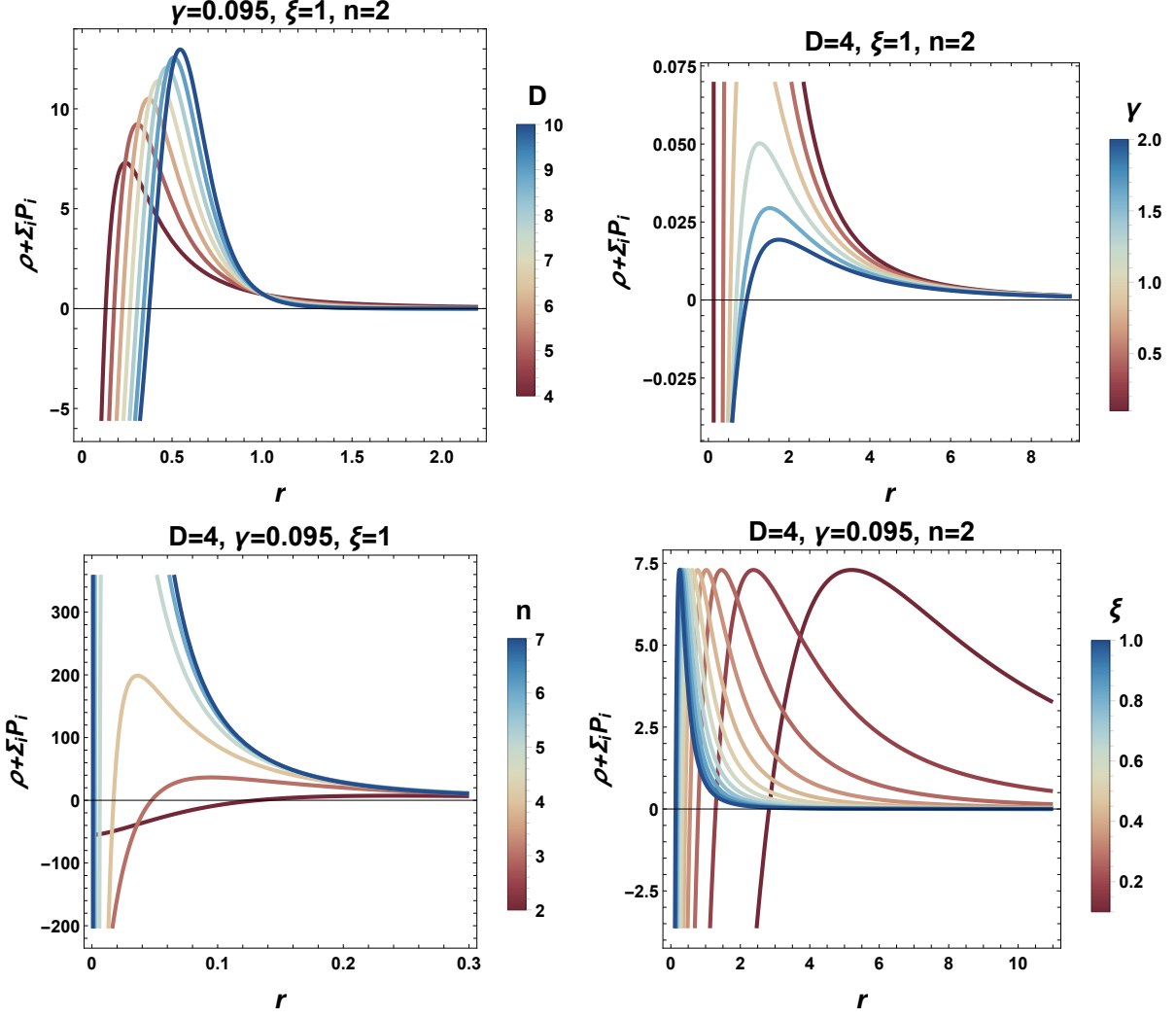


FIG. 2: Strong $(\rho + \sum_{i=1}^3 P_i)$ energy condition for several fixed parameters

where M represents the mass of the BH, in this case we are treating the BH as a point mass, which means that M is a constant. Here, ${}_2F_1[a_1, a_2; a_3; a_4]$ is a hypergeometric function which describes the regular solution of the hypergeometric differential equation, is held to hold for $|a_4| < 1$ and is specified by a series of powers of the form

$${}_2F_1(a_1, a_2; a_3; a_4) = \sum_{p=0}^{\infty} \left(\frac{(a_1)_p (a_2)_p}{(a_3)_p} \right) a_4^p / p!, \quad (47)$$

with $(k)_p$ is the (rising) Pochhammer symbol [83].

For the sake of disclosure of the asymptotic behaviour of the BH solution, such a large distance analysis is taken into account with respect to the metric function $F(r)$, resulting in

$$F(r) \rightarrow 1 + \frac{r^2}{L^2}, \quad (48)$$

which demonstrates that in the asymptotic limit, our BH solution is uniquely expressed by the AdS length L . Furthermore, a thorough analysis showed that the BH solution modeling of the

background can be brought back to the higher-dimensional Einstein-Maxwell theory as [84]

$$F(r) |_{\gamma \rightarrow \infty} = 1 - \frac{2M}{r^{D-3}} + \frac{q^2}{r^{2(D-3)}} + \frac{r^2}{L^2}. \quad (49)$$

A concrete visualization of the behavior of the metric function $F(r)$ is shown in a two-dimensional representation for different values of the parameters (D, γ) with a fixed set of rest parameters in Fig. 3. In broad terms, it can be observed that the metric function exhibits two possible horizon radii, namely the Cauchy horizon (inner horizon) and the event horizon radius (outer horizon).

Next, we investigate in terms of curvature singularity tools the relevant features of the BH solution. Thus, the verification of the uniqueness and singularity of the BH solution is carried out by analysing the Ricci scalar (\mathcal{R}) and Kretschmann scalar ($\mathcal{R}_{\alpha\beta\mu\nu}\mathcal{R}^{\alpha\beta\mu\nu}$) invariants given, respectively, in the essence of the metric function (46) by

$$\mathcal{R} = -\frac{D(D-1)}{L^2} + \frac{2\left(\gamma + \xi^2 r^{\frac{D-1}{n}}\right)^{-n} \left(D\gamma r^{\frac{1}{n}} + \xi^2 r^{D/n}\right)}{(D-2)\left(\xi^2 r^{D/n} + \gamma r^{\frac{1}{n}}\right)} - (D-4)(D-3)q^2 r^{4-2D}, \quad (50)$$

and

$$\begin{aligned} \mathcal{R}_{\alpha\beta\mu\nu}\mathcal{R}^{\alpha\beta\mu\nu} = & -\left(\frac{\left(\xi^2 r^{\frac{D-1}{n}} + \gamma\right)^{-n} \left(2(2D-5)\xi^2 r^{D/n} + 2\gamma(D-4)r^{\frac{1}{n}}\right)}{(D-2)\left(\xi^2 r^{D/n} + \gamma r^{\frac{1}{n}}\right)} - \frac{2(D-3)\gamma^{-n} {}_2F_1\left(n, n; n+1; -\frac{r^{\frac{D-1}{n}}\xi^2}{\gamma}\right)}{D-1}\right. \\ & - 2(D-3)r^{1-2D} \left(\left((D-2)Mr^D + (5-2D)q^2 r^3\right) + \frac{2}{L^2}\right)^2 + 2(D-3)(D-2) \left(-\frac{2\gamma^{-n} {}_2F_1\left(n, n; n+1; -\frac{r^{\frac{D-1}{n}}\xi^2}{\gamma}\right)}{(D-2)(D-1)}\right. \\ & \left. + r^{1-2D} \left(q^2 r^3 - 2Mr^D\right) + \frac{1}{L^2}\right)^2 + 8(D-2) \left(\frac{(D-3)\gamma^{-n} {}_2F_1\left(n, n; n+1; -\frac{r^{\frac{D-1}{n}}\xi^2}{\gamma}\right)}{(D-2)(D-1)} + (D-3)r^{1-2D} \left(Mr^D - q^2 r^3\right)\right. \\ & \left. - \frac{\gamma^{-n} \left(\frac{\xi^2 r^{\frac{D-1}{n}}}{\gamma} + 1\right)^{-n}}{D-2} + \frac{1}{L^2}\right)^2. \end{aligned} \quad (51)$$

By carefully examining the expressions (50) and (51), we can confirm that the BH solution by means of the metric function (46) is singular. This holds for any given set of parameter spaces with the given constraint $D > 3$. For practical considerations, the occurrence of the singularity is caused by the mass, the charge, and polytropic structure terms in the BH metric. However, opposing alternative situations can be thought of to abolish the singularity, such as the choice of $D = 3$ leading to elimination of the singularity. Notably, to implement such removal of singular behavior, numerous studies invented such practical mechanisms for this purpose (see, for example, [85]). Throughout the sequel, we will consider no such situation and rely instead on the metric function (46). In a more concrete inspection, the singularity is evidenced on the basis of the Ricci scalar and the Kretschmann scalar at the centre $r = 0$, which yields the results

$$\lim_{r \rightarrow 0} \mathcal{R} \approx \infty, \quad (52)$$

$$\lim_{r \rightarrow 0} \mathcal{R}_{\alpha\beta\mu\nu}\mathcal{R}^{\alpha\beta\mu\nu} \approx \infty. \quad (53)$$

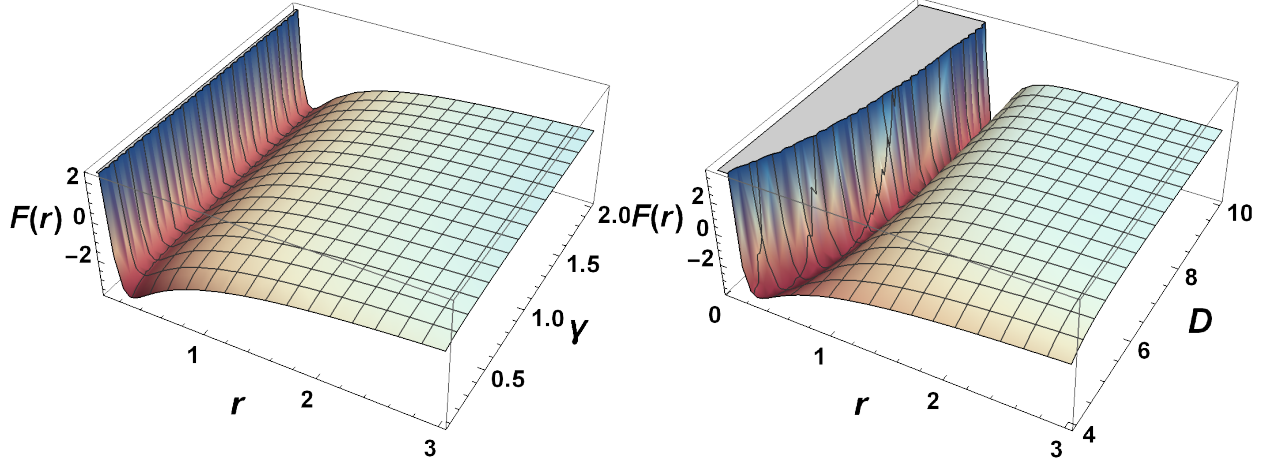


FIG. 3: Left panel: The behavior of $F(r)$ (46) by varying γ and setting $D = 4$. Right panel: The behavior of $F(r)$ with varying D and setting $\gamma = 0.095$. For the two panels, set $M = 1, L = 1, q = 0.5, \xi = 1$ and $n = 2$.

On the other hand, looking at large distance behavior is a worthwhile follow-up feature, since

$$\lim_{r \rightarrow \infty} \mathcal{R} \approx -\frac{D(D-1)}{L^2}, \quad (54)$$

$$\lim_{r \rightarrow \infty} \mathcal{R}_{\alpha\beta\mu\nu} \mathcal{R}^{\alpha\beta\mu\nu} \approx \frac{2(D^2 - D - 4)}{L^2}, \quad (55)$$

which point out that the Kretschmann and Ricci scalars exhibit a finite term at large distances. In summary, the scalar tools demonstrate that the BH solution is unique and significantly altered by the AdS backgrounds.

IV. THERMODYNAMICS AND SMARR RELATION

In the context of gauge/gravity duality, strongly coupled gauge theories can be interrelated with the closely associated weakly coupled string theories. From the holographic perspective, bulk string theory can in turn be apt to inform boundary gauge theory. By means of the AdS/CFT correspondence [86, 87], in which the conformal field theory maps onto the asymptotically AdS spacetime in a higher dimension, the thermodynamic characteristics of a BH can be made to disclose the characteristics of the dual physical state. Analogously, the BH horizon in the asymptotically AdS spacetime provides insight into the finite temperature of its dual field theory.

In the remainder of this part, we shall explore the thermodynamic quantities of charged AdS BHs solution with a surrounding polytropic structure and ascertain the first law of thermodynamics as well as the Smarr relation. So as to establish the Hawking temperature, it needs initially to be considered the surface gravity, given by [88]

$$\kappa = \left(-\frac{1}{2} \nabla_\mu \xi_\nu \nabla^\mu \xi^\nu \right)^{1/2} = \frac{1}{2} F'(r_h), \quad (56)$$

with $\xi^\mu = \partial/\partial t$ is a Killing vector for the metric. Thus, the formula $T = \kappa/2\pi$ gives the Hawking temperature expressed in terms of the parameters of the BH system, as follows,

$$T = \frac{1}{4\pi r_h} \left\{ r_h^2 \left(-\frac{2 \left(\gamma + \xi^2 r_h^{\frac{D-1}{n}} \right)^{-n}}{D-2} + 3q^2 r_h^{4-2D} - \frac{1}{L^2} \right) + \left(-q^2 r_h^{6-2D} + \frac{r^2}{L^2} + 1 \right) D - 3 \right\}, \quad (57)$$

where the horizon constraint $F(r_h) = 0$ has been taken into account.

On the other hand, entropy might arise from the fact that it is computed in accordance with the so-called area law [89, 90], which states that S_{BH} is one quarter of the area of the BH event horizon given by

$$S_{BH} = \frac{\omega_{D-2}}{4} r_h^{D-2}. \quad (58)$$

In the limit as r approaches infinity, the mass of the AdS black hole solution with an encompassing polytropic structure is expressed as

$$M_{ADM} = \frac{(D-2)\omega_{D-2}}{16\pi} M, \quad (59)$$

where M is defined by the formula $F(r_h) = 0$ in Eq. (46). Thus, the Arnowitt-Deser-Misner equation may be understood in terms of the parameter BH spacetime as (ADM) [91, 92] mass is given by

$$M_{ADM} = \frac{(D-2)\omega_{d-2}}{8\pi} r_h^{D-3} \left\{ 4\pi^{3-D} Q^2 r_h^{6-2D} \Gamma \left(\frac{D-1}{2} \right)^2 + \frac{r^2}{L^2} + 1 - \frac{2r^2 \gamma^{-n} {}_2F_1 \left(n, n; n+1; -\frac{\xi^2 r_h^{\frac{D-1}{n}}}{\gamma} \right)}{(D-2)(D-1)} \right\}. \quad (60)$$

To achieve a proper derivation of the relevant thermodynamic quantities, a useful insight is the implementation of the first law of BH thermodynamics. Concretely, the first law can be written as [93]

$$dM = TdS + \sum_i \mu_i d\mathcal{N}_i, \quad (61)$$

where μ_i represent the chemical potentials associated with the conserved charges \mathcal{N}_i . Consequently, the first law of black hole thermodynamics is fulfilled by the physical properties of black holes with a surrounding polytropic configuration defined by

$$dM = TdS + \mathcal{L}dL + UdQ + \mathcal{A}d\gamma. \quad (62)$$

Here, T corresponds to the Hawking temperature, which is correlated with the horizon's gravity, and \mathcal{L} refers to the thermodynamic variable dual to L , U is the electric potential, and \mathcal{A} represents the thermodynamic variable associated with γ . To guarantee that the fundamental equation depends only on extensive variables, the variable L , which is related to the cosmological constant, should be considered.

Based on the specific volume $v = \frac{4r_h}{D-2}$ and making use of equation (59), the conjugate quantity of the pressure results in the following amount:

$$V = \frac{\omega_{D-2}}{D-1} r_h^{D-1}. \quad (63)$$

In parallel, to properly set up the thermodynamic phase space environment, the parameter function $F(r_h, M, L, Q, \gamma)$ ought to vanish under any given parameter transformation. Related notes offer analogous arguments for recognising the constraints $F(r_h, M, L, Q, \gamma) = 0$ and $\delta F(r_h, M, L, Q, \gamma) = 0$ on the evolution along the parameter space. However, an alternative solution is envisaged by treating the mass parameter, M , as a function of the parameters $M(r_h, L, Q, \gamma)$ as well.

More specifically, the thermodynamic variables in question are entropy S , pressure P , physical charge Q and the variable \mathcal{A} , which is the conjugate potential of the parameter ζ . It is then fairly straightforward to redefine $M = M(S, Q, L, \gamma)$ as a 1-form differential such that

$$dM = \left(\frac{\partial M}{\partial S} \right)_{Q,L,\gamma} dS + \left(\frac{\partial M}{\partial Q} \right)_{S,L,\gamma} dQ + \left(\frac{\partial M}{\partial L} \right)_{S,Q,\gamma} dL + \left(\frac{\partial M}{\partial \gamma} \right)_{S,Q,L} d\gamma, \quad (64)$$

where the components stand for temperature T , thermodynamic volume V , the related electric potential, and the conjugate potential of the parameter ζ which are giving as

$$T = \left(\frac{\partial M}{\partial S} \right)_{Q,L,\gamma}, \quad U = \left(\frac{\partial M}{\partial Q} \right)_{S,L,\gamma}, \quad \mathcal{L} = \left(\frac{\partial M}{\partial L} \right)_{S,Q,\gamma}, \quad \mathcal{A} = \left(\frac{\partial M}{\partial \gamma} \right)_{S,L,Q}. \quad (65)$$

The above findings can otherwise be expressed as a function of the variation in parameter space of the condition identified by $F(r_h, M, Q, L, \gamma)$ as

$$\begin{aligned} 0 &= dF(r_h, M, Q, L, \gamma) \\ &= \frac{\partial F}{\partial r_h} dr_h + \frac{\partial F}{\partial M} dM + \frac{\partial F}{\partial Q} dQ + \frac{\partial F}{\partial L} dL + \frac{\partial F}{\partial \gamma} d\gamma, \end{aligned} \quad (66)$$

which can be recast into another term for dM , whichever gives the following:

$$\begin{aligned} dM &= \left(\frac{1}{4\pi} \frac{\partial F}{\partial r_h} \right) \left(-\frac{1}{4\pi} \frac{\partial F}{\partial M} \right)^{-1} dr_h + \left(-\frac{\partial F}{\partial M} \right)^{-1} \left(\frac{\partial F}{\partial Q} \right) dQ \\ &+ \left(-\frac{\partial F}{\partial M} \right)^{-1} \left(\frac{\partial F}{\partial L} \right) dL + \left(-\frac{\partial F}{\partial M} \right)^{-1} \left(\frac{\partial F}{\partial \gamma} \right) d\gamma. \end{aligned} \quad (67)$$

To be more specific, Eq. (62) would be consistent with Eq. (67) which involves the presence of temperature, geometrically defined as follows

$$T = \frac{1}{4\pi} \frac{\partial F}{\partial r_h}, \quad (68)$$

and then, the entropy can be defined by

$$dS = \left(-\frac{1}{4\pi} \frac{\partial F}{\partial M} \right)^{-1} dr_h. \quad (69)$$

This can also be derived using Wald's formalism; in other words, $\delta S = \int \frac{\partial \mathcal{L}}{\partial R}$ as long as $dF = 0$ is satisfied.

Furthermore, the thermodynamic volume and the conjugate potential are defined according to the formula:

$$U = \left(\frac{\partial M}{\partial Q} \right)_{S,L,\gamma} = \left(- \frac{\partial F}{\partial M} \right)^{-1} \left(\frac{\partial F}{\partial Q} \right), \quad (70)$$

$$\mathcal{L} = \left(\frac{\partial M}{\partial L} \right)_{S,Q,\gamma} = \left(- \frac{\partial F}{\partial M} \right)^{-1} \left(\frac{\partial F}{\partial L} \right), \quad (71)$$

$$\mathcal{A} = \left(\frac{\partial M}{\partial \gamma} \right)_{S,Q,L} = \left(- \frac{\partial F}{\partial M} \right)^{-1} \left(\frac{\partial F}{\partial \gamma} \right). \quad (72)$$

As far as the black hole system is concerned, the enthalpy is represented by the total mass of the system. Depending on the parameters of the black hole system and in the extended phase space environment, the thermodynamic volume, electric potential, and \mathcal{A} can be expressed as follows:

$$U = \left(\frac{\partial M}{\partial Q} \right)_{S,L,\gamma} = \frac{2\pi^{-\frac{D+3}{2}} \Gamma(\frac{D-1}{2})}{r_h^{-3+D}} Q, \quad (73)$$

$$\mathcal{L} = \left(\frac{\partial M}{\partial L} \right)_{S,Q,\gamma} = -\frac{r_h^{D-1}}{L^3}, \quad (74)$$

$$\mathcal{A} = \left(\frac{\partial M}{\partial \xi} \right)_{S,Q,L} = \frac{nr_h^{D-1} \left(\gamma + \xi^2 r_h^{\frac{D-1}{n}} \right)^{-n}}{\gamma(D-2)(D-1)}, \quad (75)$$

and the Hawking temperature is found to be in the extended phase space as follows:

$$T = \left(\frac{\partial M}{\partial S} \right)_{P,Q} = \frac{1}{4\pi r_h} \left\{ r_h^2 \left(-\frac{2 \left(\gamma + Q^2 r_h^{\frac{D-1}{n}} \right)^{-n}}{D-2} - \frac{1}{L^2} \right) + \frac{r_h^2 D}{L^2} \right. \\ \left. - 4(D-3)\pi^{3-D} Q^2 r_h^{6-2D} \Gamma \left(\frac{D-1}{2} \right)^2 + D-3 \right\}. \quad (76)$$

Inspecting the related Smarr relation is useful. For that reason, the application of Euler's theorem [94, 95] can provide the dimensional analysis for the implication of the polytropic structure such that $[M] = (D-3)$, $[L] = 1$, $[S] = (D-2)$, $[Q] = (D-3)$, $[\gamma] = 2/n$ and $[\xi] = -(D-3)/2n$. We find

$$(D-3)M = (D-2)TS + \mathcal{L}L + (D-3)UQ + \frac{2}{n}\mathcal{A}\gamma. \quad (77)$$

It is worth mentioning that for a particular case of the parameter n , the Smarr formula relation brings to a reduced one, such that for $n = 1$,

$$(D-3)M = (D-2)TS + \mathcal{L}L + (D-3)UQ + 2\mathcal{A}\gamma, \quad (78)$$

and for $n = 2$, one has

$$(D-3)M = (D-2)TS + \mathcal{L}L + (D-3)UQ + \mathcal{A}\gamma, \quad (79)$$

where all the thermodynamic variables emerge. These quantities in the classical limit where ($Q = 0$ & $\xi = 0$) are consistent with the corresponding quantities for the AdS Schwarzschild BH [96].

Barrow introduced a fractal shape for the BH horizon, which enhances its surface area. According to Barrow's modifications, the modified entropy relation is represented by [40–44]

$$S = \left(\frac{A}{A_0} \right)^{1+\frac{\Delta}{2}}. \quad (80)$$

So, the next stage consists of drawing up a thermodynamic structure based on Barrow entropy. We might begin by identifying the link between the horizon radius and Barrow entropy by means of S_{BH} as

$$S = \left(\frac{\omega_{D-2}}{4} r_h^{D-2} \right)^{1+\frac{\Delta}{2}}, \quad (81)$$

where a reciprocal link can be illustrated in terms of the horizon radius as

$$r_h = \left(\frac{4}{\omega_{D-2} S^{\frac{2}{1+\Delta}}} \right)^{\frac{1}{D-2}}. \quad (82)$$

V. THERMODYNAMIC TOPOLOGY

Recent developments in the study of black hole thermodynamics have highlighted the significance of thermodynamic topology as a tool for exploring the complex phase structure of black holes. Initially, topological methods were applied to investigate phenomena such as light rings and time-like circular orbits in black hole spacetimes [97–106]. The application of topological techniques in black hole thermodynamics was first introduced in [107], drawing inspiration from the earlier work of Duan [108, 109] in relativistic particle systems. This approach revolves around the concept of topological defects represented by zero points of a vector field, which correspond to the critical points of the system. These zero points serve as indicators of phase transitions and can be classified by their winding numbers, offering a way to categorize black hole systems into distinct topological classes based on shared thermodynamic properties.

In particular, the classification into different topological classes is determined by the structure and nature of these critical points. This methodology has been widely employed in various black hole models across the literature [110–131].

In this paper, we utilize the topological framework discussed in [132], which is particularly well-suited for studying black hole thermodynamics. By adopting the off-shell free energy method, black holes are treated as topological defects within their thermodynamic structure. This method provides insights into both the local and global topological aspects of black holes, using winding numbers to describe their topological charge and stability. Crucially, the stability of a black hole can be inferred from the sign of its winding number, underscoring the connection between thermodynamic topology and black hole stability. This method has been successfully applied to numerous black hole systems in a variety of gravitational frameworks [133–171].

The general form of generalized off-shell free energy was introduced in [132, 172], defined as:

$$\mathcal{F} = E - \frac{S}{\tau}, \quad (83)$$

where E refers to the black hole's energy (or mass M), and S denotes its entropy. The variable τ represents a varying time scale, which can be interpreted as the inverse of the equilibrium temperature at the shell surrounding the black hole. Using this generalized free energy, a vector field ϕ is formulated as [132]:

$$\phi = (\phi^r, \phi^\Theta) = \left(\frac{\partial \mathcal{F}}{\partial S}, -\cot \Theta \csc \Theta \right). \quad (84)$$

The zero points of this vector field are essential, since they denote the critical points of the black hole solutions. Specifically, these zero points are located at $(\tau, \Theta) = \left(\frac{1}{T}, \frac{\pi}{2} \right)$, where T is the black hole's equilibrium temperature within the surrounding cavity. Each of these defects, or zero points, carries a topological charge, which can be calculated using Duan's ϕ -mapping method. To determine this charge, the unit vector n is derived from the field ϕ . The unit vector n^a must satisfy the following conditions:

$$n^a n^a = 1 \quad \text{and} \quad n^a \partial_\nu n^a = 0. \quad (85)$$

A topological current j^μ can then be defined in the coordinate space $x^\nu = \{t, S, \Theta\}$ as:

$$j^\mu = \frac{1}{2\pi} \epsilon^{\mu\nu\rho} \epsilon_{ab} \partial_\nu n^a \partial_\rho n^b, \quad (86)$$

where $\epsilon^{\mu\nu\rho}$ is the Levi-Civita symbol, and $\partial_\nu = \frac{\partial}{\partial x^\nu}$. This current is conserved, implying:

$$\partial_\mu j^\mu = 0. \quad (87)$$

The current j^μ can be re-expressed in terms of the topological density as:

$$j^\mu = \delta^2(\phi) J^\mu \left(\frac{\phi}{x} \right), \quad (88)$$

where J^μ relates to the Jacobi tensor $\epsilon^{ab} J^\mu \left(\frac{\phi}{x} \right) = \epsilon^{\mu\nu\rho} \partial_\nu \phi^a \partial_\rho \phi^b$. Utilizing the Laplacian Green function $\Delta_{\phi^a} \ln \|\phi\| = 2\pi \delta^2(\phi)$, the previous expression is derived.

The topological charge W is determined by integrating the zeroth component of the current density:

$$W = \int_{\Sigma} j^0 d^2x = \sum_{i=1}^N w_i, \quad (89)$$

where w_i represents the winding number associated with each zero point of the vector field ϕ , and Σ denotes the region over which the winding numbers are calculated. The contours used to define this region are constructed as:

$$\begin{cases} S = S_1 \cos \nu + S_0, \\ \Theta = S_2 \sin \nu + \frac{\pi}{2}, \end{cases} \quad (90)$$

where $\nu \in (0, 2\pi)$, and S_1, S_2 determine the size of the contour, while S_0 marks its center. The relationship between the winding number and the deflection angle Ω is given by:

$$w = \frac{\Omega(2\pi)}{2\pi}, \quad (91)$$

where Ω is computed as:

$$\Omega(v) = \int_0^v \epsilon_{12} n^1 \partial_v n^2 dv. \quad (92)$$

The sum of all winding numbers provides the total topological charge:

$$W = \sum_i w_i. \quad (93)$$

This topological charge W characterizes the structural features of black hole solutions within the framework of thermodynamic topology. Importantly, j^l is nonzero only at the zero points of the vector field ϕ ; if no such points exist in the parameter space, the total topological charge remains zero. In this section, we will conduct an in-depth investigation of the thermodynamic topology of these black holes within the Barrow entropy framework, with a focus on both 4-dimensional and 5-dimensional solutions. Our study will consider two distinct ensembles: the canonical ensemble and the grand canonical ensemble. We will begin with the analysis of 5-dimensional black holes.

VI. THERMODYNAMICS OF $D = 5$ CHARGED ADS BLACK HOLES IMMERSSED IN POLYTROPIC DARK ENERGY

Before starting our analysis, we would like to draw attention towards an important assumption. The integration constant q is related to charge Q as:

$$Q = \frac{q}{4\pi} \omega_{D-2}.$$

From the area law of entropy in eq. (58), we draw the expression of ω_{D-2} as

$$\omega_{D-2} = \frac{4S_{BH}}{r_h^{d-2}}.$$

Again, the general form of entropy for D -dimensional black holes is given by

$$S_{BH} = \int \frac{dM}{T} = \frac{2\pi r^{D-2}}{D-2}. \quad (94)$$

Using Eq. (94), we can establish a relation between integration q and charge Q as,

$$Q = \frac{2q}{D-2},$$

hence Q can be considered equivalent to q as both are mere constants. So, throughout the topological analysis, we will consider q as charge.

We start with evaluating mass of the 5D black holes by solving the equation $F(r = r_h) = 0$, which comes out to be

$$M = \frac{1}{2} r_h^2 \left(r_h^2 \left(\frac{1}{L^2} - \frac{1}{6} \gamma^{-n} {}_2F_1 \left(n, n; n+1; -\frac{\xi^2 r_h^{4/n}}{\gamma} \right) \right) + \frac{q^2}{r_h^4} + 1 \right). \quad (95)$$

The temperature of these black holes is evaluated to be

$$T = \frac{r_h^6 \left(\frac{6}{L^2} - \gamma^{-n} \left(\frac{\xi^2 r_h^{4/n}}{\gamma} + 1 \right)^{-n} \right) + 3r_h^4 - 3q^2}{6\pi r_h^5}, \quad (96)$$

for $D = 5$ we found $S_{BH} = \frac{2\pi r^3}{3}$. The black hole mass in terms of black hole entropy S_{BH} is calculated as

$$M = - \frac{\sqrt[3]{\frac{3}{2}} S_{BH}^{4/3} \gamma^{-n} {}_2F_1 \left(n, n; n+1; -\frac{\left(\frac{3}{2\pi}\right)^{\frac{4}{3n}} \xi^2 S_{BH}^{\frac{4}{3n}}}{\gamma} \right)}{8\pi^{4/3}} + \frac{3\sqrt[3]{\frac{3}{2}} S_{BH}^{4/3}}{4\pi^{4/3} L^2} + \frac{\pi^{2/3} q^2}{\sqrt[3]{2} 3^{2/3} S_{BH}^{2/3}} + \frac{1}{2} \left(\frac{3}{2\pi} \right)^{2/3} S_{BH}^{2/3}. \quad (97)$$

The relation between GB entropy, S_{BH} and Barrow entropy S is given by

$$S_{BH} = S^{\frac{2}{\Delta+2}}.$$

Replacing the entropy S_{BH} by Barrow entropy S in the expression for mass will give us the new mass as :

$$M = - \frac{\sqrt[3]{\frac{3}{2}} \gamma^{-n} \left(S^{\frac{2}{\Delta+2}} \right)^{4/3} {}_2F_1 \left(n, n; n+1; -\frac{\left(\frac{3}{2\pi}\right)^{\frac{4}{3n}} \left(S^{\frac{2}{\Delta+2}} \right)^{\frac{4}{3n}} \xi^2}{\gamma} \right)}{8\pi^{4/3}} + \frac{3\sqrt[3]{\frac{3}{2}} \left(S^{\frac{2}{\Delta+2}} \right)^{4/3}}{4\pi^{4/3} L^2} + \frac{\left(\frac{\pi}{3}\right)^{2/3} q^2}{\sqrt[3]{2} \left(S^{\frac{2}{\Delta+2}} \right)^{2/3}} + \frac{1}{2} \left(\frac{3}{2\pi} \right)^{2/3} \left(S^{\frac{2}{\Delta+2}} \right)^{2/3}. \quad (98)$$

At $\Delta = 0$, the expression of mass becomes equivalent to the mass in GB statistics written in Eq. (97). The temperature is now calculated again for Barrow entropy as

$$T = - \frac{\gamma^{-n} S^{\frac{2}{\Delta+2}-1} \sqrt[3]{S^{\frac{2}{\Delta+2}}} \left(\frac{\left(\frac{3}{2\pi}\right)^{\frac{4}{3n}} \xi^2 \left(S^{\frac{2}{\Delta+2}} \right)^{\frac{4}{3n}}}{\gamma} + 1 \right)^{-n}}{\sqrt[3]{2} 3^{2/3} \pi^{4/3} (\Delta+2)} - \frac{2 \left(\frac{2\pi}{3} \right)^{2/3} q^2 S^{-\frac{2}{\Delta+2}-1} \sqrt[3]{S^{\frac{2}{\Delta+2}}}}{3(\Delta+2)} + \frac{\sqrt[3]{\frac{3}{2}} \left(S^{\frac{2}{\Delta+2}} \right)^{2/3}}{\pi^{2/3} (\Delta+2) S} + \frac{2^{2/3} \sqrt[3]{3} S^{\frac{2}{\Delta+2}-1} \sqrt[3]{S^{\frac{2}{\Delta+2}}}}{\pi^{4/3} (\Delta+2) L^2}. \quad (99)$$

The influence of the parameter Δ on black hole mass and temperature becomes more significant at higher values of Barrow entropy S . Figure 4a shows the black hole mass in the context of Barrow entropy for different values of Δ , with the parameters fixed at $q = 0.2$, $\gamma = 0.0095$, $\xi = 1$, and $L = 0.1$. Figure 4b displays the temperature T as a function of entropy S , illustrating small-to-large black hole phase transitions. For larger values of Δ , two distinct black hole phases are evident in the figure. The solid black line indicates that no phase transition occurs in GB statistics for the

same set of thermodynamic parameters. Figure 4c offers a detailed view of the phase transition phenomena in the free energy vs. entropy plot, where two distinct phases are clearly visible for higher values of Δ , while no phase transition occurs for values of Δ near zero. In Figure 4d, the same behaviour is depicted in the heat capacity C_q vs. entropy S plot. For larger values of Δ , two black hole branches are observed: the small black hole branch is stable, while the large black hole branch is unstable. For values $\Delta = 0$ or near zero, either three black hole branches or a single branch exist, depending on the values of L and q . The variation of the black hole branches with L and q is shown in Figs. 4e and 4f, respectively.

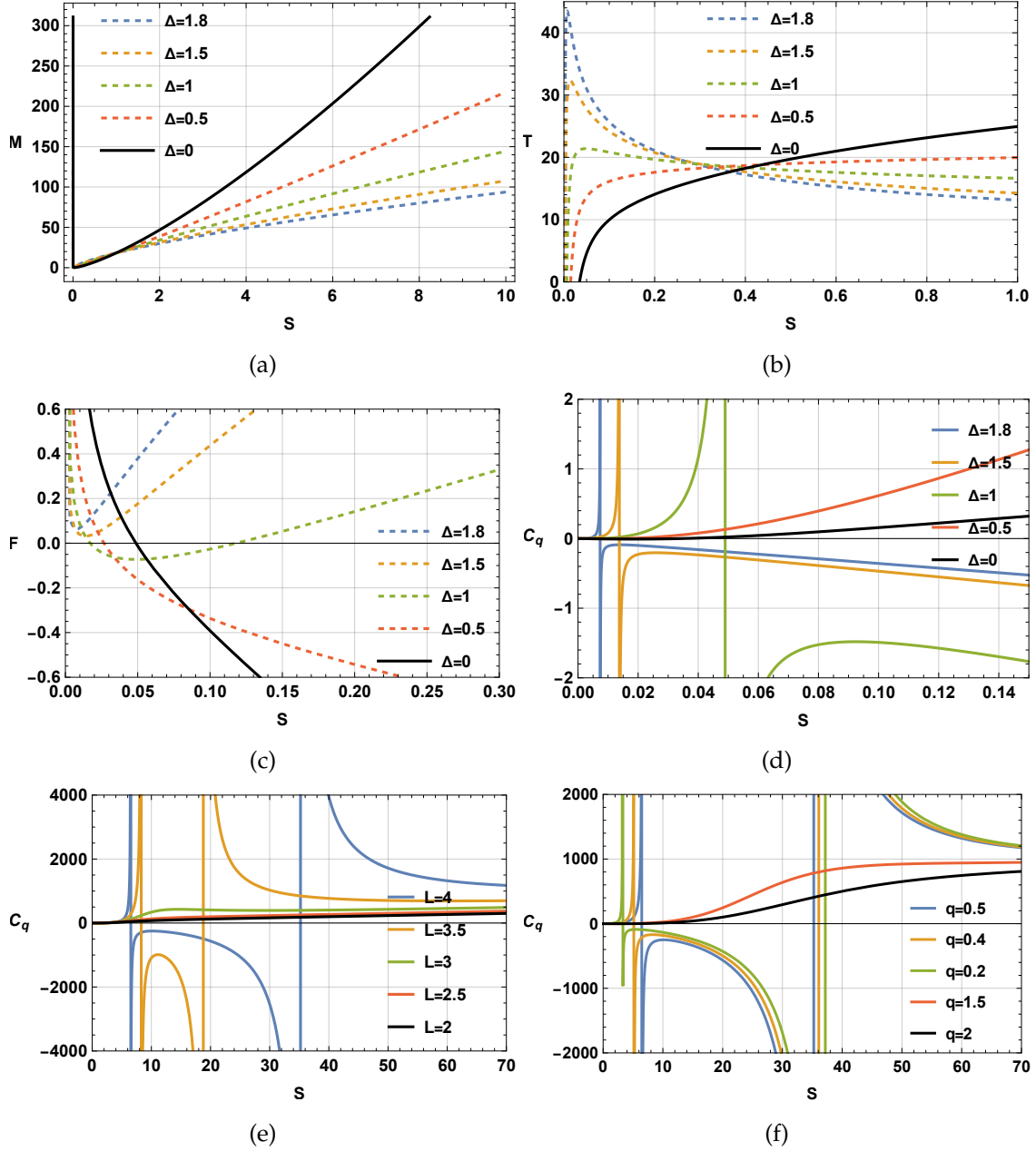


FIG. 4: Thermodynamic property of $D = 5$ dimensional charged AdS black holes immersed in polytropic dark energy in the framework of Barrow entropy

In Figure 4e, with $\Delta = 0$, $q = 0.5$, $\gamma = 0.0095$, and $\xi = 1$ fixed, we observe that when three black hole branches exist, the small branch is stable, the intermediate branch is unstable, and the large branch is stable. Conversely, when only a single branch exists, it is found to be stable. Figure 4f illustrates the variation of black hole branches with q , while keeping $\Delta = 0, L = 4$, $\gamma = 0.0095$, and $\xi = 1$ fixed.

Next, we discuss the thermodynamic properties of these black holes in the grand canonical ensemble, where the potential ϕ is kept fixed instead of its conjugate parameter q . ϕ can be calculated as :

$$\phi = \frac{\partial M}{\partial q} = \frac{\left(\frac{2\pi}{3}\right)^{2/3} q}{\left(S^{\frac{2}{\Delta+2}}\right)^{2/3}}, \quad (100)$$

solving Eq. (100), we can obtain expression of q in terms of ϕ . Next q is substituted in the equation given below and the grand canonical mass M_G is obtained

$$M_G = M - q\phi = \left(\frac{3}{2\pi}\right)^{2/3} \left(S^{\frac{2}{\Delta+2}}\right)^{2/3} - \frac{\sqrt[3]{\frac{3}{2}}\gamma^{-n} \left(S^{\frac{2}{\Delta+2}}\right)^{4/3} {}_2F_1\left(n, n; n+1; -\frac{\left(\frac{3}{2\pi}\right)^{\frac{4}{3n}} \left(S^{\frac{2}{\Delta+2}}\right)^{\frac{4}{3n}} \xi^2}{\gamma}\right)}{8\pi^{4/3}} + \frac{3\sqrt[3]{\frac{3}{2}} \left(S^{\frac{2}{\Delta+2}}\right)^{4/3}}{4\pi^{4/3}L^2} - \left(\frac{3}{2\pi}\right)^{2/3} \phi^2 \left(S^{\frac{2}{\Delta+2}}\right)^{2/3}. \quad (101)$$

Similarly, the expression for temperature in the grand canonical ensemble is obtained as :

$$T_G = \frac{2^{2/3} \sqrt[3]{3} S^{-\frac{\Delta}{\Delta+2}} \sqrt[3]{S^{\frac{2}{\Delta+2}}}}{\pi^{4/3}(\Delta+2)L^2} + \frac{2\sqrt[3]{\frac{2}{3}} S^{-\frac{\Delta}{\Delta+2} - \frac{2}{\Delta+2}} \left(S^{\frac{2}{\Delta+2}}\right)^{2/3}}{\pi^{2/3}(\Delta+2)} - \frac{\gamma^{-n} S^{-\frac{\Delta}{\Delta+2}} \sqrt[3]{S^{\frac{2}{\Delta+2}} \left(\frac{\left(\frac{3}{2\pi}\right)^{\frac{4}{3n}} \xi^2 \left(S^{\frac{2}{\Delta+2}}\right)^{\frac{4}{3n}}}{\gamma} + 1\right)^{-n}}}{\sqrt[3]{2} 3^{2/3} \pi^{4/3}(\Delta+2)} - \frac{2\sqrt[3]{\frac{2}{3}} \phi^2 S^{-\frac{\Delta}{\Delta+2} - \frac{2}{\Delta+2}} \left(S^{\frac{2}{\Delta+2}}\right)^{2/3}}{\pi^{2/3}(\Delta+2)}. \quad (102)$$

In the T_G vs S graph (Fig. 5a), we observe that the system exhibits either one or two branches for different values of Δ , with parameters fixed at $\phi = 0.2$, $\gamma = 0.0095$, $\xi = 1$, and $L = 1$. The semi-positive nature of the temperature is found to depend on the parameter γ . Notably, we observe a Davis-type phase transition, rather than a van der Waals-like phase transition, as seen in the canonical ensemble. This observation is further supported by the F_G vs S plot in Fig. 5b.

The stability of these branches is described by the C_ϕ vs S graph in Fig. 5c. When two black hole branches are present, the small black hole branch is stable, while the large black hole branch is unstable. In cases where only a single branch is observed, its stability depends on the values of L and ϕ . To better understand the differences in stability and the dependence of these temperature-driven phase transitions on various thermodynamic parameters, a topological analysis is more appropriate. This analysis is discussed in the next section.

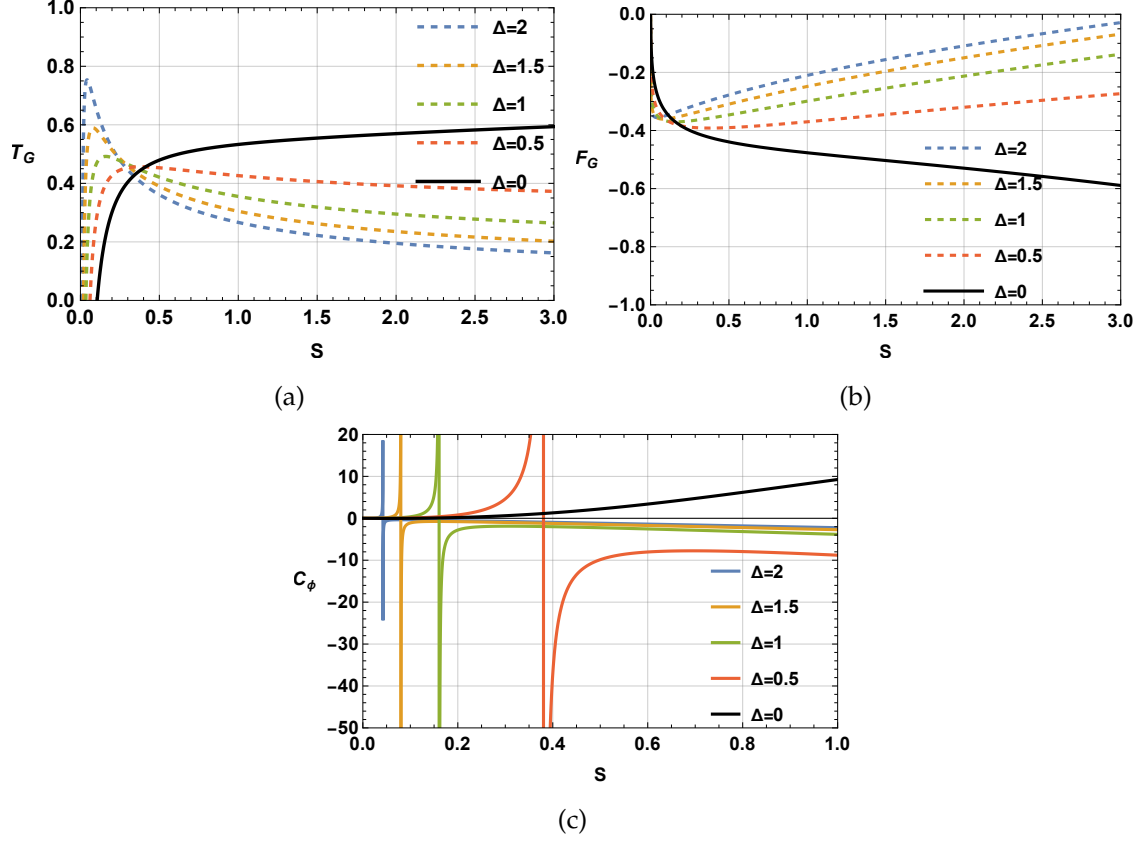


FIG. 5: Thermodynamic property of $D = 5$ dimensional charged AdS black holes in grand canonical ensemble

A. Thermodynamic Topology of 5D black holes

First we conduct our analysis in canonical ensemble. Using eqns. (83) and (98), we write the off shell free energy as :

$$\begin{aligned}
 \mathcal{F} = M - \frac{S}{\tau} = & -\frac{\sqrt[3]{\frac{3}{2}}\gamma^{-n} \left(S^{\frac{2}{\Delta+2}}\right)^{4/3}}{8\pi^{4/3}} {}_2F_1\left(n, n; n+1; -\frac{\left(\frac{3}{2\pi}\right)^{\frac{4}{3n}} \left(S^{\frac{2}{\Delta+2}}\right)^{\frac{4}{3n}} \zeta^2}{\gamma}\right) \\
 & + \frac{3\sqrt[3]{\frac{3}{2}} \left(S^{\frac{2}{\Delta+2}}\right)^{4/3}}{4\pi^{4/3}L^2} + \frac{\left(\frac{\pi}{3}\right)^{2/3} q^2}{\sqrt[3]{2} \left(S^{\frac{2}{\Delta+2}}\right)^{2/3}} + \frac{1}{2} \left(\frac{3}{2\pi}\right)^{2/3} \left(S^{\frac{2}{\Delta+2}}\right)^{2/3} - \frac{S}{\tau}. \tag{103}
 \end{aligned}$$

Using eqn. (84), components of the vector ϕ are found to be :

$$\phi^S = -\frac{1}{\tau} + \frac{2^{2/3}\sqrt[3]{3}S^{\frac{2}{\Delta+2}-1}\sqrt[3]{S^{\frac{2}{\Delta+2}}}}{\pi^{4/3}(\Delta+2)L^2} - \frac{\gamma^{-n}S^{\frac{2}{\Delta+2}-1}\sqrt[3]{S^{\frac{2}{\Delta+2}}}\left(\frac{\left(\frac{3}{2\pi}\right)^{\frac{4}{3n}}\zeta^2\left(S^{\frac{2}{\Delta+2}}\right)^{\frac{4}{3n}}}{\gamma} + 1\right)^{-n}}{\sqrt[3]{23}2^{2/3}\pi^{4/3}(\Delta+2)}$$

$$-\frac{2\left(\frac{2\pi}{3}\right)^{2/3}q^2S^{-\frac{2}{\Delta+2}-1}\sqrt[3]{S^{\frac{2}{\Delta+2}}}}{3(\Delta+2)}+\frac{\sqrt[3]{\frac{2}{3}}\left(S^{\frac{2}{\Delta+2}}\right)^{2/3}}{\pi^{2/3}(\Delta+2)S'}, \quad (104)$$

and

$$\phi^\Theta = -\cot\Theta \csc\Theta. \quad (105)$$

Subsequently, we identify the zero points or singularities of the vector field. One zero point of the vector field consistently occurs at $\Theta = \frac{\pi}{2}$ as a result of the careful selection of the Θ -component of the field. To determine the additional zero points, we get an equation for τ via solving $\phi^S = 0$, which is formulated as:

$$\tau = \frac{\alpha}{\beta}, \quad (106)$$

where

$$\alpha = 3 \cdot 6^{2/3} \pi^{4/3} (\Delta + 2) L^2 S \gamma^n \left(S^{\frac{2}{\Delta+2}} \right)^{2/3} \left(\frac{\left(\frac{3}{2\pi} \right)^{\frac{4}{3n}} \zeta^2 \left(S^{\frac{2}{\Delta+2}} \right)^{\frac{4}{3n}}}{\gamma} + 1 \right)^n \quad (107)$$

and

$$\begin{aligned} \beta = & L^2 \left(2\pi^{2/3} \gamma^n \left(3\sqrt[3]{3} \left(S^{\frac{2}{\Delta+2}} \right)^{4/3} - 2\sqrt[3]{2} \pi^{4/3} q^2 \right) \left(\frac{\left(\frac{3}{2\pi} \right)^{\frac{4}{3n}} \zeta^2 \left(S^{\frac{2}{\Delta+2}} \right)^{\frac{4}{3n}}}{\gamma} + 1 \right)^n - 3\sqrt[3]{2} S^{\frac{4}{\Delta+2}} \right) \\ & + 18\sqrt[3]{2} \gamma^n S^{\frac{4}{\Delta+2}} \left(\frac{\left(\frac{3}{2\pi} \right)^{\frac{4}{3n}} \zeta^2 \left(S^{\frac{2}{\Delta+2}} \right)^{\frac{4}{3n}}}{\gamma} + 1 \right)^n. \end{aligned} \quad (108)$$

By plotting the defect curve in Fig. 6, we observe three distinct behaviours depending on the values of the thermodynamic parameters. To determine the topological class in the canonical ensemble, we analyze each pattern and calculate the corresponding topological charge. Fig. 6a illustrates the variation of the defect curve with different values of Δ , while keeping $q = 0.2$, $\gamma = 0.0095$, $\zeta = 1$, and $L = 1$ fixed. The solid black line represents the behaviour in the case of GB statistics. For higher values of Δ , two black hole branches are present, while for values of Δ near zero, we observe only a single branch for the same set of thermodynamic parameters. Next, we examine the effect of varying the parameters L, q and γ on the defect curve. The impact is not significant for larger Δ values; however, when Δ is fixed at lower values, the phase transition behavior changes noticeably. Fig. 6b and Fig. 6c demonstrate the effects of varying L and q , respectively. It is clear that as the values of L and q change, the number of black hole branches transitions from one to three. Similar observations were made when we vary the γ parameter.

In Barrow entropy framework, when considering the parameters $q = 0.2$, $\gamma = 0.0095$, $\zeta = 1$, $\Delta = 1$, and $L = 1$, two black hole branches are observed, as shown in Fig. 7a. The black solid line represents the smaller black hole branch ($S < 0.95862$), while the red solid line represents the larger black hole branch ($S > 0.95862$). The winding number calculation is illustrated in Fig.

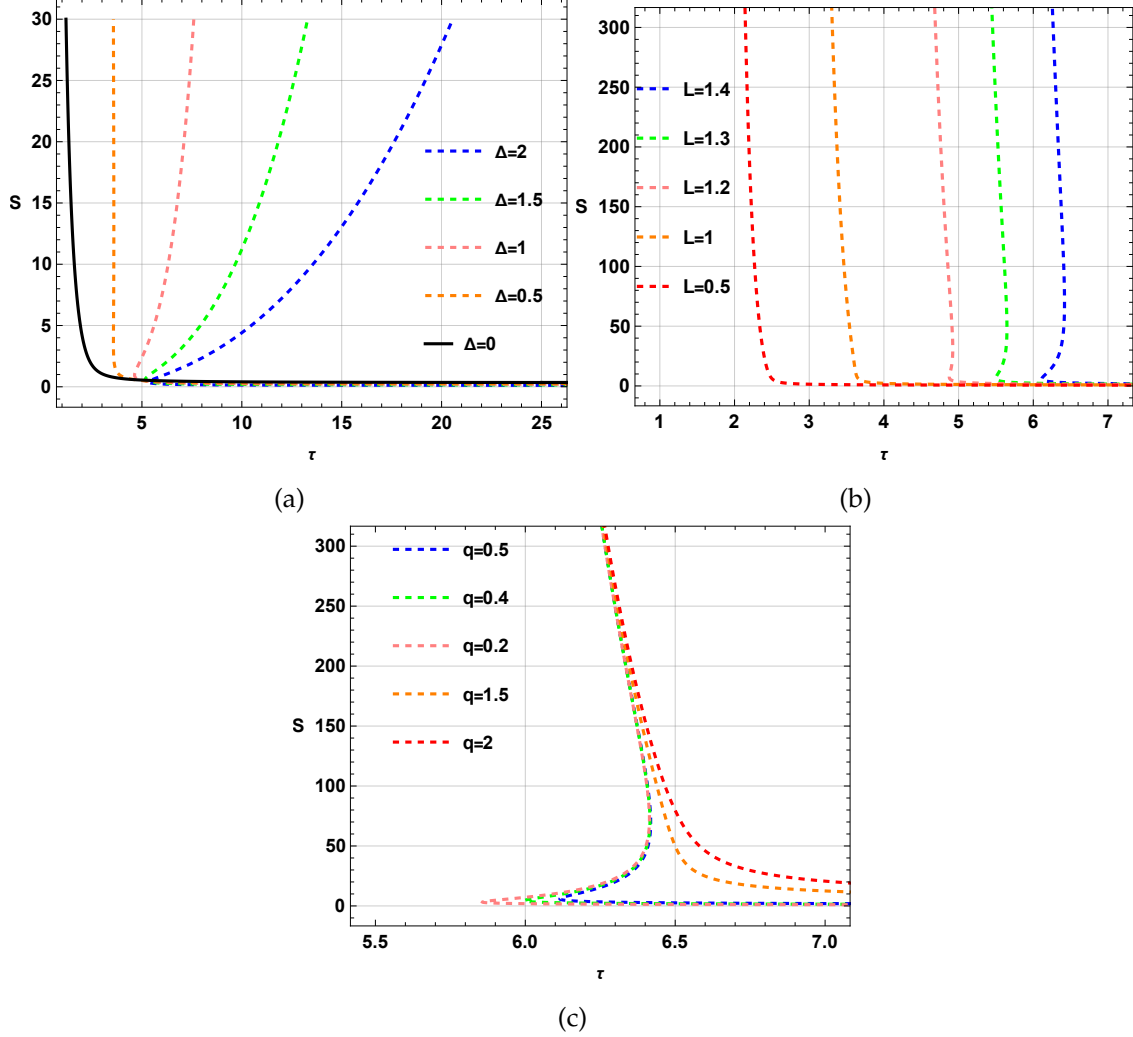


FIG. 6: Variation of defect curve of $D = 5$ dimensional charged AdS black holes in canonical ensemble

7d, where we focus on the zero points for $\tau = 4.8$. Two zero points are identified at $S = 0.613272$ and $S = 1.71772$, corresponding to the smaller black hole (SBH) and the larger black hole (LBH), respectively. Figs. 7b and 7c display the vector plots of the normalized vector field, with the zero points located at $\theta = \pi/2$. The winding number for the SBH is calculated as $+1$, indicating its stability, while the LBH has a winding number of -1 , signifying instability. The overall topological charge is determined by summing the winding numbers, resulting in a total topological charge of $-1 + 1 = 0$ for this particular defect curve. The point at which phase transition occurs, i.e $S = 0.95862$ the point is identified to be annihilation point as the stable phase ends here and an unstable phase starts.

Now we move to GB statistics framework where we consider small value of Δ . Considering the parameters $q = 0.5$, $\gamma = 0.0095$, $\zeta = 1$, $\Delta = 0.5$, and $L = 4$, we observe the presence of three distinct black hole branches, as depicted in Fig. 8. The black solid line represents the smaller black hole branch (SBH), the blue dashed line corresponds to the intermediate black hole branch

(IBH), and the red solid line represents the larger black hole branch (LBH). For $\tau = 42$, three zero points are identified at $S = 1.1016$, $S = 18.5452$, and $S = 62.4727$, corresponding to the SBH, IBH, and LBH, respectively. We observe a generation point $S = 35.2148$ and an annihilation point at $S = 6.5074$. Upon varying the values of L , q , and γ , these three branches converge into a single black hole branch, exhibiting behavior similar to that observed in GB statistics. Thus, for values Δ near zero the thermodynamic topological properties of the black hole solution demonstrate a pattern consistent with that seen in GB statistics.

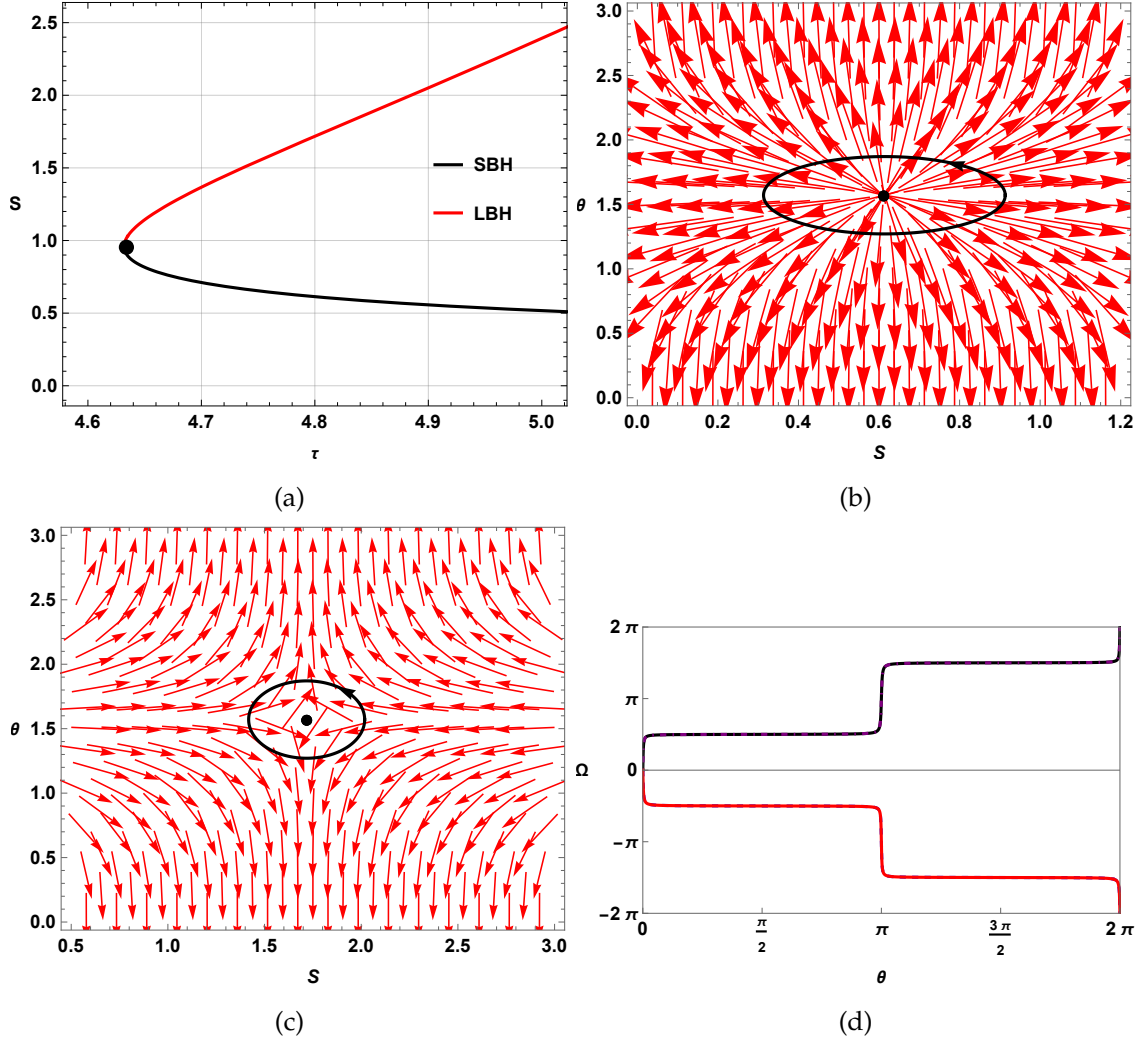


FIG. 7: Variation of defect curve of $D = 5$ dimensional charged AdS black holes in canonical ensemble

Figs. 9a, 9b, and 9c show the vector plots of the normalized vector field. The winding number for both the smaller black hole (SBH) and larger black hole (LBH) is calculated to be $+1$, indicating stability, while the intermediate black hole (IBH) has a winding number of -1 , signifying its instability. By summing the winding numbers, the total topological charge for this particular defect curve is found to be $1 - 1 + 1 = 1$. In the scenario where the three phases merge into a single black hole phase, we obtain a stable black hole branch with a topological charge of 1.

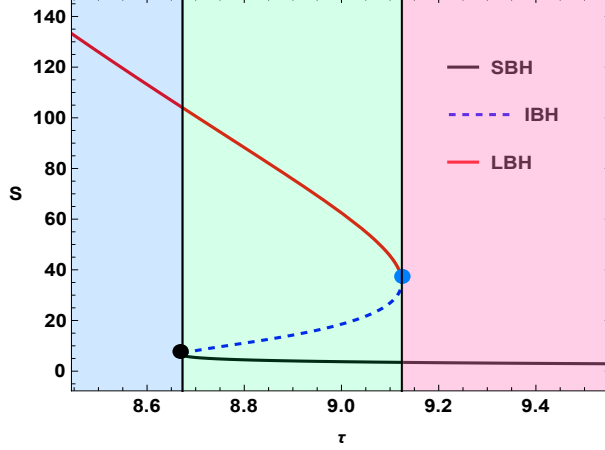


FIG. 8: Defect curve of $D = 5$ dimensional charged AdS black holes in canonical ensemble

Therefore, in the canonical ensemble, the topological charge of the black hole in GB statistics is 1. However, in the Barrow entropy framework, the topological charge can either be 1 or 0. We move our attention to grand canonical ensemble. The expression for τ in grand canonical ensemble is given by :

$$\tau_G = \frac{\mathcal{X}}{\mathcal{Y}}, \quad (109)$$

where,

$$\mathcal{X} = 6^{2/3} \pi^{4/3} (\Delta + 2) L^2 S \gamma^n \left(\frac{\left(\frac{3}{2\pi}\right)^{\frac{4}{3n}} \zeta^2 \left(S^{\frac{2}{\Delta+2}}\right)^{\frac{4}{3n}}}{\gamma} + 1 \right)^n, \quad (110)$$

and

$$\begin{aligned} \mathcal{Y} = & 6\sqrt[3]{2} \gamma^n \left(S^{\frac{2}{\Delta+2}}\right)^{4/3} \left(\frac{\left(\frac{3}{2\pi}\right)^{\frac{4}{3n}} \zeta^2 \left(S^{\frac{2}{\Delta+2}}\right)^{\frac{4}{3n}}}{\gamma} + 1 \right)^n - L^2 \left(S^{\frac{2}{\Delta+2}}\right)^{2/3} \left(4\sqrt[3]{3} \pi^{2/3} (\phi^2 - 1) \right. \\ & \left. \times \gamma^n \left(\frac{\left(\frac{3}{2\pi}\right)^{\frac{4}{3n}} \zeta^2 \left(S^{\frac{2}{\Delta+2}}\right)^{\frac{4}{3n}}}{\gamma} + 1 \right)^n + \sqrt[3]{2} \left(S^{\frac{2}{\Delta+2}}\right)^{2/3} \right). \end{aligned} \quad (111)$$

In this ensemble, three distinct topological classes are identified based on the values of Δ , L , q , and γ . To illustrate, we examine three specific scenarios where these topological classes emerge.

For the first scenario, the thermodynamic parameter values are altered to $\phi = 0.5$, $\gamma = 0.0095$, $\zeta = 1$, $\Delta = 1.5$, and $L = 1$. Here, two black hole branches are observed, as shown in Fig. 10a. The black solid line corresponds to the smaller black hole branch (SBH), while the red solid line represents the larger black hole branch (LBH). The winding number calculations, depicted in Fig. 10b, focus on the zero points for $\tau = 3$. Two zero points are identified at $S = 0.07005$ for the SBH and

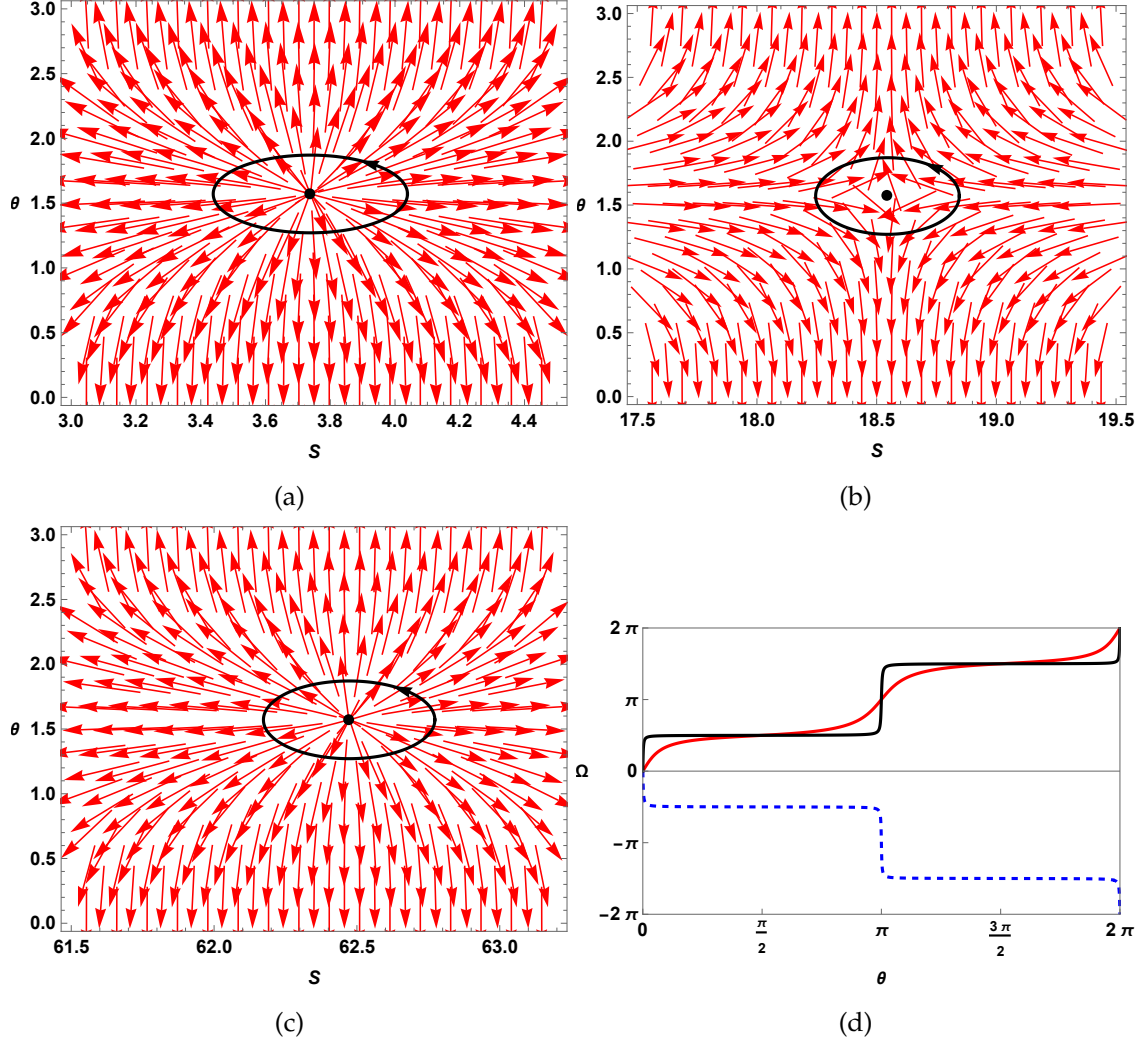


FIG. 9: Thermodynamic topology of $D = 5$ dimensional charged AdS black holes in the canonical ensemble.

$S = 0.4010$ for the LBH. The SBH exhibits a winding number of $+1$, indicating stability, whereas the LBH has a winding number of -1 , suggesting instability. The total topological charge for this defect curve is the sum of these winding numbers, yielding $-1 + 1 = 0$. Additionally, an annihilation point is observed at $S = 0.139431$ in this case. An intriguing scenario arises with parameters $\phi = 0.2$, $\gamma = 0.1$, $\xi = 1$, $\Delta = 0.5$, and $L = 1$. In this case, the local topology undergoes a significant change, with the small black holes (SBH) becoming unstable and the large black holes (LBH) gaining stability. Despite this shift in local topology, the global topology remains unchanged. The winding number calculation for $\tau = 3.26$ is illustrated in Fig. 11b, where the winding number of the SBH is found to be -1 , signifying its instability, while the LBH has a winding number of $+1$, indicating stability. A blue dot in the figure marks a generation point at $S = 81.13101$, representing the transition from an unstable to a stable phase. The overall topological class is still found to be 0.

Next, we consider $\phi = 0.5$, $\gamma = 0.01$, $\xi = 1$, $\Delta = 0.5$, and $L = 1$, we find a single black hole

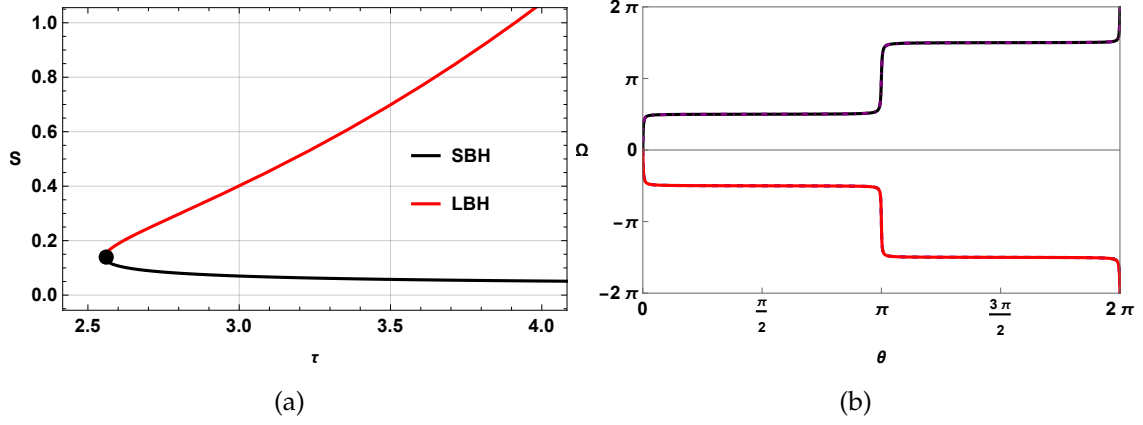


FIG. 10: Topological charge $W = 0$

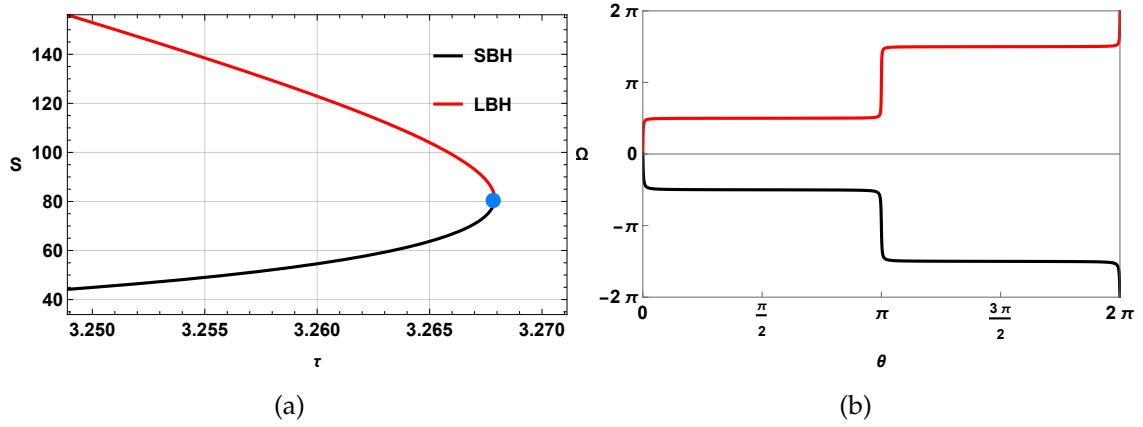


FIG. 11: Topological class $W=0$ with a generation point

branch, but now with a winding number of $+1$ as illustrated in Fig. 12a and Fig. 12b

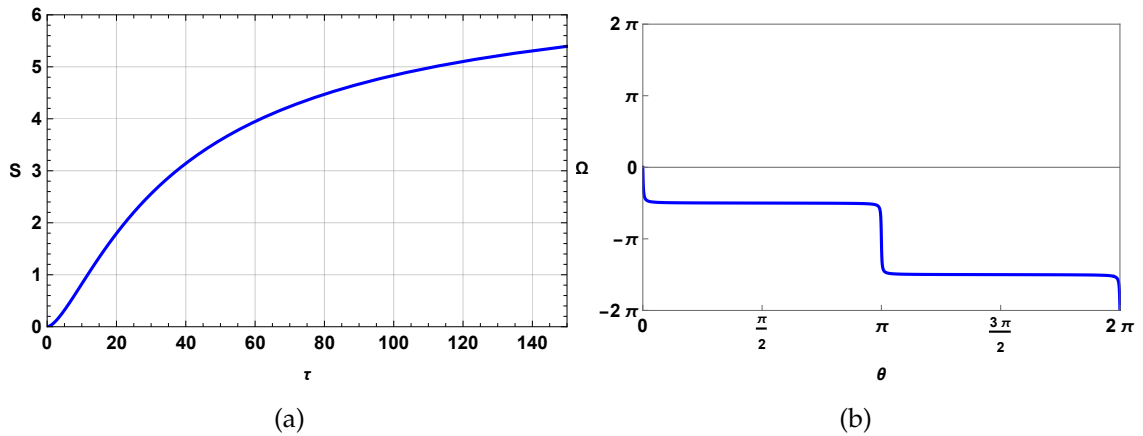


FIG. 12: Topological class $W=1$

VII. THERMODYNAMICS OF $D = 4$ CHARGED ADS BLACK HOLES

The expression for mass is obtained as :

$$M = -\frac{\gamma^{-n} \left(S^{\frac{2}{\Delta+2}}\right)^{3/2} {}_2F_1\left(n, n; n+1; -\frac{\pi^{-\frac{3}{2n}} \left(S^{\frac{2}{\Delta+2}}\right)^{\frac{3}{2n}} \xi^2}{\gamma}\right)}{6\pi^{3/2}} + \frac{\left(S^{\frac{2}{\Delta+2}}\right)^{3/2}}{2\pi^{3/2}L^2} + \frac{\sqrt{\pi}q^2}{2\sqrt{S^{\frac{2}{\Delta+2}}}} + \frac{\sqrt{S^{\frac{2}{\Delta+2}}}}{2\sqrt{\pi}}. \quad (112)$$

At $\Delta = 0$, the mass term effectively corresponds to the mass in GB statistics. The temperature is now calculated again for Barrow entropy as

$$T = \frac{dM}{dS} = \frac{3S^{\frac{2}{\Delta+2}-1}\sqrt{S^{\frac{2}{\Delta+2}}}}{2\pi^{3/2}(\Delta+2)L^2} - \frac{\gamma^{-n}S^{\frac{2}{\Delta+2}-1}\sqrt{S^{\frac{2}{\Delta+2}}}\left(\frac{\pi^{-\frac{3}{2n}}\xi^2\left(S^{\frac{2}{\Delta+2}}\right)^{\frac{3}{2n}}}{\gamma} + 1\right)^{-n}}{2\pi^{3/2}(\Delta+2)} - \frac{\sqrt{\pi}q^2S^{-\frac{2}{\Delta+2}-1}\sqrt{S^{\frac{2}{\Delta+2}}}}{2(\Delta+2)} + \frac{\sqrt{S^{\frac{2}{\Delta+2}}}}{2\sqrt{\pi}(\Delta+2)S}. \quad (113)$$

Next we calculate the heat capacity C_q and free energy at constant charge q using the formulas

$$C_q = \frac{dM}{dT} = \frac{dM}{dS} \frac{dS}{dT}, \quad (114)$$

$$F = M - TS. \quad (115)$$

The effect of Δ on the black hole properties is more evident for a higher range of values of parameter Δ and Barrow entropy S . Fig.13 shows the thermodynamic properties of the black hole in the framework of Barrow entropy where the effect of Δ is shown on each parameter while keeping $q = 0.5, \Xi = 1, \gamma = 0.095, L = 0.1$ fixed. Fig.13a, shows the plot between mass M and the Barrow entropy S . The black solid line that shows the M vs S plot, when Δ is set to zero which is the reference line for comparison between GB and Barrow entropy framework. As the parameter Δ increases from zero, the plots of M versus S begin to diverge from the solid black line. These deviations become more pronounced for larger values of Δ , indicating that the effect on the black hole mass becomes significant at lower entropy values when Δ is larger, compared to when Δ is smaller. Similarly, temperature T is plotted against S in Fig.13b. where we see two black hole phases for higher values of Δ . The black hole branch is also visible in free energy F against the Barrow entropy S . The thermal stability of the black hole branch is depicted by Fig.13d where we have plotted C_q against the Barrow entropy S . It is seen that for all values of q and L , the heat capacity is positive for small black hole branch(SBH) which means SBH branch is thermally stable and the opposite is spotted for large black hole(LBH) branch. Here it is seen that there exist Davies type phase transition as at some point, the specific heat diverges.

Next we discuss the thermodynamic properties of these black hole in grand canonical ensemble

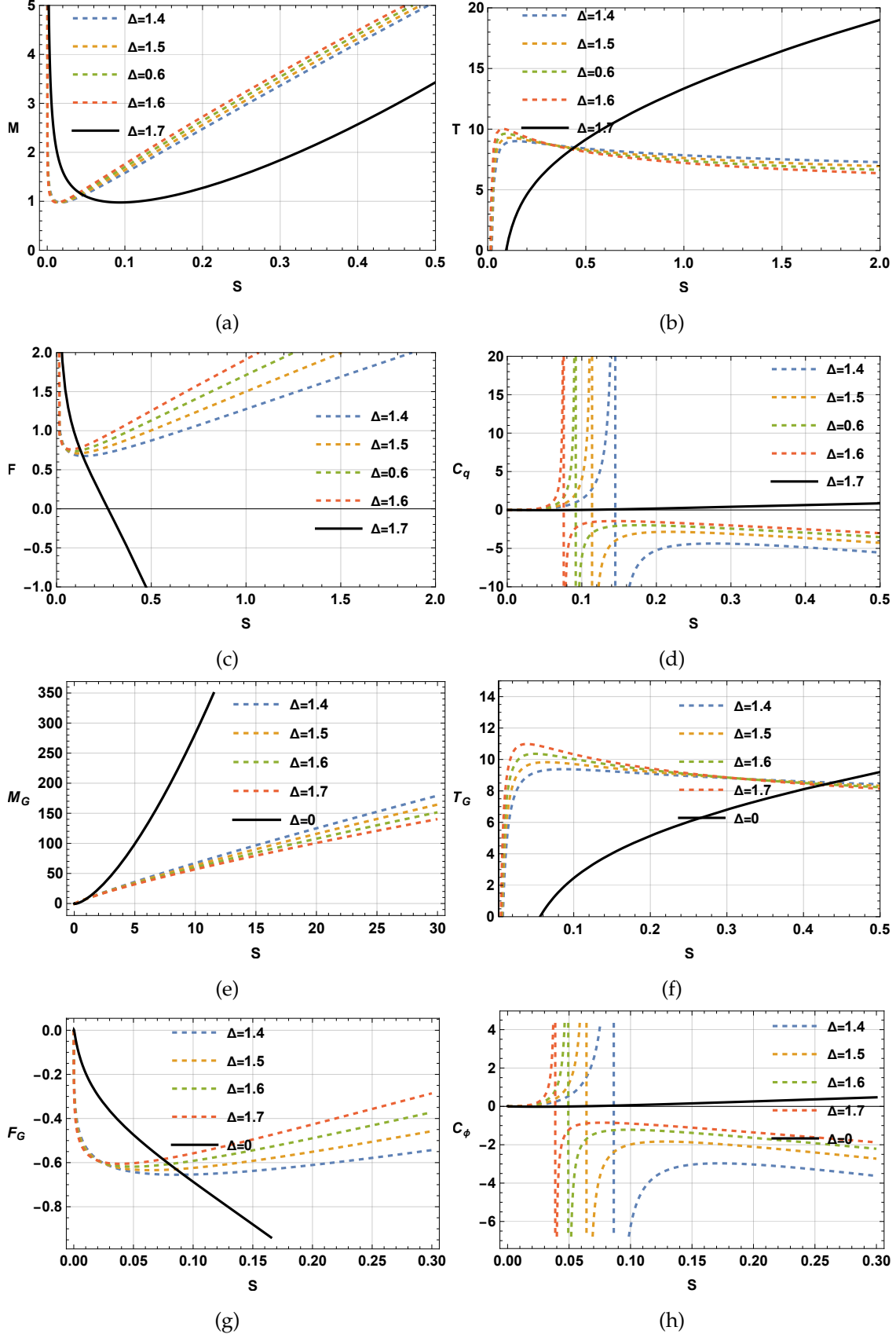


FIG. 13: Thermodynamic property of $D = 4$ dimensional charged AdS black holes immersed in polytropic dark energy in the framework of Barrow entropy

within the Barrow entropy framework, where the potential ϕ is kept fixed instead of its conjugate parameter q . ϕ can be calculated as :

$$\phi = \frac{\partial M}{\partial q} = \frac{\sqrt{\pi}q}{\sqrt{S^{\frac{2}{\Delta+2}}}}, \quad (116)$$

solving Eq. (116), we can obtain expression of q in terms of ϕ . Next q is substituted in the equation given below and the grand canonical mass M_G is obtained

$$M_G = M - q\phi$$

$$= \frac{\left(S^{\frac{2}{\Delta+2}}\right)^{3/2}}{2\pi^{3/2}L^2} - \frac{\phi^2 \sqrt{S^{\frac{2}{\Delta+2}}}}{2\sqrt{\pi}} + \frac{\sqrt{S^{\frac{2}{\Delta+2}}}}{2\sqrt{\pi}} - \frac{\gamma^{-n} \left(S^{\frac{2}{\Delta+2}}\right)^{3/2} {}_2F_1\left(n, n; n+1; -\frac{\pi^{-\frac{3}{2n}} \left(S^{\frac{2}{\Delta+2}}\right)^{\frac{3}{2n}} \zeta^2}{\gamma}\right)}{6\pi^{3/2}}, \quad (117)$$

following the same steps as explained above, the other thermodynamic quantities are obtained. It is seen that they follow the same thermodynamic behaviour as that of canonical ensemble. The grand canonical mass and temperature is plotted in Fig.13e and Fig.13f respectively while keeping $\phi = 0.5, \Xi = 1, \gamma = 0.0095, L = 0.1$ constant. The free energy and heat capacity plot in GC ensemble found to be showing similar behaviour to that in canonical ensemble which depicts that in GC ensemble also, the black hole shows Davies-type phase transition within the Barrow entropy framework.

To study the thermodynamic properties of these black holes in GB statistics, we consider smaller value of the parameter Δ . The phase transition properties are most evident in the heat capacity vs entropy curve, hence we have decided to plot only the heat capacity curve. From Fig.14a, it is evident that in canonical ensemble, these 4D black holes exhibit Van der Waals-like phase transitions within GB statistics framework depending upon the values of q and L . On the other hand, in Barrow statistics, they exhibit Davies type phase transition. For grand canonical ensemble, we do not see any phase transition in GB statistics. The Fig.14b depicts there exist only one stable black hole branch for all values of ϕ and L .

A. Thermodynamic topology of 4D black holes

The expression for τ is obtained as :

$$\tau = \frac{\mathcal{A}}{\mathcal{B}}, \quad (118)$$

where

$$\mathcal{A} = 6\pi^2(\Delta+2)L^2\gamma^n S^{\frac{2(\Delta+4)}{\Delta+2}} \left(\frac{\left(\frac{\pi}{2}\right)^{2/n} \zeta^2 \left(S^{\frac{2}{\Delta+2}}\right)^{2/n}}{\gamma} + 1 \right)^n, \quad (119)$$

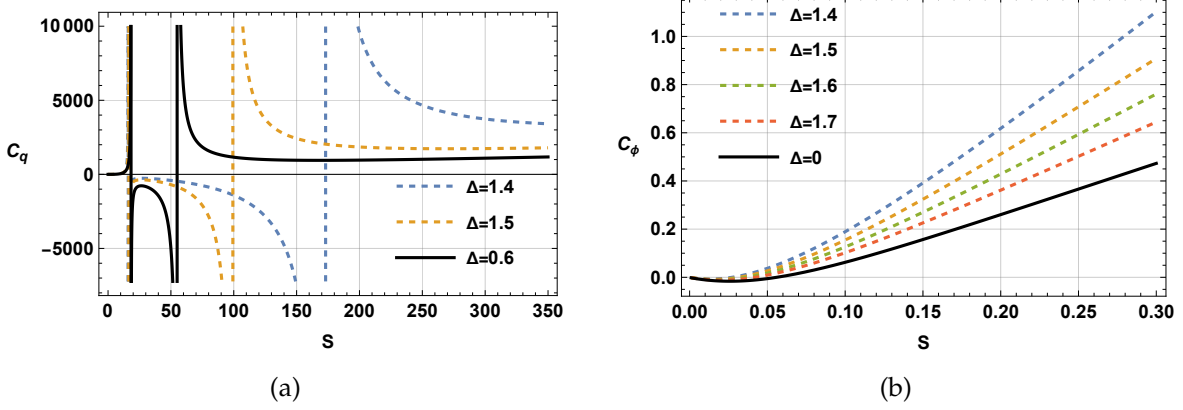


FIG. 14: Comparison of heat capacity curve in both ensemble within GB statistics framework

and

$$\mathcal{B} = 3\pi^4 \gamma^n S^{\frac{\Delta+10}{\Delta+2}} \left(\frac{\left(\frac{\pi}{2}\right)^{2/n} \zeta^2 \left(S^{\frac{2}{\Delta+2}}\right)^{2/n}}{\gamma} + 1 \right)^n - L^2 \left(\pi^4 S^{\frac{\Delta+10}{\Delta+2}} + 48q^2 S \left(\left(\frac{\pi}{2}\right)^{2/n} \zeta^2 \left(S^{\frac{2}{\Delta+2}}\right)^{2/n} + \gamma \right)^n \right). \quad (120)$$

The defect curve (τ vs S) is plotted for Barrow entropy case in Fig.15b. As it is seen from this figure that there are two branches in the defect curve for different values of Δ while we have kept $q = 0.5, L = 1, \Xi = 1, \gamma = 0.0095$ constant. Next, to calculate the topological charge, we choose any value of τ from the defect curve and draw the normalized vector plot around the selected zero point as shown in Fig.15b. From all the curves in Fig.15b we choose the purple dashed curve where $\Delta = 1.8$. For $\tau = 22$, the zero points are located at $S_0 = 3.31139$ and $S_0 = 7.47261$ represented by black dots in Fig.15b. Hence we draw the normalized vector field in the range $1 \leq S \leq 9$ with the component ϕ^S and ϕ^θ .

For the calculation of topological charge, we construct a contour around each zero point using the Eq.(90) as represents by the black contours in Fig.15b:

$$\begin{cases} S = 0.3 \cos \nu + S_0, \\ \theta = 0.3 \sin \nu + \frac{\pi}{2}. \end{cases} \quad (121)$$

We find the deflection from Eq.(92) where we solve the contour integration by simply substituting S and θ by this parametrized contour values in Eq.(121). From deflection, winding number can be calculated using Eq.(91). Fig. 15c displays the contour plots which illustrate that the value of deflection at $\theta = 2\pi$. The winding number for $S_0 = 3.31139$ is found to $+1$ as shown by the black line and that for $S_0 = 7.47261$ is calculated to be -1 illustrated by the blue line. A positive winding number implies a stable black hole branch. Hence, the SBH is stable and the LBH is unstable. Since the phase transition is taking place from winding number $+1$ to -1 , hence we identify the critical points as annihilation points,

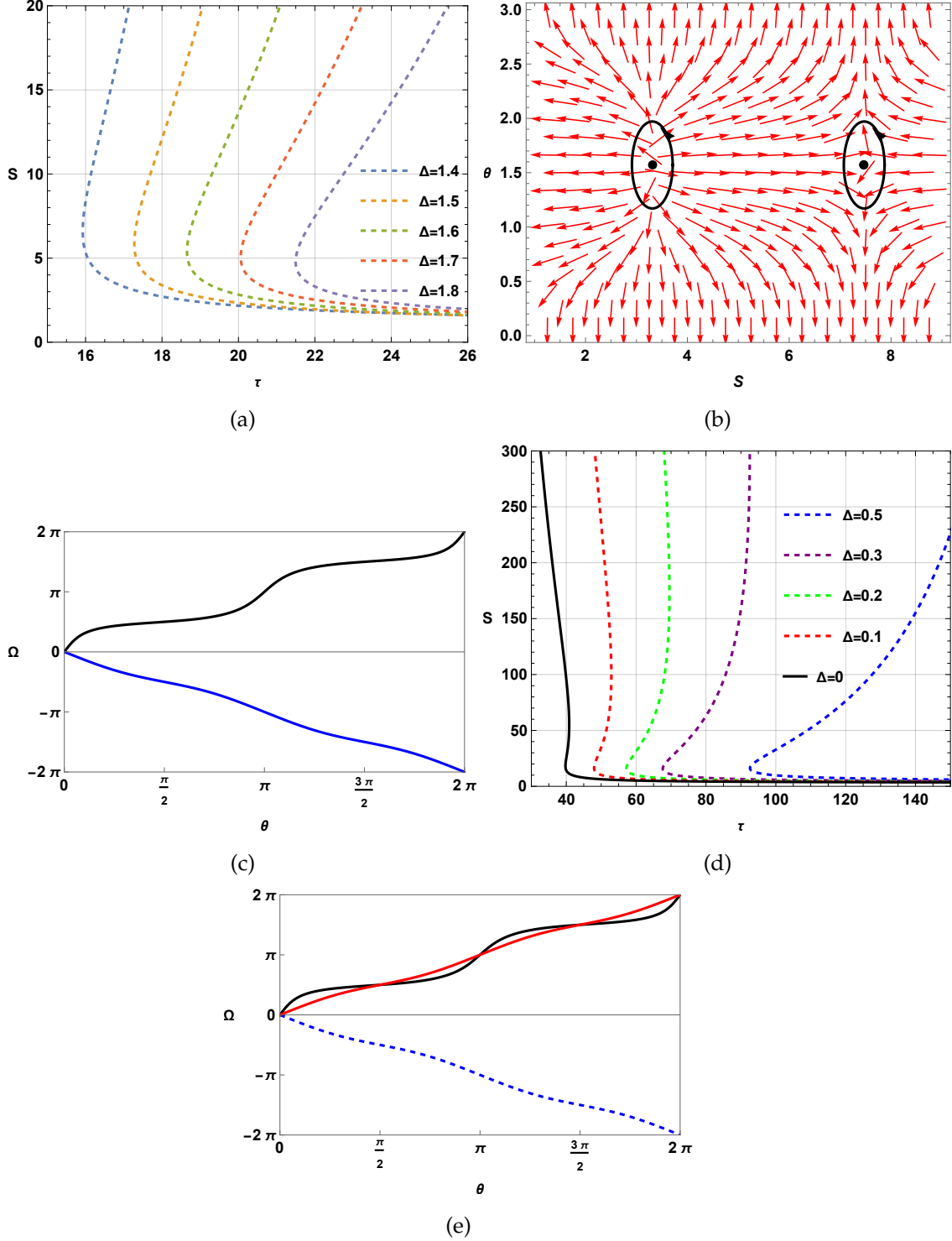


FIG. 15: Topological classes of 4D charged AdS black holes immersed in polytropic dark energy using Barrow entropy. The upper panel corresponds to topological class of black holes in canonical ensemble in Barrow entropy framework and the lower panel shows the same in GB statistics framework

Now we move on to GB statistics frame work. As it is evident in Fig.15d, the number of branch for lower value of Δ is found to be either one or three. From our previous analysis, it is well expected that the topological charge must be +1. In Fig.15e, we confirmed it by plotting the parametrized contours for $\Delta = 40, q = 0.5, L = 10, \Xi = 1, \gamma = 0.0095$ and $\tau = 40$. The black and red solid line in Fig.15e, represents the winding number calculation for SBH and LBH respectively which is found to be +1. The blue dashed line depicts the winding number for IBH which is -1. Adding all the winding number for each branches, we found topological charge of +1 as expected. Hence, 4D charged black holes in canonical ensemble immersed in polytropic dark energy within the framework of Barrow entropy has topological charge of 0 but the same is found to be +1 within GB statistics framework. The topological charge does not change with change in value of all the thermodynamic parameters apart from the Barrow entropy parameter Δ

In grand canonical ensemble, the expression for τ is given by :

$$\tau_G = \frac{\mathcal{A}_1}{\mathcal{B}_1}, \quad (122)$$

where,

$$\mathcal{A}_1 = 2\pi^{3/2}(\Delta + 2)L^2 S \gamma^n \left(\frac{\pi^{-\frac{3}{2n}} \zeta^2 \left(S^{\frac{2}{\Delta+2}} \right)^{\frac{3}{2n}}}{\gamma} + 1 \right)^n, \quad (123)$$

and

$$\mathcal{B}_1 = \sqrt{S^{\frac{2}{\Delta+2}}} \left(3\gamma^n S^{\frac{2}{\Delta+2}} \left(\frac{\pi^{-\frac{3}{2n}} \zeta^2 \left(S^{\frac{2}{\Delta+2}} \right)^{\frac{3}{2n}}}{\gamma} + 1 \right)^n - L^2 \left(\pi \left(\phi^2 - 1 \right) \gamma^n \left(\frac{\pi^{-\frac{3}{2n}} \zeta^2 \left(S^{\frac{2}{\Delta+2}} \right)^{\frac{3}{2n}}}{\gamma} + 1 \right)^n + S^{\frac{2}{\Delta+2}} \right) \right). \quad (124)$$

In Fig.16a, the defect curve for 4D black holes in the grand canonical ensemble is shown. The dashed lines represent the τ vs S curve within the Barrow entropy framework, while the black solid line corresponds to the same curve in GB statistics. As depicted in the Fig.16a, the topological charge in the Barrow entropy framework is found to be $W = 0$, with the small black hole (SBH) being stable and the large black hole (LBH) unstable, where we observe annihilation points. In contrast, the topological charge in the GB statistics framework is $W = 1$. Additionally, within the Barrow entropy framework, the topological charge changes to $W = -1$ depending on the parameter γ . In Fig.16b, black holes in the single branch belong to the topological class $W = -1$, while black holes with two branches belong to the topological class $W = 0$, featuring an annihilation point. Meanwhile, Fig.16c shows that the topological class in GB statistics remains consistently $W = +1$, independent of any thermodynamic parameters. Notably, no Van der Waals-like phase transition is observed in the grand canonical ensemble.

VIII. SPARSITY OF BLACK HOLE RADIATION

As an interesting further characteristic of BHs and the Hawking radiation flux, we now proceed to the study of sparsity, defined as the average time difference between the emission of

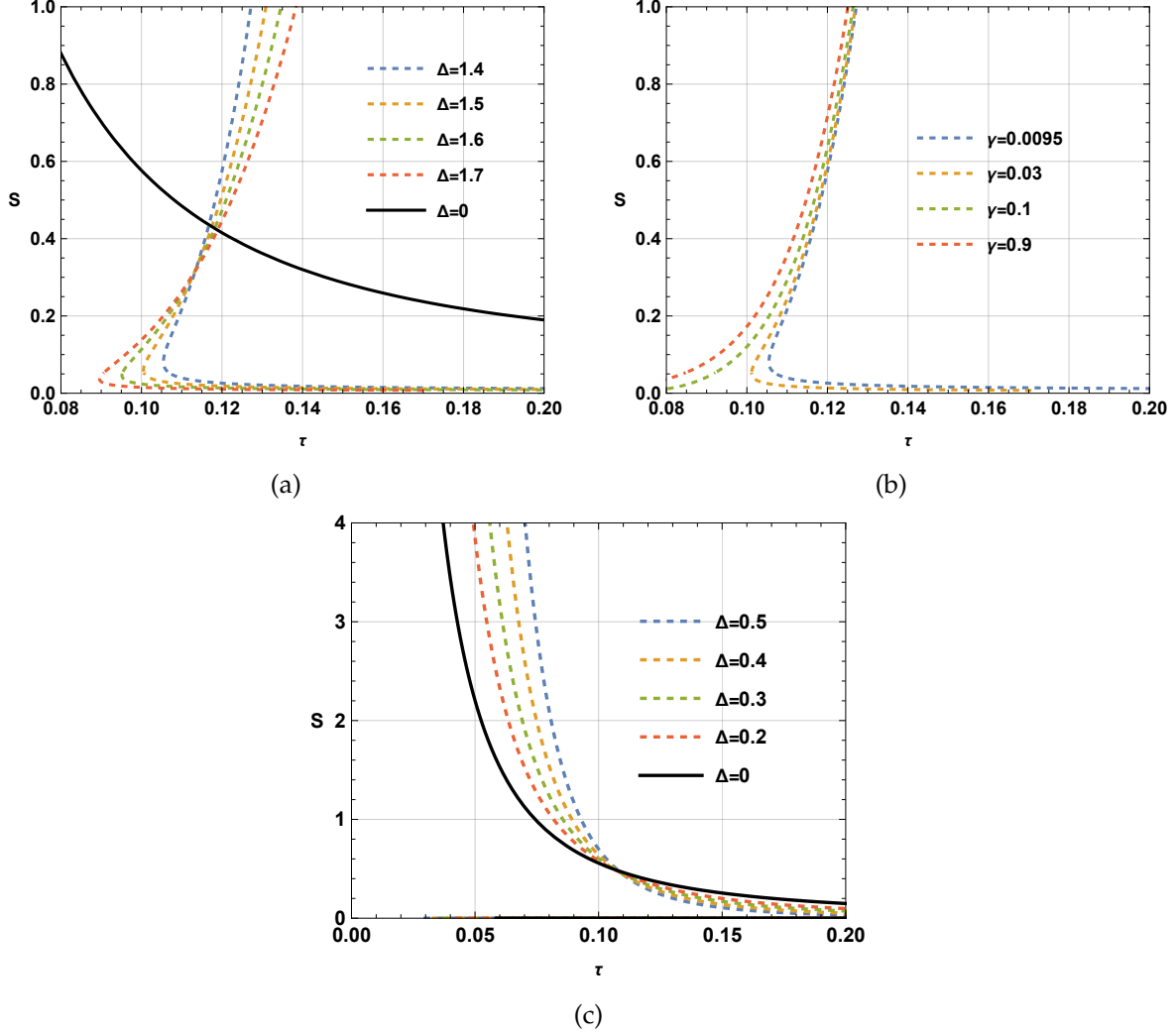


FIG. 16: Topological classes of 4D charged AdS black holes immersed in polytropic dark energy in grand canonical ensemble.

successive quanta. Relative to the black body, Hawking radiation is considerably sparser, as evidenced, in particular, e.g., in [173]. This is a key feature that distinguishes the two distinct kinds of radiation system.

For D -dimensional BHs, sparsity is governed by the parameter,

$$\eta = \frac{\mathcal{H}}{\tilde{g}} \left(\frac{\lambda_t^{D-2}}{\mathcal{A}_{eff}} \right), \quad (125)$$

which corresponds to the well-known expression for $D = 4$ [173]. For this purpose, \mathcal{H} is a dimensionless constant, \tilde{g} is the spin degeneracy factor of the emitted quanta, $\lambda_t = 2\pi/T$ represents their thermal wavelength, and $\mathcal{A}_{eff} = \sigma_{\text{capt}}\mathcal{A}_{BH}$ refers to the effective area of the BH where σ_{capt} stands for the capture cross-section of the photon by the Schwarzschild BH [174]. In the most straightforward case of Schwarzschild BHs of dimension $(1 + 3)$, taking into account the emission of massless bosons, the constant is $\eta = 64\pi^3/27 \simeq 73.49$. For the sake of comparison, we note that $\eta \ll 1$ for black bodies.

Accordingly, with a view to uncovering on how the polytropic structure affects the sparsity characteristic relevant to higher-dimensional charged AdS BHs, consider, responsive to this, the corresponding high-dimensional effective area of BH involved in the capture cross-section as follows [174]

$$\mathcal{A}_{eff} = \mathcal{A}_{BH} \frac{2^{4/(D-3)}(D-3)(D-1)^{(D-1)(D-3)}}{\left[2^{3/(D-3)}(D-1) - 2^{D/(D-3)}\right]^2} \pi, \quad (126)$$

where the BH area in higher-dimensions can be represented by

$$\mathcal{A}_{BH} = \frac{2\pi^{(D-1)/2}}{\Gamma\left(\frac{D-1}{2}\right)} r_h^{D-2}. \quad (127)$$

Corrections imposed on Eq. (125) by generalized entropies and / or uncertainty relations were investigated in [72, 175–180]. Furthermore, the computation of sparsity in D -dimensional generic Tangherlini BHs has been carried out in [181]. The aim herein is to explore how Eq. (125) arises for charged AdS BHs with a surrounding polytropic structure in high-dimensional spacetimes. In this respect, we point out that the straightforward substitution of the modified Hawking temperature which is obtained by using (82) in (76), such that

$$\begin{aligned} T = \frac{1}{\pi} & \left\{ 4^{\frac{1}{2-D}-1} \left(\frac{S_{\Delta+2}^2}{\omega_{D-2}} \right)^{\frac{1}{2-D}} \left(4^{\frac{1}{D-2}} \left(\frac{S_{\Delta+2}^2}{\omega_{D-2}} \right)^{\frac{1}{D-2}} \left(-\frac{2}{D-2} \left(\gamma + \zeta^2 \left(4^{\frac{1}{D-2}} \left(\frac{S_{\Delta+2}^2}{\omega_{D-2}} \right)^{\frac{1}{D-2}} \right)^{\frac{D-1}{n}} \right)^{-n} \right. \right. \right. \\ & \left. \left. - \frac{1}{L^2} + \frac{48\pi^2 Q^2 \left(4^{\frac{1}{D-2}} \left(\frac{S_{\Delta+2}^2}{\omega_{D-2}} \right)^{\frac{1}{D-2}} \right)^{4-2D}}{\omega_{D-2}^2} \right) + D \left(-\frac{16\pi^2 Q^2 \left(4^{\frac{1}{D-2}} \left(\frac{S_{\Delta+2}^2}{\omega_{D-2}} \right)^{\frac{1}{D-2}} \right)^{6-2D}}{\omega_{D-2}^2} + 1 \right) \right. \\ & \left. \left. + 4^{\frac{2}{D-2}} \frac{D}{L^2} \left(\frac{S_{\Delta+2}^2}{\omega_{D-2}} \right)^{\frac{2}{D-2}} - 3 \right) \right\}, \quad (128) \end{aligned}$$

into Eq. (125) yields

$$\eta = (D-1)^{(3-D)(D-1)} \pi^{\frac{1}{2}(D(D+2)-9)} \left(\frac{\mathcal{C}}{D-3} \right) \Gamma\left(\frac{D-1}{2}\right) \frac{2^{3D-\frac{4}{D-3}-5} \left(2^{\frac{D}{D-3}} - 8^{\frac{1}{D-3}}(D-1) \right)^2}{\left(\left(\pi^{\frac{1}{2}-\frac{D}{2}} \Gamma\left(\frac{D-1}{2}\right) S_{\Delta+2}^2 \right)^{\frac{1}{D-2}} \right)^{D-2}}, \quad (129)$$

where we have defined

$$\begin{aligned} \mathcal{C} &= \left(\frac{\mathcal{C}_1}{\mathcal{C}_2 - 8Q^2 \Gamma\left(\frac{D-1}{2}\right)^{\frac{2(D-1)}{D-2}} \pi^{\frac{-3}{D-2}} \left(2^{\frac{4}{2}} + 1S \right)^{\frac{12}{(\Delta+2)(D-2)}}} \right)^{D-2} \\ \mathcal{C}_1 &= (D-2)(\Delta+2)S \left(\pi^{\frac{1-D}{2}} \Gamma\left(\frac{D-1}{2}\right) S_{\Delta+2}^2 \right)^{\frac{3}{D-2}} \Gamma\left(\frac{D-1}{2}\right) \left(2^{\frac{1}{D-2}} \left(\pi^{\frac{1-D}{2}} \Gamma\left(\frac{D-1}{2}\right) S_{\Delta+2}^2 \right)^{\frac{1}{D-2}} \right)^D, \end{aligned}$$

$$\begin{aligned}
\mathcal{C}_2 = & \left\{ \frac{(D-2)(D-1) \left(\pi^{\frac{1-D}{2}} \Gamma\left(\frac{D-1}{2}\right) \left(2^{\frac{\Delta}{2}+1} S\right)^{\frac{2}{\Delta+2}} \right)^{\frac{2}{D-2}}}{L^2} D^2 - 2 \left(\pi^{\frac{1-D}{2}} \Gamma\left(\frac{D-1}{2}\right) \left(2^{\frac{\Delta}{2}+1} S\right)^{\frac{2}{\Delta+2}} \right)^{\frac{2}{D-2}} \right. \\
& \times \left. \left(\gamma + \zeta^2 \left(2^{2^{\frac{1}{D-2}}} \left(\pi^{\frac{1-D}{2}} \Gamma\left(\frac{D-1}{2}\right) S^{\frac{2}{\Delta+2}} \right)^{\frac{1}{D-2}} \right)^{\frac{D-1}{n}} \right)^{-n} - 5D + 6 \right\} \pi^D \left(2^{2^{\frac{1}{D-2}}} \left(\pi^{\frac{1-D}{2}} \Gamma\left(\frac{D-1}{2}\right) S^{\frac{2}{\Delta+2}} \right)^{\frac{1}{D-2}} \right)^{2D}.
\end{aligned} \tag{130}$$

Examination of the plot in Figs. 17 and 18 offers some interesting information about the dimensions of $4D/5D$ spacetime. Unlike Schwarzschild's BHs, the sparsity fluctuates (i.e. decreases) as S increases, i.e. as the size of the BHs increases. For S sufficiently large, $\eta \ll 1$ is achieved: in this regime, the radiation emitted by AdS BHs with a surrounding polytropic structure appears to be almost classical and completely consistent with the spectrum of a black body. Alternatively, we observe that for a given S , the larger the size of the BH, the sparser the radiation, and vice versa.

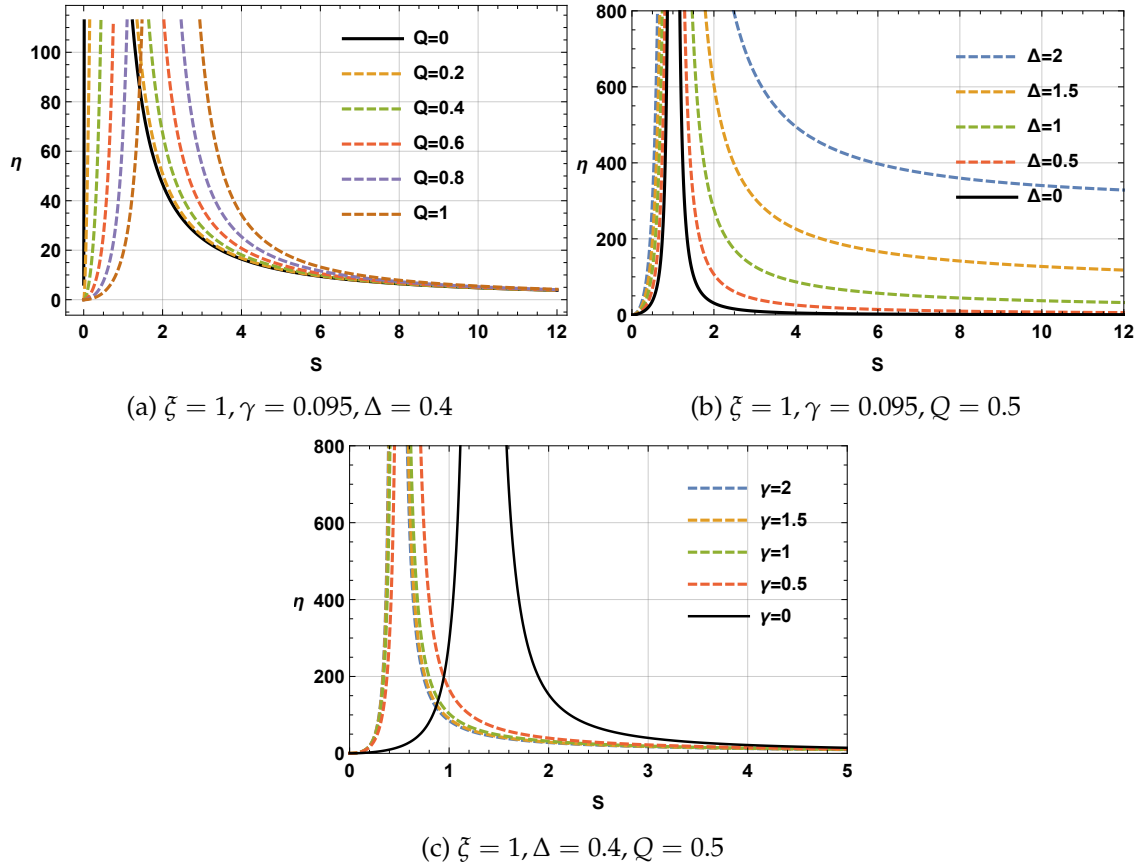


FIG. 17: Sparsity effects for the fixed-parameter polytropic structure of the BH system in $4D$ spacetime.

On the one hand, this is caused by the surround polytropic structure (γ decreases), which slows down the emission of quanta and therefore increases the density of the radiation as Q and Δ increases (see Figs. 17a- 17a and Figs. 18a- 18b), while remaining observed as D decreases ($5D \rightarrow 4D$) from a point of view regarding Figs. 17 and 18. For the sake of comparison, we

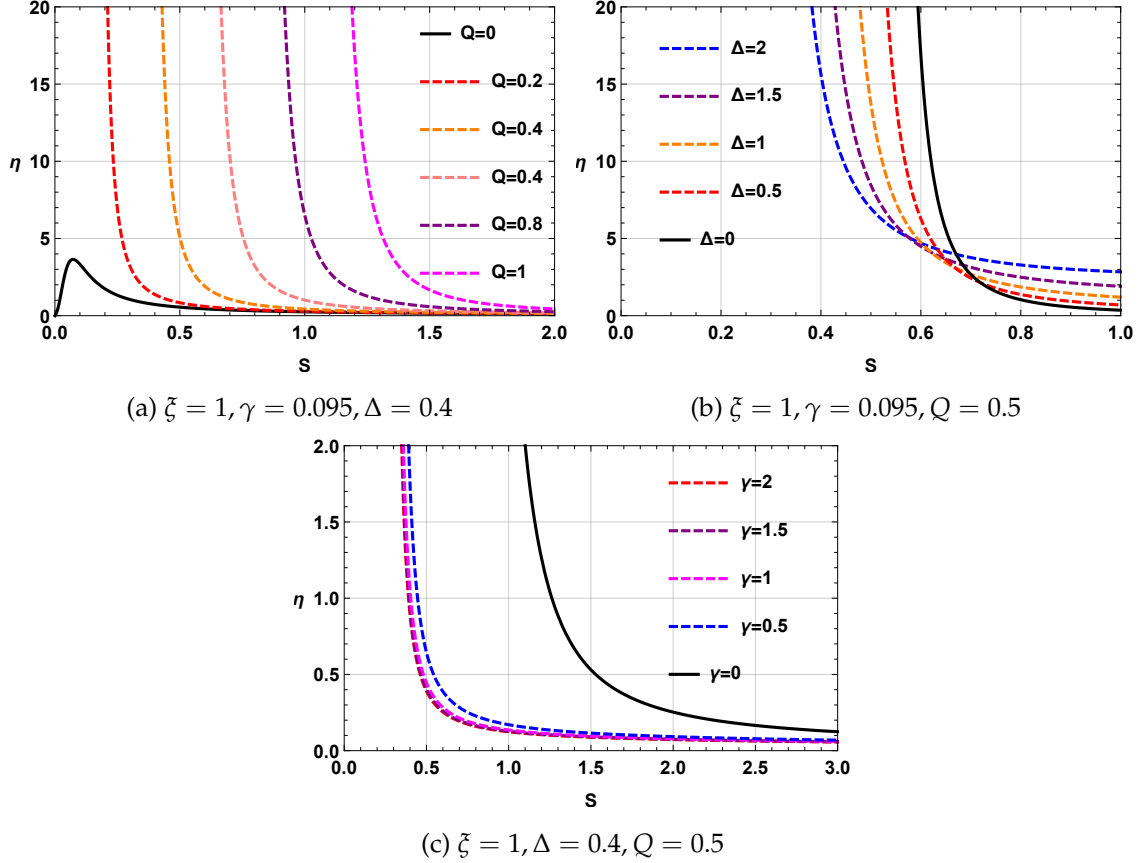


FIG. 18: Sparsity effects for the fixed-parameter polytropic structure of the BH system in 5D spacetime.

note that in [181] - where no polytropic structure is being considered - the density is lossy in high dimensions. Broadly speaking, this outcome is valid and serves to highlight the impact of the polytropic structure on the fluctuation of the Hawking radiation sparsity.

IX. THERMAL GEOMETRY

In investigating in a depth-way the relevant heat capacity phase transition points, an alternative approach revealing this feature can be taken into account, such as geometrical thermodynamics (GT). In particular, the characteristic of the heat capacity phase transition points are correlated to divergent points of the thermodynamic Ricci curvature scalar. Applying the GT tools offer on the other hand a practical way to gain a better understanding about thermodynamic phase transitions from a geometric point of view, especially from the Ricci scalar curvature of the thermodynamic metric. In the realm of these endeavors, a wide number of GT tools are regarded efficiently to predict the phase transition point of heat capacity such as Weinhold, Ruppeiner and Quevedo [182–185]. However, it has been demonstrated that the phase transition points provided by this family of metrics are not consistent with those provided by the canonical ensemble approach. For that reason, the application of the so-called Hendi, Panahiyan, Eslam Panah and Momennia (HPEM) metric is therefore efficace to set out a presice exact position of the heat capacity phase

transition points [186–189]. The associated metric for HPEM is given by

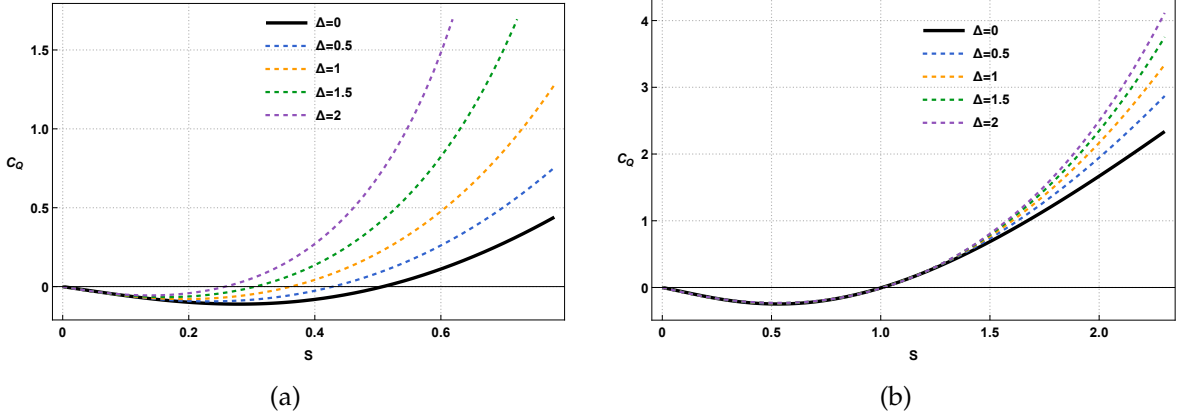


FIG. 19: Heat capacity C_Q variation against S (C_Q roots, i.e., physical limitation point) for various values of the Barrow parameter Δ with setting $\gamma = 0.095$, $L = 1$, $Q = 0.5$, $\xi = 1$, and $n = 2$.

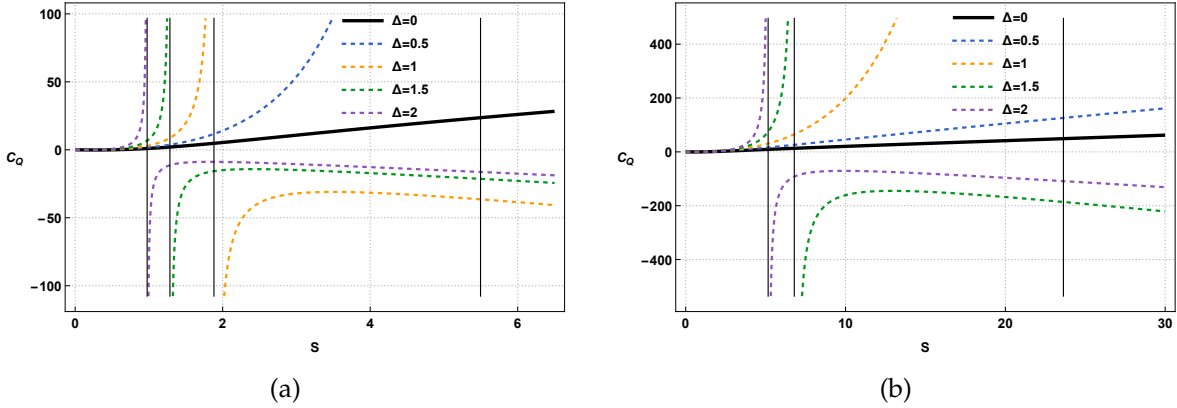


FIG. 20: Heat capacity C_Q variation against S (C_Q^{-1} roots, i.e., phase transition critical point) for various values of the Barrow parameter Δ with setting $\gamma = 0.095$, $L = 1$, $Q = 0.5$, $\xi = 1$, and $n = 2$.

$$dS_{HPEM}^2 = \frac{S M_S}{\left(\prod_{i=2}^n \frac{\partial^2 M}{\partial \xi_i^2}\right)^3} \left(-M_{SS} dS^2 + \sum_{i=2}^n \left(\frac{\partial^2 M}{\partial \chi_i^2} \right) d\chi_i^2 \right), \quad (131)$$

where, χ ($\chi \neq S$), $M_S = \frac{\partial M}{\partial S}$, and $M_{SS} = \frac{\partial^2 M}{\partial S^2}$ are, respectively, extensive parameters. Accordingly, the background of metrics expressed in view of the first law of BH thermodynamics as follows

$$dS_{HPEM}^2 = \frac{S M_S}{\left(\frac{\partial^2 M}{\partial L^2} \frac{\partial^2 M}{\partial Q^2} \frac{\partial^2 M}{\partial \gamma^2}\right)^3} \left(-M_{SS} dS^2 + M_{LL} dL^2 + M_{QQ} dQ^2 + M_{\gamma\gamma} d\gamma^2 \right). \quad (132)$$

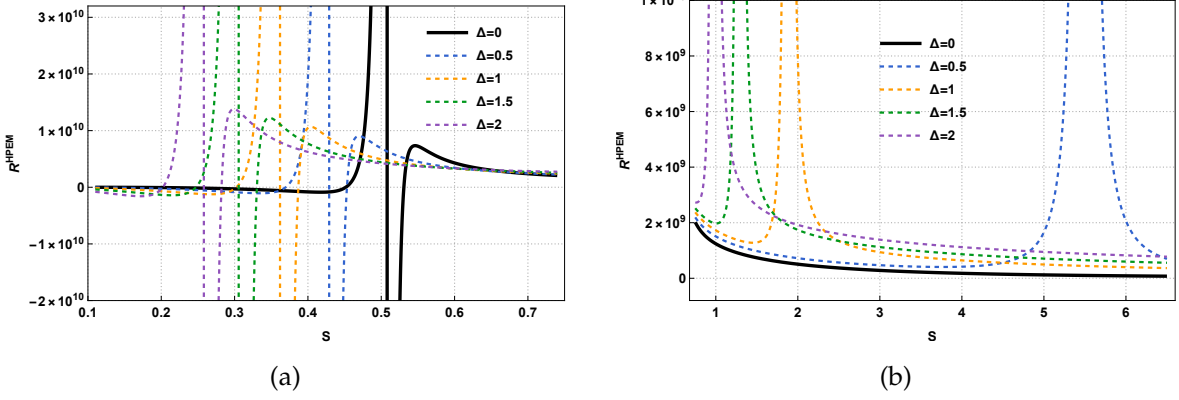


FIG. 21: Ricci scalar of HPEM's metric R^{HPEM} against S for various values of the Barrow parameter Δ in 5D spacetime.

Likewise, in the realm of mass representation, a diagonal matrix form relevant to HPEM geometry can be established according to the following expression :

$$g^{\text{HPEM}} = \frac{S M_S}{\left(\frac{\partial^2 M}{\partial L^2} \frac{\partial^2 M}{\partial Q^2} \frac{\partial^2 M}{\partial \gamma^2} \right)^3} \begin{pmatrix} -M_{SS} & & & \\ & M_{LL} & & \\ & & M_{QQ} & \\ & & & M_{\gamma\gamma} \end{pmatrix}. \quad (133)$$

In this formalism, the associated Ricci scalar curvature employed to carry out these measurements

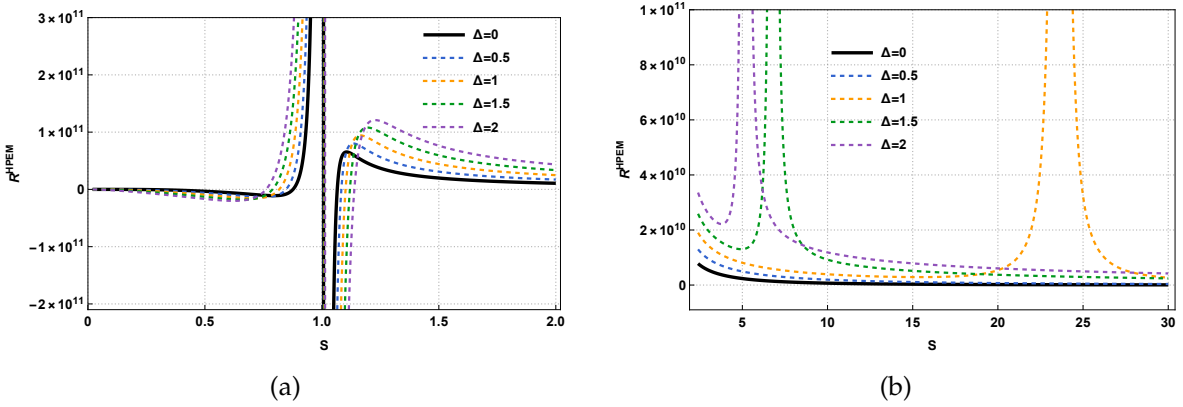


FIG. 22: Ricci scalar of HPEM's metric R^{HPEM} against S for various values of the Barrow parameter Δ in 4D spacetime.

has the following denominator

$$\text{denom}(R^{\text{HPEM}}) = 2M_{SS}^2 S^3 M_S^3, \quad (134)$$

where solving $\text{denom}(R^{\text{HPEM}}) = 0$ gives us a precise insight into the number and location of each specific heat capacity phase transition point.

In order to draw out information and gain a detailed insight into the behaviour of the HPEM R^{HPEM} scalar curvature, Figs. 21 and 22 depict an intrinsic analysis. For this purpose, a mandatory step is to take into account the behavior of the heat capacity at constant Q (see Figs. 19 and 20) to establish such a one-to-one correspondence with the features of R^{HPEM} . Manifestly, the HPEM scalar curvature for a given Δ parameter spectrum involves, whether in the case of 5D or 4D, two divergent points (one with a change of sign and the second refers to a positive divergent point). Practically speaking, these two divergent points are consistently linked to the heat capacity phase transition points. To be concrete, the heat capacity phase transition point entails what is called the physical limitation point by solving the set, $\left(\frac{\partial M}{\partial S}\right) = 0$ [190, 191], while the other specific point refers to the phase transition critical point emerging by solving $\left(\frac{\partial^2 M}{\partial S^2}\right) = 0$ [190–192]. Therefore, it is straightforward that the set of physical limitation points in 5D (see Fig. 19a) is perfectly predicted by the HPEM scalar curvature, as shown in Fig. 21a. However, similar findings are explored in 4D (see Figs. 19b and 22a). On the other hand, with respect to the exploration of the phase transition critical points relevant for the heat capacity (divergent point), the HPEM scalar curvature predicts these exactly by means of a positive divergent point. For the 5D case, the phase transition critical points (Fig. 20a) are correlated to the divergent point of R^{HPEM} (see Fig. 21b), while for the 4D case, Fig. 20b coherently maps to Fig. 22b. Furthermore, it is of interest to note that the impact carried out by the Barrow parameter Δ in a decreasing sense reduced the set of phase transition critical points (divergent points of the heat capacity), which are predicted in terms of positive divergent points pertinent to the HPEM scalar curvature R^{HPEM} . This is graphically shown in the case of 5D where for $\Delta < 0.5$, the system features not any phase transition critical point; in turn, in the case of 4D, the HPEM scalar curvature R^{HPEM} remains a feature with three positive divergent points satisfying the observation condition such that $\Delta \geq 1$.

TABLE II: Topological Classes in Different Black Hole Dimensions and Ensembles

Dimension	Ensemble	Barrow Entropy	Gibbs-Boltzmann (GB)
5D	Canonical	$W = 1, W = 0$	$W = 1$
	Grand Canonical	$W = 0$ (annihilation), $W = 0$ (generation)	$W = 0$ (generation), $W = 1$
4D	Canonical	$W = 1, W = 0$ (annihilation), Van der Waals-like phase transition	$W = 1$
	Grand Canonical	$W = 0, W = -1, W = 1$	$W = 1$

X. CONCLUSION

The sections II to IV were for the polytropic solution and thermodynamics basis needed for the higher dimension AdS BH detailed thermodynamic study. These section provide us the material on polytropic gases pressure and density solutions useful for the thermodynamic topology of the Barrow entropy in higher dimensions and its possible generalizations. The possibilities of possible dark energy states for the background have been treated for the main fluid models allowing AdS BHs, whether quintessence, chaplygin gas and in general polytropic fluids as showed in Table I. In Figs. 2 and 3, we present in addition the strong energy condition evolution and the metric function $F(r)$ with the radius coordinate in terms of fixed parameter to better simulate the

parameter impacts on the AdS BH models by the thermodynamic topology approach. The $F(r)$ evolution indicates the thermodynamic effects on the metric, but also on curvature and Einstein FEs. This is essential for higher dimensions BH solutions.

The section IV concerns the thermodynamic variables themselves evolution for polytropic gases and typically AdS BHs expected thermodynamic quantities evolutions. This implies the BH temperature profile, entropy, conserved charges, mass evolution, the heat capacity and so on... All these variables are essential for polytropic Barrow entropy parameters determination for 4 and 5 dimensional AdS BHs solution and spacetime topology. From these ingredients, we can study all possible higher-dimensional AdS BH solutions without any constraints.

In Section V, we conducted a detailed analysis of the thermodynamic topology of these black holes within the Barrow entropy framework, with a particular focus on both 4-dimensional and 5-dimensional black hole solutions. Our analysis was performed in two distinct ensembles: the canonical ensemble and the grand canonical ensemble.

Starting with the 5-dimensional black holes, where the behavior became more intricate, we evaluated their thermodynamic quantities and analyzed their topological structure. In the canonical ensemble, we identified topological classes characterized by the charges $W = 1$ and $W = 0$ within the Barrow entropy framework, while only the topological class $W = 1$ appeared in the Gibbs-Boltzmann (GB) statistics framework. Next, in the grand canonical ensemble, we observed a topological class $W = 0$ with an annihilation point in the Barrow entropy framework, alongside another topological class $W = 0$ with a generation point. Under the GB statistics framework, we found the topological classes $W = 0$ and $W = 1$, with $W = 0$ featuring a generation point.

Extending our study to 4-dimensional black holes, we found two distinct topological classes with charges $W = 1$ and $W = 0$ in the canonical ensemble, depending on the values of the thermodynamic parameters within the Barrow entropy framework. The topological charge $W = 0$ also contained annihilation points. In the GB statistics framework, only the topological class $W = 1$ was present. Furthermore, we observed a Van der Waals-like phase transition in this ensemble. In contrast, the grand canonical ensemble revealed three topological classes with charges $W = 0$, $W = -1$, and $W = 1$ within the Barrow entropy framework, while only the topological class $W = 1$ was found in the GB statistics framework, showcasing an even richer structure. Notably, the topological charge in both ensembles was found to depend on the thermodynamic and ensemble parameters. A key feature of both black hole solutions was the significant influence of the Barrow entropy parameter Δ . For values of Δ close to zero, the thermodynamic topology closely resembled the behavior predicted by Gibbs-Boltzmann (GB) statistics. However, as Δ deviated from zero, the system exhibited substantial deviations from GB statistics, both globally and locally, under Barrow statistics. The results are summarized in the Table II for highlighting and comparing 4D and 5D AdS Black Hole main results. These 4 and 5 dimensional AdS BH solutions are the necessary cases for generalization to the $D > 5$ AdS BH solution classes with respect to the Barrow statistic and still by using Canonical and Grand Canonical statistic approaches. Once again, we have to take into account the main differences between these Canonical and Grand Canonical solutions.

In sect VIII, we found that the inter-quanta average time difference is impacted by the higher-dimensional AdS BH for the Hawking Radiation (an highly sparser case). For polytropic struc-

tures, the AdS charge BH area is corrected according to eqns (126) and (127). The Hawking radiation temperature is then corrected in these case. The sparsity effect also implies several corrections for polytropic fluid parameters and ultimately the spacetime structure around an AdS BH versus a Schwarzschild BH under this background. The 4 and 5 dimensions AdS BHs solutions clearly show the impacts on the main polytropic variables and parameters when we look at the Fig. 17 and 18. We may obtain similar effect for $D > 5$ AdS BHs cases solutions.

In sect IX, we finally determined the thermodynamic-dependent spacetime structures for polytropic AdS BHs. These structures directly clarify the effects of Barrow thermal radiation on the higher-dimensional spacetime structure $D > 3$. Yes, thermodynamics and Barrow entropy directly influence the metric representation of spacetime. We plotted the effects for the 4 and 5-dimensional AdS BHs studied in detail in this paper to make this clear. We could do the same for the cases of BHs with $D > 5$. This was at the same time the ultimate goal of this paper.

We did the detailed study of polytropic Barrow Entropy system and topology for higher dimension AdS BHs. There are naturally several possible extension of this study such as Mur-naghan fluids and more complex fluids. We can ask us how the current paper 4D and 5D BH solution could be generalized to more complex fluid and thermodynamic topological structures. In these cases, it would be good to know how thermodynamic topologies will behave for more complex structures. How will the 4 and 5-dimensional AdS BHs solutions change, both for the temperature, mass, entropy profiles and for the invariants involved. Would additional dimensional solutions $D > 5$ be needed that are more suited to more complex fluids? How will sparsity be possible for such cases? This will have to be investigated tactfully. Beyond GR, one could in some future study these types of topological thermodynamic phenomena and structures for alternative theories, such as in teleparallel $F(T)$ gravity [51–53]. In such a case, one would base the study on the evolution of the spacetime torsion tensor and scalar. Another implication can be the Tsallis entropy arising within teleparallel frameworks [53]. One could also repeat such a challenge for symmetric teleparallel $F(Q)$ gravity and other intermediate theories. Even though the challenge is very big, it is good and reasonable to believe in these possibilities.

ACKNOWLEDGMENTS

The author SKM acknowledges that this research work is supported by the TRC Project (Grant No. BFP/RGP/CBS/24/203). SKM is also thankful for continuous support and encouragement from the administration of the University of Nizwa for this research work. B. Hazarika would like to thank DST-INSPIRE, Ministry of Science and Technology fellowship program, Govt. of India for awarding the DST/INSPIRE Fellowship[IF220255] for financial support.

-
- [1] S.W. Hawking, Particle creation by black holes, *Comm. in Math. Phys.*, 43, 199 (1975).
 - [2] S.W. Hawking, Black hole explosions?, *Nature*, 248, 30 (1974).
 - [3] M. Isi, W.M. Farr, M. Giesler, M.A. Scheel & S.A. Teukolsky, Testing the Black-Hole Area Law with GW150914, *Phys. Rev. Lett.* 127, 011103 (2021).
 - [4] M.-I. Park, Notes on the area theorem, *Classical Quantum Gravity* 25(9), 095013 (2008).

- [5] E.-A. Kontou & V. Sacchi, A generalization of the Hawking black hole area theorem, *Gen. Relativ. Gravit.* **56**, 62 (2024).
- [6] E.-A. Kontou, B. Freivogel & D. Krommydas, A singularity theorem for evaporating black holes, *The Sixteenth Marcel Grossmann Meeting*, 822 (2023).
- [7] D.N. Page, Hawking radiation and black hole thermodynamics, *New Journal of Physics* **7**, 203 (2005).
- [8] D.N. Page, Finite Upper Bound for the Hawking Decay Time of an Arbitrarily Large Black Hole in Anti-de Sitter Spacetime, *Phys. Rev. D* **97**, 024004 (2018).
- [9] S. Abdolrahimi, D.N. Page, Hawking Radiation Energy and Entropy from a Bianchi-Smerlak Semi-classical Black Hole, *Phys. Rev. D* **92**, 083005 (2015).
- [10] D.N. Page, Time Dependence of Hawking Radiation Entropy, *J. Cosmol. Astropart. Phys.* **09**, 028 (2013).
- [11] K. Sfetsos & K. Skenderis, Microscopic derivation of the Bekenstein-Hawking entropy formula for non-extremal black holes, *Nucl. Phys. B* **517**, 179 (1998).
- [12] L.C.B. Crispino, A. Higuchi & G.E.A. Matsas, The Unruh effect and its applications, *Review of Modern Physics* **80**, 787 (2008).
- [13] P. Longhi & R. Soldati, Unruh effect revisited, *Phys. Rev. D* **83**, 107701 (2011).
- [14] F. Hammad, A. Landry & D. Dijamco, The influence of the dispersion relation on the Unruh effect according to the relativistic Doppler shift method, *Phys. Rev. D* **103**, 085010 (2021).
- [15] B. Carter, Large number coincidences and the anthropic principle in cosmology, in *Confrontation of cosmological theories with observational data*, M.S. Longair, 291, D. Reidel, Dordrecht (1974).
- [16] J.D. Barrow, *The anthropic cosmological principle*, New York: Oxford University Press. Edited by Frank J. Tipler (1986).
- [17] J.D. Barrow, Anthropic definitions, *Quarterly Journal of the Royal Astronomical Society* **24**, 146 (1997).
- [18] J. Leslie, Probabilistic phase transitions and the anthropic principle, *Origin and early history of the Universe: Liege 26*, Knudsen, 439 (1986).
- [19] L.A. Barnes, The Fine-Tuning of the Universe for Intelligent Life, *Publications of the Astronomical Society of Australia* **29**(4), 529 (2012).
- [20] L. Susskind, "The anthropic landscape of string theory". The Davis Meeting on Cosmic Inflation, 26 (2003), [arXiv:hep-th/0302219](https://arxiv.org/abs/hep-th/0302219)
- [21] D.N. Page, Inflation does not explain time asymmetry, *Nature* **304** (5921), 39 (1983).
- [22] K. Karami, S. Ghaffari & J. Fehri, Interacting polytropic gas model of phantom dark energy in non-flat universe, *Eur. Phys. J. C* **64**, 85 (2009).
- [23] K. Karami, Z. Safari & S. Asadzadeh, Cosmological constraints on polytropic gas model, *International Journal Theoretical Physics* **53**, 1248 (2014).
- [24] K. Karami & A. Abdolmaleki, Reconstructing interacting new agegraphic polytropic gas model in non-flat FRW universe, *Astrophysical and Space Science* **330**, 133 (2010).
- [25] K. Karami & M.S. Khaledian, Polytropic and Chaplygin $f(R)$ -gravity models, *Int. J. Mod. Phys. D* **21**, 1250083 (2012).
- [26] S. Banerjee & A. Paul, Effect of Accretion on the evolution of Primordial Black Holes in the context of Modified Gravity Theories, preprint (2024), [arXiv:2406.04605](https://arxiv.org/abs/2406.04605).
- [27] M.S. Aboueisha, M.I. Nouh, E.A-B. Abdel-Salam, T.M. Kamel, M.M. Beheary & K.A.K. Gadallah, Analysis of the Fractional Relativistic Polytropic Gas Sphere, *Scientific Reports* **13**, 14304 (2023).
- [28] V.H. Cardenas, M. Cruz, Emulating dark energy models with known equation of state via the created cold dark matter scenario, *Phys. Dark Univ.* **44**, 101452 (2024).
- [29] Y. Jia, T.-Y. He, W.-Q. Wang, Z.-W. Han, R.-J. Yang, Accretion of matter by a Charged dilaton black hole, *Eur. Phys. J. C* **84**, 501 (2024).
- [30] I. Zlatev, L. Wang & P. Steinhardt, Quintessence, Cosmic Coincidence, and the Cosmological Constant, *Phys. Rev. Lett.* **82**(5), 896 (1999).

- [31] P. Steinhardt, L. Wang & I. Zlatev, Cosmological tracking solutions, *Phys. Rev. D* **59**(12), 123504 (1999)
- [32] R.R. Caldwell, A phantom menace? Cosmological consequences of a dark energy component with super-negative equation of state, *Phys. Lett. B* **545**, 23 (2002).
- [33] Y. Kucukakca, A. R. Akbarieh & S. Ashrafi, Exact solutions in teleparallel dark energy model, *Chinese Journal of Physics* **82** (2023) 47–61.
- [34] A.A. Coley, A. Landry & F. Gholami, Teleparallel Robertson-Walker Geometries and Applications, *Universe*, **9**, 454 (2023).
- [35] P.K.S. Dunsby, O. Luongo, M. Muccino & V. Pillay, Double polytropic cosmic acceleration from the Murnaghan equation of state, *Phys. Dark Univ.* **46**, 101563 (2024).
- [36] P.K.S. Dunsby, O. Luongo, M. Muccino, Unifying the dark sector through a single matter fluid with non-zero pressure, preprint (2024), [arXiv:2308.15776](https://arxiv.org/abs/2308.15776).
- [37] N. Bilic, G.B. Tuppe & R.D. Viollier, Unification of dark matter and dark energy: the inhomogeneous Chaplygin gas, *Phys. Lett. B* **535**, 17 (2002).
- [38] M. Makler, S.Q. de Oliveira & I. Waga, Observational constraints on Chaplygin quartessence: Background results, *Phys. Rev. D* **68**, 123521 (2003).
- [39] Z.-H. Zhu, Generalized Chaplygin gas as a unified scenario of dark matter/energy: Observational constraints, *Astronomy and Astrophysics* **423**, 421 (2004)
- [40] J.D. Barrow, The Area of a Rough Black Hole, *Phys. Lett. B* **808**, 135643 (2020).
- [41] A. Sheykhi, Modified cosmology through Barrow entropy, *Phys. Rev. D* **107**, 023505 (2023).
- [42] P.S. Ens & A.F. Santos, An attempt to add Barrow entropy in $f(R)$ gravity, *Phys. Lett. B* **835**, 137562 (2022).
- [43] G. Leon, J. Magana, A. Hernandez-Almada, M.A. Garcia-Aspeitia, T. Verdugo & V. Motta, Barrow Entropy Cosmology: an observational approach with a hint of stability analysis, *J. Cosmol. Astropart. Phys.* **12**, 032 (2021).
- [44] G.G. Luciano, Constraining Barrow entropy-based Cosmology with power-law inflation, *Eur. Phys. J. C* **83**, 329 (2023).
- [45] Y. Ladghami, B. Asfour, A. Bouali, A. Errahmani & T. Ouali, Barrow Entropy and AdS Black Holes in RPS Thermodynamics, *Phys. Dark Univ.* **44**, 101470 (2024).
- [46] J. Xia & Y.C. Ong, Upper Bound of Barrow Entropy Index from Black Hole Fragmentation, *Universe*, **10**, 177 (2024).
- [47] A. Sheykhi, Barrow Entropy Corrections to Friedmann Equations, *Phys. Rev. D* **103**, 123503 (2021).
- [48] A. Sheykhi & S. Ghaffari, Note on agegraphic dark energy inspired by modified Barrow entropy, *Phys. Dark Univ.* **41**, 101241 (2023).
- [49] A. Sheykhi & M.S. Hamedan, Holographic dark energy in modified Barrow cosmology, *Entropy* **25**, 569 (2023).
- [50] M. Bousder, E. Salmani & H. Ez-Zahraouy, Entropy as logarithmic term of the central charge and modified Friedmann equation in AdS/CFT correspondence, *Journal of High Energy Astrophysics* **38**, 49 (2023).
- [51] M. Yasir, X. Tiecheng & A. Jawad, Topological charges via Barrow entropy of black hole in metric-affine gravity, *Eur. Phys. J. C* **84**, 946 (2024).
- [52] T. Ghorui, P. Rudra, F. Rahaman, A new type of $f(T)$ gravity from Barrow entropy, preprint (2024), [arXiv:2406.08006](https://arxiv.org/abs/2406.08006).
- [53] S. Di Gennaro, H. Xu, Y.C. Ong, How Barrow entropy modifies gravity: with comments on Tsallis entropy, *Eur. Phys. J. C* **82**, 1066 (2022).
- [54] S. Nojiri, S.D. Odintsov & T. Paul, Different aspects of entropic cosmology, *Universe*, **10**(9), 352 (2024), [arXiv:2409.01090](https://arxiv.org/abs/2409.01090).
- [55] A. Sheykhi & B. Farsi, Growth of Perturbations in Tsallis and Barrow Cosmology, *Eur. Phys. J. C* **82**, 1111 (2022).
- [56] C. Tsallis, L.J.L. Cirto, Black hole thermodynamical entropy, *Eur. Phys. J. C* **73**, 2487 (2013).

- [57] Y. Sekhmani, G.G. Luciano, S.K. Maurya, J. Rayimbaev, B. Pourhassan, M.K. Jasim and A. Rincon, Exploring Tsallis thermodynamics for boundary conformal field theories in gauge/gravity duality, *Chinese Journal of Physics*, pre-proof, (2024).
- [58] G. Kaniadakis, Statistical Mechanics in the Context of Special Relativity, *Phys. Rev. E* **66**, 056125 (2002).
- [59] G. Kaniadakis, Statistical Mechanics in the Context of Special Relativity II, *Phys. Rev. E* **72**, 036108 (2005).
- [60] N. Drepanou, A. Lymperis, E.N. Saridakis, K. Yesmakhanova, Kaniadakis Holographic Dark Energy and Cosmology, *Eur. Phys. J. C* **82**, 82, 449 (2022).
- [61] A.Y. Kamenshchik, U. Moschella, V. Pasquier, An alternative to quintessence, *Phys. Lett. B* **511**, 265 (2001).
- [62] V.V. Kiselev, Quintessence and black holes, *Classical Quantum Gravity* **20**, 1187 (2003).
- [63] G.-Q. Li, Effects of dark energy on P–V criticality of charged AdS black holes, *Phys. Lett. B* **735**, 256 (2014).
- [64] M.R. Setare, Holographic Chaplygin gas model, *Phys. Lett. B* **648**, 329 (2007).
- [65] H.B. Benaoum, Modified Chaplygin Gas Cosmology, *Adv. High Energy Phys.* **2012**, 357802 (2002).
- [66] S. b. Chen and J. I. Jing, Quasinormal modes of a black hole surrounded by quintessence, *Class. Quant. Grav.* **22** (2005), 4651-4657.
- [67] K. Arun, S.B. Gudennavar and C. Sivaram, Dark matter, dark energy, and alternate models: A review, *Advances in Space Research*, **60**(1) (2017), 166.
- [68] D. Kubiznak and R. B. Mann, Black hole chemistry, *Can. J. Phys.* **93** (2015) no.9, 999-1002
- [69] M. R. Garousi, Tachyon couplings on nonBPS D-branes and Dirac-Born-Infeld action, *Nucl. Phys. B* **584** (2000), 284-299.
- [70] C.E. Magalhaes Batista, J.C. Fabris and M. Morita, Power spectrum in the Chaplygin gas model: Tachyonic, fluid and scalar field representations, *Gen. Rel. Grav.* **42** (2010), 839–849.
- [71] G. Raposo, P. Pani, M. Bezares, c. Palenzuela and v. Cardoso, Anisotropic stars as ultracompact objects in General Relativity, *Phys. Rev. D* **99** no.10 (2019), 104072.
- [72] Y. Sekhmani, G. G. Luciano, J. Rayimbaev, M. K. Jasim, A. Al-Badawi and S. K. Maurya, Topological AdS black holes surrounded by Chaplygin dark fluid: From stability to geometrothermodynamic analysis, *Phys. Dark Univ.* **46** (2024), 101567
- [73] K. Migkas and T. H. Reiprich, Anisotropy of the galaxy cluster X-ray luminosity–temperature relation, *Astron. Astrophys.* **611** (2018), A50
- [74] K. Migkas, G. Schellenberger, T. H. Reiprich, F. Pacaud, M. E. Ramos-Ceja and L. Lovisari, Probing cosmic isotropy with a new X-ray galaxy cluster sample through the $L_X - T$ scaling relation, *Astron. Astrophys.* **636** (2020), A15.
- [75] K. Migkas, F. Pacaud, G. Schellenberger, J. Erler, N. T. Nguyen-Dang, T. H. Reiprich, M. E. Ramos-Ceja and L. Lovisari, Cosmological implications of the anisotropy of ten galaxy cluster scaling relations, *Astron. Astrophys.* **649** (2021), A151.
- [76] S. Del Campo, V. H. Cardenas and R. Herrera, Presence of anisotropic pressures in Lemaître-Tolman-Bondi cosmological models, *Mod. Phys. Lett. A* **27** (2012), 1250213.
- [77] E.-A. Kontou & K. Sanders, Energy conditions in general relativity and quantum field theory, *Classical Quantum Gravity* **37**, 193001 (2020).
- [78] C. S. Santos, J. Santos, S. Capozziello and J. S. Alcaniz, Strong energy condition and the repulsive character of f(R) gravity, *Gen. Rel. Grav.* **49** (2017) no.4, 50
- [79] S. Capozziello, R. D’Agostino, A. Lapponi & O. Luongo, Black hole thermodynamics from logotropic fluids, *Eur. Phys. J. C* **83**, 175 (2023).
- [80] Z.-Y. Fan, Critical phenomena of regular black holes in anti-de Sitter space-time, *Eur. Phys. J. C* **77**, 266 (2017).

- [81] M.E. Rodrigues, M.V. de S. Silva, & A.S. de Siqueira, Regular multihorizon black holes in General Relativity, *Phys. Rev. D* **102**, 084038 (2020).
- [82] B. Toshmatov, C. Bambi, B. Ahmedov, A. Abdujabbarov & Z. Stuchlík, Energy conditions of non-singular black hole spacetimes in conformal gravity, *Eur. Phys. J. C* **77**, 542, (2017).
- [83] M. Abramowitz and I.A. Stegun, Handbook of Mathematical Functions, ISBN:978-0486612720, Dover (1965).
- [84] A. Chamblin, R. Emparan, C. V. Johnson and R. C. Myers, Charged AdS black holes and catastrophic holography, *Phys. Rev. D* **60** (1999), 064018.
- [85] L. Balart & E.C. Vagenas, Regular black holes with a nonlinear electrodynamics source, *Phys. Rev. D* **90**, 124045 (2014).
- [86] J. Maldacena, The Large N limit of superconformal field theories and supergravity, *Adv. Theor. Math. Phys.* **2**, 231 (1998).
- [87] E. Witten, Anti-de Sitter space and holography, *Adv. Theor. Math. Phys.* **2**, 253 (1998).
- [88] D. Kubizňák, R.B. Mann & M. Teo, Black hole chemistry: thermodynamics with Lambda, *Classical Quantum Gravity* **34**, 063001 (2017).
- [89] G.W. Gibbons & S.W. Hawking, Cosmological Event Horizons, Thermodynamics, and Particle Creation, *Phys. Rev. D* **15**, 2738 (1977).
- [90] J.D. Bekenstein, Black holes and entropy, *Phys. Rev. D* **7**, 2333 (1973).
- [91] A. Ashtekar and A. Magnon, Asymptotically anti-de Sitter space-times, *Class. Quant. Grav.* **1** (1984), L39-L44.
- [92] A. Ashtekar and S. Das, Asymptotically Anti-de Sitter space-times: Conserved quantities, *Class. Quant. Grav.* **17** (2000), L17-L30.
- [93] R.-G. Cai & K.-S. Soh, Topological black holes in the dimensionally continued gravity, *Phys. Rev. D* **59**, 044013 (1999).
- [94] D. Kastor, S. Ray & J. Traschen, Enthalpy and the Mechanics of AdS Black Holes, *Classical Quantum Gravity* **26**, 195011 (2009).
- [95] N. Altamirano, D. Kubiznak, R.B. Mann & Z. Sherkatghanad, Thermodynamics of rotating black holes and black rings: phase transitions and thermodynamic volume, *Galaxies*, **2**(1), 89-159 (2014).
- [96] A. Kumar, S.G. Sushant and S.D. Maharaj, Nonsingular black hole chemistry, *Phys. Dark Univ.*, **30**, 100634 (2020).
- [97] P.V.P. Cunha, E. Berti, & C.A.R. Herdeiro, Light Ring Stability in Ultra-Compact Objects, *Phys. Rev. Lett.* **119**, 251102 (2017).
- [98] P.V.P. Cunha, & C.A.R. Herdeiro, Stationary Black Holes and Light Rings, *Phys. Rev. Lett.* **124**, 181101 (2020).
- [99] S.-W. Wei, Topological charge and black hole photon spheres, *Phys. Rev. D* **102**, 064039 (2020).
- [100] M. Guo & S. Gao, Universal properties of light rings for stationary axisymmetric spacetimes, *Phys. Rev. D* **103**, 104031 (2021).
- [101] M. Guo, Z. Zhong, J. Wang, & S. Gao, Light rings and long-lived modes in quasiblack hole spacetimes, *Phys. Rev. D* **105**, 024049 (2022).
- [102] S.-P. Wu & S.-W. Wei, Topology of light rings for extremal and nonextremal Kerr-Newman-Taub-NUT black holes without Z_2 symmetry, *Phys. Rev. D* **108**, 104041 (2023).
- [103] P.V.P. Cunha, C.A.R. Herdeiro, & J.P.A. Novo, Light rings on stationary axisymmetric spacetimes: blind to the topology and able to coexist, *Phys. Rev. D* **109**, 064050 (2024).
- [104] S.-W. Wei & Y.-X. Liu, Topology of equatorial timelike circular orbits around stationary black holes, *Phys. Rev. D* **107**, 064006 (2023).
- [105] X. Ye & S.-W. Wei, Topological study of equatorial timelike circular orbit for spherically symmetric (hairy) black holes, *J. Cosmol. Astropart. Phys.* **07** (2023) 049.
- [106] X. Ye & S.-W. Wei, Novel topological phenomena of timelike circular orbits for charged test particles, [arXiv:2406.13270](https://arxiv.org/abs/2406.13270).

- [107] S.-W. Wei & Y.-X. Liu, Topology of black hole thermodynamics, *Phys. Rev. D* **105**, 104003 (2022).
- [108] Y. S. Duan, *The structure of the topological current*, SLAC-PUB-3301, 1984.
- [109] Yi-Shi Duan & Mo-Lin Ge. *SU(2) Gauge Theory and Electrodynamics with N Magnetic Monopoles*, *Sci.Sin. Math*, **9**, 1072, 1979.
- [110] P.K. Yerra & C. Bhamidipati, Topology of black hole thermodynamics in Gauss-Bonnet gravity, *Phys. Rev. D* **105**, 104053 (2022).
- [111] P.K. Yerra & C. Bhamidipati, Topology of Born-Infeld AdS black holes in 4D novel Einstein-Gauss-Bonnet gravity. *Phys. Lett. B* **835**, 137591 (2022).
- [112] M.B. Ahmed, D. Kubiznak, & R.B. Mann, Vortex/anti-vortex pair creation in black hole thermodynamics, *Phys. Rev. D* **107**, 046013 (2023).
- [113] N.J. Gogoi & P. Phukon, Topology of thermodynamics in R-charged black holes, *Phys. Rev. D* **107**, 106009 (2023).
- [114] M. Zhang & J. Jiang, Bulk-boundary thermodynamic equivalence: a topology viewpoint, *J. High Energy Phys.* **06** (2023) 115.
- [115] M.R. Alipour, M.A.S. Afshar, S.N. Gashti, & J. Sadeghi, Topological classification and black hole thermodynamics, *Phys. Dark Univ.* **42**, 101361 (2023).
- [116] Z.-M. Xu, Y.-S. Wang, B. Wu, & W.-L. Yang, Riemann surface, winding number and black hole thermodynamics, [arXiv:2305.05916](https://arxiv.org/abs/2305.05916).
- [117] M.-Y. Zhang, H. Chen, H. Hassanabadi, Z.-W. Long, & H. Yang, Topology of nonlinearly charged black hole chemistry via massive gravity, *Eur. Phys. J. C* **83**, 773 (2023).
- [118] T.N. Hung & C.H. Nam, Topology in thermodynamics of regular black strings with Kaluza-Klein reduction, *Eur. Phys. J. C* **83**, 582 (2023).
- [119] J. Sadeghi, M.R. Alipour, S.N. Gashti, & M.A.S. Afshar, Bulk-boundary and RPS thermodynamics from topology perspective, [arXiv:2306.16117](https://arxiv.org/abs/2306.16117).
- [120] P.K. Yerra, C. Bhamidipati & S. Mukherji, Topology of critical points and Hawking-Page transition, *Phys. Rev. D* **106**, 064059 (2022).
- [121] Z.-Y. Fan, Topological interpretation for phase transitions of black holes, *Phys. Rev. D* **107**, 044026 (2023).
- [122] N.-C. Bai, L. Li & J. Tao, Topology of black hole thermodynamics in Lovelock gravity, *Phys. Rev. D* **107**, 064015 (2023).
- [123] N.-C. Bai, L. Song, & J. Tao, Reentrant phase transition in holographic thermodynamics of Born-Infeld AdS black hole, *Eur. Phys. J. C* **84**, 43 (2024).
- [124] R. Li, C.H. Liu, K. Zhang, & J. Wang, Topology of the landscape and dominant kinetic path for the thermodynamic phase transition of the charged Gauss-Bonnet AdS black holes, *Phys. Rev. D* **108**, 044003 (2023).
- [125] P.K. Yerra, C. Bhamidipati, & S. Mukherji, Topology of critical points in boundary matrix duals, [arXiv:2304.14988](https://arxiv.org/abs/2304.14988).
- [126] C.X. Fang, J. Jiang & M. Zhang, Revisiting thermodynamic topologies of black holes, *J. High Energy Phys.* **01** (2023) 102.
- [127] Y.-Z. Du, H.-F. Li, Y.-B. Ma, & Q. Gu, Topology and phase transition for EPYM AdS black hole in thermal potential, [arXiv:2309.00224](https://arxiv.org/abs/2309.00224).
- [128] P.K. Yerra, C. Bhamidipati, & S. Mukherji, Topology of Hawking-Page transition in Born-Infeld AdS black holes, *J. Phys. Conf. Ser.* **2667**, 012031 (2023).
- [129] K. Bhattacharya, K. Bamba, & D. Singleton, Topological interpretation of extremal and Davies-type phase transitions of black holes, *Phys. Lett. B* **854**, 138722 (2024)
- [130] H. Chen, M.-Y. Zhang, H. Hassanabadi, B.C. Lutfuoglu, & Z.-W. Long, Topology of dyonic AdS black holes with quasitopological electromagnetism in Einstein-Gauss-Bonnet gravity, [arXiv:2403.14730](https://arxiv.org/abs/2403.14730).
- [131] B. Hazarika, N.J. Gogoi, & P. Phukon, Revisiting thermodynamic topology of Hawking-Page and Davies type phase transitions, [arXiv:2404.02526](https://arxiv.org/abs/2404.02526).

- [132] S.-W. Wei, Y.-X. Liu, & R.B. Mann, Black Hole Solutions as Topological Thermodynamic Defects, *Phys. Rev. Lett.* **129**, 191101 (2022).
- [133] C.H. Liu & J. Wang, The topological natures of the Gauss-Bonnet black hole in AdS space, *Phys. Rev. D* **107**, 064023 (2023).
- [134] D. Wu, Topological classes of rotating black holes, *Phys. Rev. D* **107**, 024024 (2023).
- [135] D. Wu & S.-Q. Wu, Topological classes of thermodynamics of rotating AdS black holes, *Phys. Rev. D* **107**, 084002 (2023).
- [136] N. Chatzifotis, P. Dorlis, N.E. Mavromatos, & E. Papantonopoulos, Thermal stability of hairy black holes, *Phys. Rev. D* **107**, 084053 (2023).
- [137] S.-W. Wei, Y.-P. Zhang, Y.-X. Liu, & R.B. Mann, Implementing static Dyson-like spheres around spherically symmetric black hole, *Phys. Rev. Res.* **5**, 043050 (2023).
- [138] Y. Du & X. Zhang, Topological classes of black holes in de-Sitter spacetime, *Eur. Phys. J. C* **83**, 927 (2023).
- [139] C. Fairros & T. Sharqui, *Int. J. Mod. Phys. A* **38**, 2350133 (2023).
- [140] D. Chen, Y. He, & J. Tao, Thermodynamic topology of higher-dimensional black holes in massive gravity, *Eur. Phys. J. C* **83**, 872 (2023).
- [141] N.J. Gogoi & P. Phukon, Thermodynamic topology of 4d dyonic AdS black holes in different ensembles, *Phys. Rev. D* **108**, 066016 (2023).
- [142] J. Sadeghi, S.N. Gashti, M.R. Alipour, & M.A.S. Afshar, Bardeen black hole thermodynamics from topological perspective, *Ann. Phys. (Amsterdam)* **455**, 169391 (2023).
- [143] M.S. Ali, H.E. Mourni, J. Khalloufi, & K. Masmar, Topology of Born-Infeld-AdS black hole phase transition, *Ann. Phys. (Amsterdam)* **465**, 169679 (2024).
- [144] D. Wu, Classifying topology of consistent thermodynamics of the four-dimensional neutral Lorentzian NUT-charged spacetimes, *Eur. Phys. J. C* **83**, 365 (2023).
- [145] D. Wu, Consistent thermodynamics and topological classes for the four-dimensional Lorentzian charged Taub-NUT spacetimes, *Eur. Phys. J. C* **83**, 589 (2023).
- [146] D. Wu, Topological classes of thermodynamics of the four-dimensional static accelerating black holes, *Phys. Rev. D* **108**, 084041 (2023).
- [147] J. Sadeghi, M.A.S. Afshar, S.N. Gashti, & M.R. Alipour, Thermodynamic topology and photon spheres in the hyperscaling violating black holes, *Astropart. Phys.* **156**, 102920 (2024).
- [148] F. Barzi, H.E. Mourni, & K. Masmar, Rényi topology of charged-flat black hole: Hawking-Page and Van-der-Waals phase transitions, *JHEAp* **42**, 63 (2024).
- [149] M.U. Shahzad, A. Mehmood, S. Sharif, & A. Övgün, Criticality and topological classes of neutral Gauss-Bonnet AdS black holes in 5D, *Ann. Phys. (Amsterdam)* **458**, 169486 (2023).
- [150] C.-W. Tong, B.-H. Wang, & J.-R. Sun, Topology of black hole thermodynamics via Rényi statistics, [arXiv:2310.09602](https://arxiv.org/abs/2310.09602).
- [151] A. Mehmood & M.U. Shahzad, Thermodynamic topological classifications of well-known black holes, [arXiv:2310.09907](https://arxiv.org/abs/2310.09907).
- [152] M. Rizwan & K. Jusufi, Topological classes of thermodynamics of black holes in perfect fluid dark matter background, *Eur. Phys. J. C* **83**, 944 (2023).
- [153] C. Fairros, Topological interpretation of black hole phase transition in Gauss-Bonnet gravity, *Int. J. Mod. Phys. A* **39**, 2450030 (2024).
- [154] D. Chen, Y. He, J. Tao, & W. Yang, Topology of Hořava-Lifshitz black holes in different ensembles, *Eur. Phys. J. C* **84**, 96 (2024).
- [155] J. Sadeghi, M.A.S. Afshar, S.N. Gashti, & M.R. Alipour, Thermodynamic topology of black holes from bulk-boundary, extended, and restricted phase space perspectives, *Ann. Phys. (Amsterdam)* **460**, 169569 (2023).
- [156] B. Hazarika & P. Phukon, Thermodynamic topology of $D = 4, 5$ Horava Lifshitz black hole in two ensembles, [arXiv:2312.06324](https://arxiv.org/abs/2312.06324).

- [157] N.J. Gogoi & P. Phukon, Thermodynamic topology of 4D Euler-Heisenberg-AdS black hole in different ensembles, *Phys. Dark Univ.* **44**, 101456 (2023).
- [158] M.-Y. Zhang, H. Chen, H. Hassanabadi, Z.-W. Long, & H. Yang, Thermodynamic topology of Kerr-Sen black holes via Rényi statistics, [arXiv:2312.12814](https://arxiv.org/abs/2312.12814).
- [159] J. Sadeghi, M.A.S. Afshar, S.N. Gashti, & M.R. Alipour, Topology of Hayward-AdS black hole thermodynamics, *Phys. Scripta* **99**, 025003 (2024).
- [160] B. Hazarika & P. Phukon, Thermodynamic topology of black holes in $f(R)$ gravity, *PETP* **2024**, 043E01 (2024).
- [161] A. Malik, A. Mehmood, & M.U. Shahzad, Thermodynamic topological classification of higher dimensional and massive gravity black holes, *Ann. Phys. (Amsterdam)* **463**, 169617 (2024).
- [162] M.U. Shahzad, A. Mehmood, A. Malik, & A. Övgün, Topological behavior of 3D regular black hole with zero point length, *Phys. Dark Univ.* **44**, 101437 (2024).
- [163] S.-P. Wu & S.-W. Wei, Thermodynamical topology of quantum BTZ black hole, [arXiv:2403.14167](https://arxiv.org/abs/2403.14167).
- [164] H. Chen, M.-Y. Zhang, H. Hassanabadi, & Z.-W. Long, Thermodynamic topology of phantom AdS black holes in massive gravity, [arXiv:2404.08243](https://arxiv.org/abs/2404.08243).
- [165] B. Hazarika & P. Phukon, Topology of restricted phase space thermodynamics in Kerr-Sen-AdS black holes, [arXiv:2405.02328](https://arxiv.org/abs/2405.02328).
- [166] Z.-Q. Chen & S.-W. Wei, Thermodynamical topology with multiple defect curves for dyonic AdS black holes, [arXiv:2405.07525](https://arxiv.org/abs/2405.07525).
- [167] B.E. Panah, B. Hazarika, & P. Phukon, Thermodynamic topology of topological black hole in $F(R)$ -ModMax gravity's rainbow, [arXiv:2405.20022](https://arxiv.org/abs/2405.20022).
- [168] H. Wang & Y.-Z. Du, Topology of the charged AdS black hole in restricted phase space, [arXiv:2406.08793](https://arxiv.org/abs/2406.08793).
- [169] A.S. Mohamed & E.E. Zotos, Motion of test particles and topological interpretation of generic rotating regular black holes coupled to non-linear electrodynamics, *Astron. Comput.* **48**, 100853 (2024).
- [170] D. Wu, S.-Y. Gu, X.-D. Zhu, Q.-Q. Jiang, & S.-Z. Yang, Topological classes of thermodynamics of the static multi-charge AdS black holes in gauged supergravities: novel temperature-dependent thermodynamic topological phase transition, *J. High Energy Phys.* **06** (2024) 213.
- [171] X.-D. Zhu, D. Wu, D. Wen, Topological classes of thermodynamics of the rotating charged AdS black holes in gauged supergravities, *Phys. Lett. B* **856** (2024) 138919.
- [172] J. W. York, Black-hole thermodynamics and the Euclidean Einstein action, *Phys. Rev. D* **33**, 2092 (1986).
- [173] F. Gray, S. Schuster, A. Van-Brunt and M. Visser, The Hawking cascade from a black hole is extremely sparse, *Class. Quant. Grav.* **33** (2016) no.11, 115003
- [174] B. Ahmedov, O. Rahimov and B. Toshmatov, Gravitational Capture Cross-Section of Particles by Schwarzschild-Tangherlini Black Holes, *Universe* **7** (2021) no.8, 307
- [175] I. Cimidikier, M.P. Dabrowski and H. Gohar, Generalized uncertainty principle impact on nonextensive black hole thermodynamics, *Class. Quant. Grav.* **40** (2023) no.14, 145001
- [176] A. Alonso-Serrano, M. P. Dabrowski and H. Gohar, Nonextensive Black Hole Entropy and Quantum Gravity Effects at the Last Stages of Evaporation, *Phys. Rev. D* **103** (2021) no.2, 026021
- [177] Z. W. Feng, X. Zhou, S. Q. Zhou and D. D. Feng, Rainbow gravity corrections to the information flux of a black hole and the sparsity of Hawking radiation, *Annals Phys.* **416** (2020), 168144
- [178] G. G. Luciano and A. Sheykhi, Black hole geometrothermodynamics and critical phenomena: A look from Tsallis entropy-based perspective, *Phys. Dark Univ.* **42** (2023), 101319
- [179] Y. Sekhmani, S. K. Maurya, J. Rayimbaev, M. K. Jasim, A. Z. Kaczmarek, S. Malik and A. Yadav, Phase transitions and structure of 5D AdS black holes immersed in Chaplygin-like dark fluid from Kaniadakis statistics, *JHEAp* **44** (2024), 79-98
- [180] Y. Sekhmani, D. J. Gogoi, R. Myrzakulov, G. G. Luciano and J. Rayimbaev, Four STU black holes shadows, *Class. Quant. Grav.* **41** (2024) no.18, 185002

- [181] S. Schuster, Sparsity of Hawking radiation in $D + 1$ space-time dimensions for massless and massive particles, *Class. Quant. Grav.* **38** (2021) no.4, 4
- [182] H. Quevedo, Geometrothermodynamics, *J. Math. Phys. (N.Y.)* **48**, 013506 (2007).
- [183] F. Weinhold, Metric geometry of equilibrium hermodynamics, *J. Chem. Phys.* **63** (1975) 6, 2479
- [184] G. Ruppeiner, Riemannian geometry in thermodynamic fluctuation theory, *Rev. Mod. Phys.* **67** (1995), 605-659 [erratum: *Rev. Mod. Phys.* **68** (1996), 313-313]
- [185] H. Quevedo and A. Sanchez, Geometrothermodynamics of asymptotically de Sitter black holes, *JHEP* **09** (2008), 034
- [186] S.H. Hendi, S. Panahiyan, B. Eslam Panah & M. Momennia, A new approach toward geometrical concept of black hole thermodynamics, *Eur. Phys. J. C* **75**, 507 (2015).
- [187] S.H. Hendi, A. Sheykhi, S. Panahiyan & B. Eslam Panah, Phase transition and thermodynamic geometry of Einstein-Maxwell-dilaton black holes, *Phys. Rev. D* **92**, 064028 (2015).
- [188] S.H. Hendi, B. Eslam Panah & S. Panahiyan, Einstein-Born-Infeld-massive gravity: adS-black hole solutions and their thermodynamical properties, *J. High Energy Phys.* **2015**, 157, (2015).
- [189] S. H. Hendi, B. Eslam Panah and S. Panahiyan, Massive charged BTZ black holes in asymptotically (a)dS spacetimes, *JHEP* **05** (2016), 029
- [190] P. C. W. Davies, Thermodynamics of Black Holes, *Proc. Roy. Soc. Lond. A* **353** (1977), 499-521.
- [191] B. Eslam Panah, Effects of energy dependent spacetime on geometrical thermodynamics and heat engine of black holes: gravity's rainbow, *Phys. Lett. B* **787** (2018), 45-55.
- [192] A. G. Tzikas, Bardeen black hole chemistry, *Phys. Lett. B* **788** (2019), 219-224.